AD_____

Award Number: DAMD17-98-1-8224

TITLE: Applications of a Novel Nucleic Acid Detection Method in Breast Cancer: Analysis of Overexpression of HER-2/neu and FAK

PRINCIPAL INVESTIGATOR: Herbert H. Thorp, Ph.D.

CONTRACTING ORGANIZATION: University of North Carolina
Chapel Hill, North Carolina 27599-1350

REPORT DATE: July 2002

TYPE OF REPORT: Final

PREPARED FOR: U.S. Army Medical Research and Materiel Command
Fort Detrick, Maryland 21702-5012

REPORT DOCUMENTATION PAGE

Form Approved
OMB No. 074-0188

1. AGENCY USE ONLY (Leave blank)	2. REPORT DATE	3. REPORT TYPE AND DATES COVERED
	July 2002	Final (1 Jul 98 - 30 Jun 02)

4. TITLE AND SUBTITLE
Applications of a Novel Nucleic Acid Detection Method in Breast Cancer: Analysis of Overexpression of HER-2/neu and FAK

5. FUNDING NUMBERS
DAMD17-98-1-8224

6. AUTHOR(S)
Herbert H. Thorp, Ph.D.

7. PERFORMING ORGANIZATION NAME(S) AND ADDRESS(ES)
University of North Carolina
Chapel Hill, North Carolina 27599-1350

E-Mail: Holden@unc.edu

8. PERFORMING ORGANIZATION REPORT NUMBER

9. SPONSORING / MONITORING AGENCY NAME(S) AND ADDRESS(ES)
U.S. Army Medical Research and Materiel Command
Fort Detrick, Maryland 21702-5012

10. SPONSORING / MONITORING AGENCY REPORT NUMBER

11. SUPPLEMENTARY NOTES
report contains color

12a. DISTRIBUTION / AVAILABILITY STATEMENT
Approved for Public Release; Distribution Unlimited

12b. DISTRIBUTION CODE

13. Abstract *(Maximum 200 Words)* *(abstract should contain no proprietary or confidential information)*

The project "Applications of a Novel Nucleic Acid Detection Method in Breast Cancer: Analysis of Overexpression of Her-2/neu and FAK" is aimed at utilizing new biosensors based on guanine electron transfer to quantitate messenger RNA for breast cancer genes. In the first two years of the project, methods were developed for attaching nucleic acids to indium tin oxide electrodes and detecting these molecules electrochemically through the catalytic reaction. These methods allow for detection of 0.5 fmol per 0.1 cm^2 of electrode area. This method was applied detection of mRNA amplified by RT-PCR and to determination of repeat lengths. In the second two years, molten salts of DNA were developed that allowed for dramatically reducing the electrode size used to do the detection. These materials allowed for DNA detection on electrodes as small as 5 microns; present DNA chips are generally limited to microlocations in the 100 micron range. In the final studies, photoinduced electron transfer was used to probe these novel materials in more detail.

14. SUBJECT TERMS
breast cancer, automated nucleic acid detection, gene expression, MRNA quantitation, prognostic markers, protein kinases

15. NUMBER OF PAGES
42

16. PRICE CODE

17. SECURITY CLASSIFICATION OF REPORT	18. SECURITY CLASSIFICATION OF THIS PAGE	19. SECURITY CLASSIFICATION OF ABSTRACT	20. LIMITATION OF ABSTRACT
Unclassified	Unclassified	Unclassified	Unlimited

Table of Contents

Introduction

The project "Applications of a Novel Nucleic Acid Detection Method in Breast Cancer: Analysis of Overexpression of HER-2/neu and FAK" is aimed at utilizing new biosensors based on guanine electron transfer to quantitate messenger RNA for breast cancer genes. The biosensors are based on a scheme involving abstraction of electrons from the guanines of immobilized RNA to generate a signature current for a specific gene. The purpose of the proposed research is to demonstrate that the guanine electron transfer technology can be used to detect overexpressed RNAs in real biological samples. (Note that changes in the Statement of Work were approved as was a one-year, no-cost extension). The first Task involves demonstration of electrochemical detection of specific genes using $Ru(bpy)_3^{2+}$-mediated electrochemistry (bpy = 2,2'-bipyridine); this task was completed and described in the first report. The second task involves detection of fragment size using electrochemistry; this task was completed and described in the second report. The third task involves preparing liquid DNA samples that can be immobilized on small electrodes for ultra-miniaturized detection; this task was described in the third report. Additional progress on the characterization of these liquid-forming nucleic acids is described here. The fourth task involves use of these liquid-forming nucleic acids to perform expression analyses; this task could not be completed because we have thus far been unsuccessful at including RNA in these novel liquids.

Body

The studies on Task 1 have been published as "Modification of Metal Oxides with Nucleic Acids: Detection of Attomole Quantities of Immobilized DNA by Electrocatalysis."[1] More detailed studies on the kinetics of electron transfer at these interfaces were also published as "Oxidation Kinetics of Guanine in DNA Molecules Adsorbed to Indium Tin Oxide Electrodes."[2]

The studies on Task 2 have been published. The proof-of-principle on the concept that longer fragments containing guanine give larger signals was demonstrated in solution and published as "Kinetics of Metal-Mediated, One-Electron Oxidation of Guanine in Polymeric DNA and Oligonucleotides Containing Trinucleotide Repeat Sequences." [3] A second paper demonstrating this concept on electrode surfaces was under review at Analytical Chemistry when the last report was submitted but has now been published[4] and is attached.

The studies for Task 3 have been completed. These experiments center on forming molten salts of DNA that can be interrogated on very small (5 μm) electrodes. Studies on the formation and interrogation of these compounds have been published as "An Ionic Liquid Form of DNA: Redox-Active Molten Salts of Nucleic Acids."[5] This report describes more detailed photophysical characterization of these materials; the studies described here have been submitted to the Journal of the American Chemical Society.

Considerable attention has focused on electron transfer in nucleic acids, particularly long-range electron transfer between donors and acceptors associated with DNA molecules.[6] A major question surrounding these studies has been the importance of diffusion of one or both of the redox partners. This question was addressed initially using donors or acceptors that intercalated into DNA and were therefore expected to diffuse

slowly on the timescale of electron transfer.[7,8] Later, synthetic oligonucleotides were prepared with attached redox moieties, and the nucleobases were recognized as good electron donors for these studies. Long-range electron transfer has now been unambiguously observed in these tethered systems.[9] An alternative approach to eliminating diffusion is to place the nucleic acid in a medium where diffusion is slow. This approach was quite successful in early studies of photoinduced electron transfer involving $Ru(bpy)_3^{2+}$ (bpy = 2,2'-bipyridine) and small molecule quenchers or related reactions.[10] Inclusion of nucleic acids in highly viscous media has thus far proved elusive, but we report here a system in which photoinduced electron transfer from nucleic acids to metal complexes can be observed and diffusion cannot contribute to the redox process.

We have recently reported molten phases of nucleic acids where a polyether-decorated cation is paired with a DNA polyanion.[5] Extremely slow diffusion of the metal complex in these phases can be determined directly by electrochemical analysis of the neat melts to give values for the diffusion coefficients of the polyether-decorated cation of $D_{PHYS} < 10^{-11}$ cm^2/s. The DNA concentrations attainable in these media (0.65 M) are quite high, and the polyether tails allow maintenance of double-helical structure when melts are formed using duplex DNA. The electrochemical studies show that charge is transported through the melts by metal-centered electron hopping when the intrinsic self-exchange reaction of the participating metal complex is efficient. Ground-state electron transfer between metal centers and the DNA is apparent as catalytic currents provided the included metal complex is a sufficiently powerful oxidant to remove an electron from the guanine nucleobase (approximately 1.05 V vs SCE). Here we report on photoinduced electron transfers in analogous melts.

The complex $Ru(bpz)_3^{2+}$ is a strong excited-state oxidant ($E^{(2+*/1+)} \sim 1.35$ V vs SCE)[11] and is capable of extracting electrons from guanine upon photoexcitation (Figure 1). Quenching of the $Ru(bpz)_3^{2+*}$ emission at 610 nm in dilute aqueous solution occurs upon addition of 2'-deoxyguanosine-5'-monophosphate (dGMP) or poly(d[GC])•poly(d[GC]) and follows Stern-Volmer kinetics to give rate constants of 1.6×10^9 M^{-1} s^{-1} and 2.2×10^9 M^{-1} s^{-1}, respectively. The $Ru(bpz)_3^{2+*}$ emission is unaltered by the addition of a saturated solution of 2'-deoxycytosine-5'-monophosphate (dCMP) or thymidine-5'-monophosphate (TMP). Further, radiolabeled nucleotides photolyzed with visible light in the presence of the $Ru(bpz)_3^{2+}$ show piperidine-labile, guanine-specific cleavage as visualized by gel electrophoresis. These experiments strongly implicate electron transfer from guanine to $Ru(bpz)_3^{2+*}$ as the quenching mechanism.

Nucleic acid melts were prepared by extensive dialysis of $Ni(bpy_{350})_3(ClO_4)_2$ with either 5'-GAT GAA GTG TGA TGT AGA AGA TGT G-3' (**1**) or 5'-CAC ATC TTC TAC ATC ACA CTT CAT C-3' (**2**) (Figure 1) to produce a guanine-containing DNA melt ($Ni(bpy_{350})_3$•**1**) and a DNA melt with no guanines ($Ni(bpy_{350})_3$•**2**). The complex $Ru(bpz)_3(SO_3PEG_{350})_2$ (Figure 1) was added to these melts at a concentration of 1 Ru:10 Ni:20 nucleotides. These materials were combined to vary the concentration of the guanine sites while maintaining a constant overall proportion of nucleotides. The emission decay of $Ru(bpz)_3^{2+*}$ in the melts was determined by time correlated single photon counting, and the measured lifetimes decreased with increasing guanine content (Table 1). As normally observed for metal-DNA photochemistry, a biexponential was required to fit the emission decay, and the lifetimes given in Table 1 are weighted

averages $\langle\tau\rangle$ for the biexponential fits. As expected, the complexes $Ru(bpy)_3^{2+}$ and $Ru(bpm)_3^{2+}$ (bpm = 2,2'-bipyrimidine), which are both less potent excited-state oxidants than $Ru(bpz)_3^{2+}$, gave emission lifetimes that were the same in either $Ni(bpy_{350})_3$•**1** or $Ni(bpy_{350})_3$•**2**. The quenching in the melt did not follow Stern-Volmer kinetics for either time component (Figure 2A), which is expected since the $Ru(bpz)_3^{2+}$ diffuses less than 0.4 Å within the observed lifetimes (calculated as $(2D_{PHYS}t)^{1/2}$).

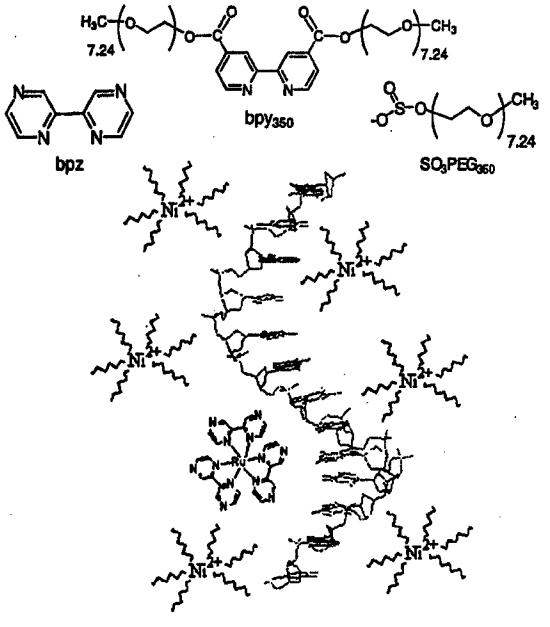

Figure 1. $Ni(bpy_{350})_3$Oligo + $Ru(bpz)_3^{2+}$, ligands, and counterion.

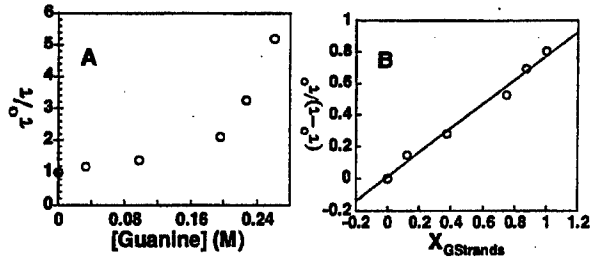

Figure 2. A. Stern-Volmer plot for quenching of $Ru(bpz)_3^{2+}$ in $Ni(bpy_{350})_3$DNA molten salts. **B.** Fraction of $Ru(bpz)_3^{2+}$quenched vs. mole fraction of G strands in $Ni(bpy_{350})_3$DNA molten salts (same data as **A**). G strand concentration was altered by varying the relative proportion of $Ni(bpy_{350})_3$•**1** and $Ni(bpy_{350})_3$•**2** while maintaining constant [nucleotides] = 0.65 M, $[Ru(bpz)_3^{2+}]$ = 0.033 M, $[Ni(bpy_{350})_3^{2+}]$ = 0.33 M.

The dependence of the lifetime on guanine concentration must be analyzed using a model designed for quenching in rigid solutions.[10] A simple sphere-of-action model assumes random distribution of the reactants and does not account for binding of $Ru(bpz)_3^{2+}$ to the phosphates along the DNA backbone; accordingly, a plot of $\ln(\tau^o/\tau)$ deviates significantly from linearity. Alternatively, Figure 2B shows that there is a linear relationship between the fraction quenched (plotted as $(\tau^o - \tau)/\tau^o$) versus the fraction of guanine-containing oligonucleotides. Oligonucleotide **1** was designed such that electrostatically associated $Ru(bpz)_3^{2+}$ is bound to phosphate that is either part of a guanine nucleotide or adjacent to a guanine nucleotide. Molecular models suggest that $Ru(bpz)_3^{2+}$ bound to a guanine nucleotide is 10 - 13 Å from a guanine. Thus, as the fraction of **1** is increased, the fraction of $Ru(bpz)_3^{2+}$ excited states bound to **1** (and hence undergoing electron transfer) increases linearly.

Table 1. Emission lifetimes of $Ru(bpz)_3^{2+}$ in DNA melts as a function of guanine concentration.

τ	[Guanine]
767 ns	**0 mM**
653 ns	**33 mM**
553 ns	**98 mM**
364 ns	**196 mM**
236 ns	**227 mM**
148 ns	**262 mM**

The average lifetime of 148 ns for the sample with 100% **1** suggests an electron-transfer rate of $7 \times 10^6\ s^{-1}$ for reaction of bound $Ru(bpz)_3^{2+*}$. Steenken[12] has estimated the potential of protonated guanine to be 1.34 V, giving a driving force for the reaction with $Ru(bpz)_3^{2+*}$ close to 0 eV. We also assume that $\beta = 1\ Å^{-1}$, and that the rate is described by $k = 10^{13}\ s^{-1}\exp[-(\Delta G + \lambda)^2/4\lambda RT]\exp(-\beta(r-r^o))$ where r is the average electron-transfer distance and r^o is the distance of closest approach of guanine and $Ru(bpz)_3^{2+}$ (approximately 10 Å). We assume a reorganizational energy λ of 1.2 eV, based on the known value for self-exchange in tailed $Ru(bpy)_3^{2+}$-type molten salts. This analysis gives an average electron-transfer distance in the melt of 12.5 Å (center-to-center), which is consistent with average distances determined from molecular models of $Ru(bpz)_3^{2+}$ and single-stranded DNA and similar to that obtained in early studies of photoinduced electron transfer in rigid glycerol solution.

In summary, we have developed redox melts for observing electron transfer from guanine in DNA to non-covalently bound metal complexes where the influence of diffusion can be rigorously neglected due to known diffusion properties of the metal complexes in the melt. The ability of these melts to stabilize DNA secondary structures should allow detailed studies of electron transfer in novel environments.

Experimental. *Materials.* Millipore ultra pure water was used for all experiments. All reagents were purchased from Sigma Aldrich unless otherwise noted. 2,2' bipyrimidine was purchased from Lancaster Synthesis and twice recrystallized from ether before use. Oligonucleotides were obtained from MWG-Biotech. **1** refers to the

following sequence: 3' G-A-T-G-A-A-G-T-G-T-G-A-T-G-T-A-G-A-A-G-A-T-G-T-G 5'. **2** is: 3' C-A-C-A-T-C-T-T-C-T-A-C-A-T-C-A-C-A-C-T-T-C-A-T-C 5'. The following molar absorptivities were used for concentration determinations: $Ni(bpy_{350})_3^{2+}$ ε_{327} = 27,850 M^{-1} cm^{-1}, $Ru(bpy)_3^{2+}$ ε_{452} = 14,000 M^{-1} cm^{-1}, $Ru(bpz)_3^{2+}$ ε_{440} = 13,000 M^{-1} cm^{-1}, $Ru(bpm)_3^{2+}$ ε_{454} = 8,600 M^{-1} cm^{-1}, oligo **1** ε_{262} = 12,075 $M^{-1}cm^{-1}$, oligo **2** ε_{258} = 10,050 $M^{-1}cm^{-1}$. Absorption measurements were determined using a Cary300Bio™ UV-Vis Spectrophotometer. Steady state luminescence measurements were performed on a Spex-fluoromax™ spectrofluorimeter.

Methods. 2,2' Bipyrazine (bpz) was prepared by the procedure of Lafferty and Case.[13] $Ru(bpz)_3Cl_2$ and $Ru(bpm)_3Cl_2$ preparations were described by Meyer.[11] Synthesis of $Ni(bpy_{350})_3(ClO_4)_2$ was as previously described.[14] Synthesis of $NaSO_3MePeg_{350}$ was described previously[15] and $Ru(bpz)_3(SO_3MePeg_{350})_2$, $Ru(bpm)_3(SO_3MePeg_{350})_2$, and $Ru(bpy)_3(SO_3MePeg_{350})_2$ were synthesized by the methods of Ritchie.[16]

Synthesis of $Ni(bpy_{350})_3$•**1** and $Ni(bpy_{350})_3$•**2** were achieved through dialysis as described previously for the $Co(bpy_{350})_3$•nucleotides[5] with slight modification. Aqueous solutions containing 1.3 equivalents of $Ni(bpy_{350})_3(ClO_4)_2$ and 2 equivalents of nucleotide were mixed in a 500 MWCO dialysis tube. The tubing was placed in a 1-L water reservoir for 4 days at 4° C. The water was changed every 24 h. The quantity of the $Ni(bpy_{350})_3(ClO_4)_2$ in the reservoir was monitored spectrophotometrically by measuring the absorbance at 327 nm (ε = 27,850 $M^{-1}cm^{-1}$).

Preparation of melts for photochemistry. Following dialysis, concentrations of solutions of the $Ni(bpy_{350})_3$•**1** or $Ni(bpy_{350})_3$•**2** were determined by UV-Vis absorption spectroscopy using ε = 27,850 M^{-1} cm^{-1} at 327 nm. From these solutions, mixtures of $Ni(bpy_{350})_3$•**1** and $Ni(bpy_{350})_3$•**2** $Ru(bpz)_3^{2+}$ were obtained by adding the following: [1 mole $Ni(bpy_{350})_3$•**2** + 0.14 mole $Ni(bpy_{350})_3$•**1**], [1 mole $Ni(bpy_{350})_3$•**2** + 0.60 mole $Ni(bpy_{350})_3$•**1**], [1 mole $Ni(bpy_{350})_3$•**2** + 3 mole $Ni(bpy_{350})_3$•**1**], [1 mole $Ni(bpy_{350})_3$•**2** + 7 mole $Ni(bpy_{350})_3$•**1**]. 1 mole equivalent of the $Ru(bpz)_3(SO_3MePeg_{350})_2$ was added to 10 equivalents of the total $Ni(bpy_{350})_3^{2+}$ concentration. This produced solutions of composition $1Ru(bpz)_3^{2+}$:$10Ni(bpy_{350})_3^{2+}$:20nucleotides that varied only in their guanine content. Solutions were reduced in volume to 10 µL and cast on quartz slides. These solultions were placed in a vacuum dessicator with drierite for 6 h followed by drying at 10^{-3} torr vacuum for 12 h. Samples containing the strong photooxidant $Ru(bpz)_3^{2+}$ were always shielded from light with aluminum foil prior to analysis. Density of dry molten salts determined by picnometry (d = 1.124 g/ml) gives $[Ni(bpy_{350})_3^{2+}]$ = 0.327 M.

Emission spectroscopy. The apparatus consists of a commercially available Argon ion laser whose continuous output is used to pump a mode-locked Ti:Sapphire laser. The Ti:Sapphire laser output is frequency doubled to 423 nm using a BBO crystal to produce ~1 ps pulses with a pulse energy of ~.26 nJ/pulse. This pulse train is cavity dumped and the repetition rate selected to be roughly 5 times the natural lifetime of the sample. Luminescence lifetime data was collected using the time-correlated single photon counting technique published earlier.[17]

Gel electrophoresis. Radiolabeled ATP was purchased from New England Nuclear. T4 Kinase was purchased from either Promega or New England Biolabs. Oligonucleotides were sythesized by the Lineburger Comprehensive Cancer Center Nucleic Acids Core facility. Photolysis was performed with a 300 W Hg lamp (Oriel)

with a 350 nm cutoff filter. Final concentrations were 50 μM HT DNA, 12.5 fM radiolabeled oligonucleotide, 2.5 μM $Ru(bpz)_3^{2+}$, and 500 mM NaP_i, pH 7. Irradiation time was 1 minute and the total volume was 80 μL. Samples were precipitated with sodium acetate and ethanol, subjected to alkaline treatment with piperdine for 30 min at 90 °C, redissolved in 0.5X TBE buffer with orange G and xylene in 80% formamide and loaded onto a denaturing (7M urea) 20% acrylamide gel. Gels were visualized using a Molecular Dynamics Phosphorimager and ImageQuant™ software.

Research Accomplishments

- New method for adsorption of double-stranded DNA to ITO electrodes. The method involves no coupling agents or reactive additives, and can be performed rapidly with no special handling.
- Detection of adsorbed DNA without labeling using catalytic electrochemistry. The sensitivity is 0.5 fmol of strand per 0.1 cm^2.
- Detection of HER-2 mRNA following RT-PCR amplification from breast cancer cells.Generation of PCR fragments with trinucleotide repeat sequences of CAG and CCG.
- Immobilization of PCR fragments on ITO electrodes with high reproducibility and good linearity based on the quantity of applied DNA.
- Detection of quantity **and** size of PCR products.
- Developed new molten salts of DNA based on polyether-tailed counterions.
- Characterized molten salts by elemental analysis and UV spectroscopy.
- Detected DNA electrochemically by catalytic guanine oxidation inside the molten salts.
- Developed new molten salts of defined oligonucleotide sequences based on $Ni(bpy_{350})_3^{2+}$.
- Demonstrated electron transfer from guanine in DNA to the excited state of $Ru(bpz)_3^{2+}$.
- Showed that electron transfer in DNA melts occurs with predictable physical parameters over logical distances.

Reportable Outcomes

- Findings reported by Ivana Yang at the Era of Hope Meeting in Atlanta, June 2000.
- Immobilization method reported in Analytical Chemistry: Modification of Metal Oxides with Nucleic Acids: Detection of Attomole Quantities of Immobilized DNA by Electrocatalysis. P. M. Armistead, H. H. Thorp* *Anal. Chem.* **2000**, *72*, 3764-3770.
- Kinetics studies of oxidation at the modified electrodes published in Analytical Chemistry: Oxidation Kinetics of Guanine in DNA Molecules Adsorbed to Indium Tin Oxide Electrodes. P. M. Armistead, H. H. Thorp* *Anal. Chem.* **2001**, *73*, 558-564. (Note that P. M. Armistead also received fellowship support from DoD as DAMD17-96-1-6067.)

- Kinetics of fragment size effects in solution reported in a paper submitted to Inorganic Chemistry: Kinetics of Metal-Mediated, One-Electron Oxidation of Guanine in Polymeric DNA and Oligonucleotides Containing Trinucleotide Repeat Sequences. I. V. Yang, H. H. Thorp* *Inorg. Chem.* **2000**, *39*, 4969-4976.
- Synthesis of molten salts of DNA, characterization of these salts, and detection of DNA inside the molten salts published in Journal of the American Chemical Society: An Ionic Liquid Form of DNA: Redox-Active Molten Salts of Nucleic Acids. A. M. Leone, S. C. Weatherly, M. E. Williams, R. W. Murray*, H. H. Thorp* *J. Am. Chem. Soc.* **2001**, *123*, 218-222.
- Detection of fragment size on modified electrodes under second review at Analytical Chemistry: Modification of Indium Tin Oxide Electrodes with Repeat Polynucleotides: Electrochemical Detection of Trinucleotide Repeat Expansion. I. V. Yang, H. H. Thorp* *Anal. Chem.* **2001**, *73*, 5316-5322.
- Photoinduced Electron Transfer in Nucleic Acid Molten Salts. A. M. Leone, M. K. Brennaman, J. D. Tibodeau, J. M. Papanikolas, R. W. Murray, H. H. Thorp *J. Am. Chem. Soc.*, submitted.

Conclusions

The work performed under this grant has provided a convenient method for immobilizing PCR fragments and quantitating these fragments quickly (Task 1). The method can also be used to determine the size of PCR fragments, which will allow for detection of genetic abnormalities, RFLP analysis, detection of trinucleotide repeat expansion, and monitoring other changes that are reflected in the size of DNA fragments (Task 2). Preparation of novel materials comprising DNA molten salts was described in the previous report (Task 3). As described in this report, these materials were further characterized using sophisticated photochemical methods. Studies aimed at addressing Task 4 were unsuccessful, because we have thus far been unable to stabilize RNA in the molten salts.

References

(1) Armistead, P. M.; Thorp, H. H. *Anal. Chem.* **2000**, *72*, 3764-3770.

(2) Armistead, P. M.; Thorp, H. H. *Anal. Chem.* **2001**, *73*, 558-564.

(3) Yang, I. V.; Thorp, H. H. *Inorg. Chem.* **2000**, *39*, 4969-4976.

(4) Yang, I. V.; Thorp, H. H. *Anal. Chem.* **2001**, *73*, 5316-5322.

(5) Leone, A. M.; Weatherly, S. C.; Williams, M. E.; Thorp, H. H.; Murray, R. W. *J. Am. Chem. Soc.* **2001**, *123*, 218-222.

(6) Barton, J. K.; Kumar, C. V.; Turro, N. J. *J. Am. Chem. Soc.* **1986**, *108*, 6391-6393.

(7) Brun, A. M.; Harriman, A. *J. Am. Chem. Soc.* **1992**, *114*, 3656.

(8) Holmlin, R. E.; Stemp, E. D. A.; Barton, J. K. *J. Am. Chem. Soc.* **1996**, *118*, 5236-5244.

(9) Hall, D. B.; Holmlin, R. E.; Barton, J. K. *Nature* **1996**, *382*, 731-735.

(10) Guarr, T.; McGuire, M.; Strauch, S.; McLendon, G. *J. Am. Chem. Soc.* **1983**, *105*, 616-618.

(11) Rillema, D. P.; Allen, G.; Meyer, T. J.; Conrad, D. *Inorg. Chem.* **1983**, *22*, 1617-1622.

(12) Steenken, S.; Jovanovic, S. V. *J. Am. Chem. Soc.* **1997**, *119*, 617-618.
(13) Lafferty, J. J.; Case, F. H. *J. Org. Chem.* **1967**, *32*, 1591-1596.
(14) Long, J. W.; Velazquez, C. S.; Murray, R. W. *J. Phys. Chem. A* **1996**, *100*, 5492-5499.
(15) Ito, K.; Ohno, H. *Electrochimica Acta* **1998**, *43*, 1247-1252.
(16) Ritchie, J. E.; Murray, R. W. *J. Phys. Chem. B* **2001**, *105*, 11523-11528.
(17) Fleming, C. N.; Maxwell, K. A.; DeSimone, J. M.; Meyer, T. J.; Papanikolas, J. M. *J. Am. Chem. Soc.*, **2001**, *123*, 10336-10347.

Appendices

Complete Bibliography. Three copies of the following are attached. Note that all except the first paper have been submitted with previous annual reports.

- Modification of Indium Tin Oxide Electrodes with Repeat Polynucleotides: Electrochemical Detection of Trinucleotide Repeat Expansion. Yang, I. V.; Thorp, H. H. *Anal. Chem.* **2001**, *73*, 5316-5322.
- Modification of Metal Oxides with Nucleic Acids: Detection of Attomole Quantities of Immobilized DNA by Electrocatalysis. P. M. Armistead, H. H. Thorp* *Anal. Chem.* **2000**, *72*, 3764-3770.
- Oxidation Kinetics of Guanine in DNA Molecules Adsorbed to Indium Tin Oxide Electrodes. P. M. Armistead, H. H. Thorp* *Anal. Chem.* **2001**, *73*, 558-564.
- Kinetics of Metal-Mediated, One-Electron Oxidation of Guanine in Polymeric DNA and Oligonucleotides Containing Trinucleotide Repeat Sequences. I. V. Yang, H. H. Thorp* *Inorg. Chem.* **2000**, *39*, 4969-4976.
- An Ionic Liquid Form of DNA: Redox-Active Molten Salts of Nucleic Acids. A. M. Leone, S. C. Weatherly, M. E. Williams, R. W. Murray*, H. H. Thorp* *J. Am. Chem. Soc.* **2001**, *123*, 218-222.

Individuals paid with award:
Kircus, Sandy
Verona, Ivana
Leone, Anthony
Thorp, Holden
Baik, M.
Paul, Jared
Hull, Dominic
Tibodeau, Jennifer
Holmberg, Rebecca

An Ionic Liquid Form of DNA: Redox-Active Molten Salts of Nucleic Acids

Anthony M. Leone, Stephanie C. Weatherly, Mary Elizabeth Williams, H. Holden Thorp, and Royce W. Murray

Contribution from the Department of Chemistry, Venable and Kenan Laboratories, University of North Carolina, Chapel Hill, North Carolina 27599-3290

JOURNAL OF THE AMERICAN CHEMICAL SOCIETY

Reprinted from
Volume 123, Number 2, Pages 218–222

An Ionic Liquid Form of DNA: Redox-Active Molten Salts of Nucleic Acids

Anthony M. Leone, Stephanie C. Weatherly, Mary Elizabeth Williams,† H. Holden Thorp,* and Royce W. Murray*

Contribution from the Department of Chemistry, Venable and Kenan Laboratories, University of North Carolina, Chapel Hill, North Carolina 27599-3290

Received September 11, 2000. Revised Manuscript Received November 13, 2000

Abstract: Ionic liquids are described that contain duplex DNA as the anion and polyether-decorated transition metal complexes based on $M(MePEG\text{-}bpy)_3^{2+}$ as the cation (M = Fe, Co; MePEG-bpy = 4,4′-$(CH_3(OCH_2CH_2)_7OCO)_2$-2,2′-bipyridine). When the undiluted liquid DNA—or molten salt—is interrogated electrochemically by a microelectrode, the molten salts exhibit cyclic voltammograms due to the physical diffusion (D_{PHYS}) of the polyether−transition metal complex. When M = Co(II), the cyclic voltammogram of the melt shows an oxidative wave due to the Co(III/II) couple at $E_{1/2} = 0.40$ V (versus Ag/AgCl) and a D_{PHYS} of 6×10^{-12} cm²/s, which is significantly lower than that for $Co(MePEG\text{-}bpy)_3(ClO_4)_2$ ($D_{PHYS} = 2.6 \times 10^{-10}$ cm²/s) due to greater viscosity provoked by the DNA polymer. When a 1:1 mixture is made of the $Co(MePEG\text{-}bpy)_3$·DNA and $Fe(MePEG\text{-}bpy)_3(ClO_4)_2$ melts, two redox waves are observed. The first is due to the Co(III/II) couple, and the second is a catalytic wave due to oxidation of guanine in DNA by electrogenerated Fe(III) in the undiluted melt. Independent experiments show that the Fe(III) form of the complex selectively oxidizes guanine in duplex DNA. These DNA molten salts constitute a new class of materials whose properties can be controlled by nucleic acid sequence and that can be interrogated in undiluted form on microelectrode arrays.

The ability of nucleic acids to store and transfer information through Watson−Crick base pairing has intriguing parallels with microelectronic circuitry.[1−3] Binding of complementary DNA sequences has been suggested as a method for forming connections between circuit elements,[3−5] directing assembly of nanoscale structures,[6,7] and computing.[1,8] In addition to providing a molecular self-assembly platform, DNA can also provide specific electronic signals through electron-transfer reactions of the guanine nucleobase.[9−11] Herein, we report on novel ionic liquid materials based on DNA salts of polyether-decorated transition metal complexes (Figure 1) that, in undiluted form, undergo electrochemical reactions and act as catalytic electron relays between a microelectrode and DNA. The DNA remains double-stranded in the ionic liquids, and the electrochemistry is performed under vacuum. The semisolid-state nature of the new DNA materials—which can be regarded as molten salts—may be useful in microelectronic circuits that utilize DNA for *both* self-assembly and electronic connections. Further, the ability to control DNA sequence and secondary structure will allow creation of new classes of molten materials that undergo well-defined structural changes programmed by sequence and monitored by electrochemical signals.

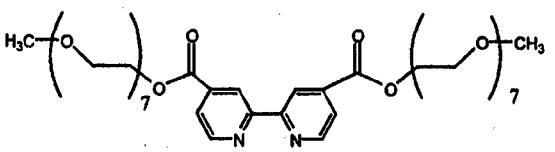

MePEG-bpy

1: $Co(MePEG\text{-}bpy)_3(ClO_4)_2$
2: $Fe(MePEG\text{-}bpy)_3(ClO_4)_2$
3: $Co(MePEG\text{-}bpy)_3$• DNA

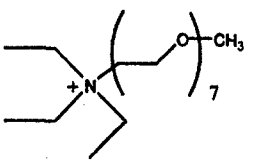

$MePEG\text{-}NEt_3^+$
4: $MePEG\text{-}NEt_3^+$ DNA

Figure 1. Structures of the hybrid redox polyether melts. In the melt formed between $Co(MePEG\text{-}bpy)_3^{2+}$ and DNA (**3**), there is one Co complex for each base pair of the DNA. In the melt formed with the $MePEG\text{-}NEt_3^+$ cation (**4**), there are two ammonium cations per base pair. Elemental analysis of the DNA melts shows that the composition is >90% of the indicated cation−DNA pair with <10% of the perchlorate or chloride salt of the polyether cation. Very little sodium ion was detected in either **3** or **4**, showing that the polyether cation replaced all of the DNA cations during the dialysis.

† Present address: Department of Chemistry, Northwestern University, 2145 Sheridan Road, Evanston, Illinois 60208.

(1) Adelman, L. M. *Science* **1994**, *266*, 1021−1024.
(2) Hopfield, J. J.; Onuchic, J. N.; Beratan, D. N. *Science* **1988**, *241*, 817−820.
(3) Mirkin, C. A.; Taton, T. A. *Nature* **2000**, *405*, 626−627.
(4) Porath, D.; Bezryadin, A.; de Vries, S.; Dekker, C. *Nature* **2000**, *403*, 635−639.
(5) Fink, H. W.; Schonenberger, C. *Nature* **1999**, *398*, 407−410.
(6) Mirkin, C. A. *Inorg. Chem.* **2000**, *39*, 2258−2272.
(7) Elghanian, R.; Storhoff, J. J.; Mucic, R. C.; Letsinger, R. L.; Mirkin, C. A. *Science* **1997**, *277*, 1078−1081.
(8) Pirrung, M. C.; Connors, R. V.; Odenbaugh, A. L.; Montague-Smith, M. P.; Walcott, N. G.; Tollett, J. J. *J. Am. Chem. Soc.* **2000**, *122*, 1873−1882.
(9) Hall, D. B.; Holmlin, R. E.; Barton, J. K. *Nature* **1996**, *384*, 731−735.
(10) Johnston, D. H.; Cheng, C.-C.; Campbell, K. J.; Thorp, H. H. *Inorg. Chem.* **1994**, *33*, 6388−6390.
(11) Schuster, G. B. *Acc. Chem. Res.* **2000**, *33*, 253−260.

10.1021/ja003332c CCC: $20.00
Published on Web 12/16/2000

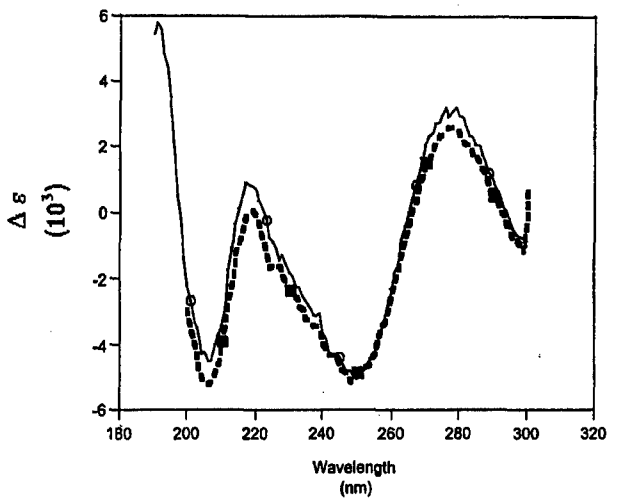

Figure 4. CD spectra of 500 μM herring testes DNA (dashed) and **4** (solid). Concentrations are in nucleotide phosphate.

of **3** showing the relative sizes of the polyether tails and DNA is shown in Figure 5.

The only electrochemical signal seen in melt **3** is that due to the Co(III/II) couple. Co(III) is not a sufficiently powerful oxidant to oxidize guanine. However, when a 1:1 mixture was made of **3** and the iron perchlorate melt **2**, two electrochemical signals were observed (Figure 3B). The first was due to the Co(III/II) wave, while the more positive wave for Fe(III/II) displayed an oxidation current much larger than the subsequent reductive current, which is characteristic of mediated electrocatalysis.[29] Faster potential scanning gave a more symmetrical Fe(III/II) wave, and repeated scanning led to smaller oxidation currents on successive scans; both of these features are indicative of electrocatalytic oxidation of guanine.[26,30,31] This behavior is ascribed to catalytic oxidation of guanine in DNA by the electrogenerated Fe(III) in the melt. The Co(III/II) couple was used in choronoamperometry experiments to determine a value of D_{PHYS} for the 1:1 **3/2** melt of 6×10^{-11} cm^2/s, which is higher than in compound **3** probably because of the higher ethylene oxide/DNA ratio.

To verify that guanines were the source of the electrons that gave the catalytic current in Figure 3B, we performed an experiment in which the tailed Fe(III) complex was reacted with a radiolabeled oligonucleotide containing a single guanine. This reaction was performed by oxidizing the Fe(II) complex with Ce^{4+} and mixing the resulting Fe(III) form with DNA in dilute aqueous solution. The DNA showed selective cleavage at the guanine residue following piperidine treatment and high-resolution gel electrophoresis. In addition, cyclic voltammetry of both **3** and **4** in the absence of Fe showed no faradaic current at potentials up to 1.5 V, showing that direct oxidation of guanine at the microelectrode does not occur at a detectable rate. We therefore ascribe the catalytic current observed in Figure 3B to oxidation of guanine by Fe(III) *in the neat DNA molten salt.*

Conclusions

The use of polyether-tailed cations to prepare ionic liquid forms of DNA raises many exciting possibilities. Tailed quaternary ammonium salts of DNA have been used to prepare aligned DNA films,[32] but these materials are not expected to possess favorable electrochemical characteristics because the tail contains only four polyether units with a C_{10} aliphatic unit on the end. The DNA materials **3** and **4** have long polyether tails terminated with only a methyl group, which facilitates ion transport and an ability to interrogate the neat liquid **3** electrochemically. Since the rate of electron hopping for Co(III/II) is slow, the currents in Figure 3 can be confidently assigned as arising from slow, physical diffusion of the Co complex in the melt. These experiments are carried out on dried materials under vacuum. The melts also show solubility in a wide range of fluid solvents, and both the dissolved forms and the neat melts are amenable to spectroscopic analysis. Recovery of the DNA from the melts and subsequent analysis shows that it is double-stranded. This new ionic phase of DNA is readily manipulated, and the cast films can be deposited onto microelectrode arrays, placed under vacuum, and still exhibit chemical reactions normally observed in dilute solution.

In these melts doped with the Fe complex, the polyether–metal complex serves a dual role: to provide a "solvent" in

Figure 5. Model showing the structure of **3** with the tailed metal complexes and the DNA molecule rendered to scale. The DNA is shown in a cartoon form and the metal complexes are shown with the metal atoms as blue spheres and the MePEG ligands in CPK colors. The polyether chains provide considerable "solvent" for the DNA molecule and diffusion of the metal ions to the electrode. Note that, for clarity, the drawing shows fewer than the actual 1 metal ion per base pair present in the melt. The model was generated using the Cerius2 software package from MSI.

(29) Bard, A. J.; Faulkner, L. R. *Electrochemical Methods*; John Wiley and Sons: New York, 1980; p 431.
(30) Szalai, V. A.; Thorp, H. H. *J. Am. Chem. Soc.* **2000**, *122*, 4524–4525.
(31) Armistead, P. M.; Thorp, H. H. *Anal. Chem.* **2000**, 72, 3764–3770.
(32) Okahata, Y.; Kobayashi, T.; Tanaka, K.; Shimomura, M. *J. Am. Chem. Soc.* **1998**, *120*, 6165–6166.

which diffusive electron transfers can occur and to mediate electron transfer from guanine to the electrode. Numerous pathways for electron transfer exist in the melts, because electrons can transfer from the guanine to the metal, from guanine to an oxidized guanine, and from metal to metal. Guanine−guanine electron transfers may occur within single DNA molecules; however, because of the relatively high concentration of Fe in the melt and its ability to carry charge by electron hopping in the polyether medium, efficient electron transfer within DNA is probably not required. In the future, we believe that these processible ionic liquid materials will provide a simple basis for microstructures that utilize DNA as both a self-assembly partner and, when electron-transfer active polyethers such as **3** are used, specific electronic signals. In addition, sequence control of the DNA combined with the maintenance of the duplex structure in the melts provides pathways to new materials where the nucleic acid structure produces designed properties of the polymer melts. The electron-transfer reactivity provides a means to study these properties on small quantities of undiluted material.

Acknowledgment. This research was supported by the Department of Energy (R.W.M.), the Department of Defense (H.H.T.), and Xanthon, Inc. (H.H.T.). We thank Dr. M. Baik for assistance with Figure 5 and Professor E. T. Samulski for helpful discussions.

JA003332C

Experimental Section

Materials and Measurements. Compounds **1** and **2** were prepared according to a published procedure[12] and characterized by NMR and electrochemistry. The MePEG-NEt_3Cl salt was prepared according to a published procedure.[13] Electrochemical measurements were conducted under vacuum at 67 °C on 3-electrode arrays with a 3.9 μm radius Pt working electrode as previously described.[12] CD spectra were acquired on an Aviv Model 62DS circular dichroism spectrometer with a 0.1 cm cell. Values of D_{PHYS} were determined from chronoamperometry data plotted as current versus $t^{-1/2}$; and linear fits were used to determine D_{PHYS} as described previously.[12] The bulk concentration of the Co complex was 0.4 M in **3** and 0.2 M in the 1:1 **3/2** melt.

Preparation of DNA Ionic Liquids. Herring testes DNA was obtained from Sigma and sheared to a size range of 50−100 bp as determined by agarose gel electrophoresis. To form compound **3**, 41.0 mL of 49 mM sheared HT DNA (2.0 mmol) was added to 1.0 mmol of **1**. The solution was diluted to 300 mL and added to Millipore brand 500 MWCO dialysis tubing that had been soaked twice for 30 min in Nanopure water. Dialysis was executed for 1 week during which the 8-L reservoir was replaced every 12 h. Following dialysis, the solution was removed from the dialysis tubing, and the water was removed by rotary evaporation at ambient temperature. The resulting melt was rinsed repeatedly with Nanopure water. Removal of water produces a viscous, transparent material that was further dried under vacuum. Elemental analysis gave P = 1.90%, Na = 0.04%, Cl = 0.77%, and Co = 1.90%. Complete conversion to Co(MePEG-bpy)$_3$·DNA would give P = 1.75%, Na = 0%, Cl = 0%, and Co = 1.66%. Compound **4** was prepared by the same method except that 2 mmol of MePEG-NEt_3Cl was used as was 100 MWCO dialysis tubing. Elemental analysis of **4** gave P = 4.63%, Na = 0.20%, and Cl = 0.87%. Complete conversion to MePEG-NEt_3·DNA would give P = 3.90%, Na = 0%, and Cl = 0%.

Gel Electrophoresis. Compound **2** was oxidized to the Fe(III) form by reaction with 1 equiv of $Ce(ClO_4)_4$ + $2HClO_4$ in an acetonitrile/perchloric acid solution (GFS Chemicals, Powell, OH). Complete oxidation to the Fe(III) form was confirmed by absorbance spectroscopy. In the cleavage reactions, a 10-μL solution of 5′-^{32}P labeled oligonucleotide (5′-AAAAATATAGTATAAAAAA-3′) and 1 equiv of calf thymus DNA was mixed with 10 μL of either a 1 mM solution of oxidized **2**, **2** that had not been oxidized, or Ce(IV) alone. The reaction was allowed to proceed until the Fe(III) was converted to Fe(II) (the color of the solution changed from green to violet). The samples were ethanol precipitated, piperidine treated, and electrophoresed on a denaturing polyacrylamide gel according to a published procedure.[14] A single cleavage site was detected on the gel at the guanine nucleotide upon reaction with oxidized **2** (the site of reaction was determined by comparison with a Maxam−Gilbert G reaction). No cleavage was observed upon reaction with **2** that had not been oxidized or with Ce(IV) in the absence of **2**.

Results and Discussion

Room temperature melts are reliably formed when one partner in a cation/anion pair is decorated with poly(ethylene glycol) tails of appropriate length (Figure 1)[12,13] and are redox-active molten salts when one of the partners is also capable of electron transfer.[12,13] The polyether tail can be attached to either the redox-active partner or the redox-inert counterion.[13] For example, the perchlorate salt Co(MePEG-bpy)$_3$(ClO_4)$_2$ (**1**), containing a redox-active metal complex with polyether tails, is a molten material.[12] When this highly viscous, amorphous compound is placed on a three-electrode array containing a 3.9 μm radius Pt microelectrode, an electrochemical signal due to the Co(III/II) oxidation reaction (0.18 V, all potentials in the text are versus Ag/AgCl) is observed in the neat liquid (Figure 2A).

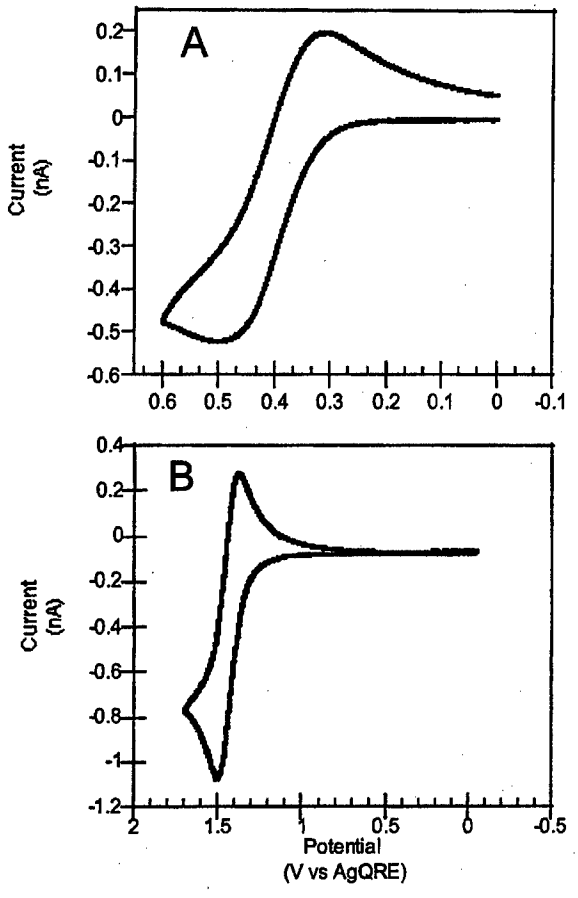

Figure 2. Cyclic voltammograms for (A) **1** and (B) **2** at 25 mV/s on the 3.9 μm Pt microelectrode with a silver quasireference and a Pt auxiliary electrode. Measurements were performed at 67 °C under vacuum using a home-built potentiostat capable of detecting 0.1 pA of current. The potentials in the figure are as-collected versus the silver quasireference, but those quoted in the text are versus aqueous Ag/AgCl after conversion with a ferrocene standard.

Diffusion-controlled currents in polyether melts reflect the summed rates of physical diffusion (D_{PHYS}) of the metal complex to the microelectrode and of electron hopping (self-exchange) between oxidized and reduced forms of the complex in the melt,[12] as embodied in the Dahms−Ruff equation:[15]

$$D_{APP} = D_{PHYS} + \frac{k_{EX}\delta^2 C}{6} \quad (1)$$

where D_{APP} is the overall (apparent) diffusion coefficient, k_{EX} is the rate constant for self-exchange, and C and δ are the concentration and average center-to-center distances between the complexes in the melts, respectively. For the Co(III/II) wave observed in **1**, electron hopping is slow, and the observed current is solely a function of D_{PHYS}. The value of D_{PHYS} for **1** is 2.6 × 10^{-10} cm^2/s; such slow diffusion is typical of the polyether melts.[12] When Co is replaced with Fe to form Fe(MePEG-bpy)$_3$(ClO_4)$_2$ (**2**), the Fe(III/II) oxidation wave appears at 1.04 V and electron hopping is much faster (while D_{PHYS} remains constant), giving higher overall currents (Figure 2B). The larger k_{EX} for Fe compared to Co is a well-understood chemical difference.[12,16] We will show below analogous electrochemical behavior of

(12) Williams, M. E.; Masui, H.; Long, J. W.; Malik, J.; Murray, R. W. *J. Am. Chem. Soc.* **1997**, *119*, 1997−2005.
(13) Dickinson, E. V.; Williams, M. E.; Hendrickson, S. M.; Masui, H.; Murray, R. W. *J. Am. Chem. Soc.* **1999**, *121*, 613−616.
(14) Farrer, B. T.; Thorp, H. H. *Inorg. Chem.* **2000**, *39*, 44−49.
(15) Majda, M. In *Molecular Design of Electrode Surfaces*; Murray, R. W., Ed.; John Wiley and Sons: New York, 1992; p 159. Dahms, H. *J. Phys. Chem.* **1968**, *72*, 362. Ruff, I.; Botar, L. *J. Chem. Phys.* **1985**, *83*, 1292.
(16) Buttry, D. A.; Anson, F. C. *J. Am. Chem. Soc.* **1983**, *105*, 685−689.

metal complex molten salts containing DNA and exhibiting evidence of its electron-transfer chemistry.

One-electron oxidation of the guanine base has been extensively scrutinized as a partial origin of oxidative DNA damage[17,18] and as a probe of long-range electron transfer along the DNA helix.[9,11,19–22] Transient formation of oxidized guanine bases appears to play a critical role in the ability of DNA to mediate remote electron transfer between two attached circuit elements where those circuit elements can either be molecular donors and acceptors or electrodes.[4,11,22–24] While direct transfer of electrons from guanine to solid electrodes in fluid, homogeneous solutions is slow, guanine oxidation can be studied indirectly by electrochemically generating small molecule redox catalysts.[10,25] Transition metal complexes with potentials ≥1.0 V, such as $Ru(bpy)_3^{2+}$ (bpy = 2,2′-bipyridine), mediate guanine electron transfer from intact DNA molecules according to the reaction scheme:[26–28]

$$Ru(bpy)_3^{2+} \rightarrow Ru(bpy)_3^{3+} + e^- \quad (2)$$

$$Ru(bpy)_3^{3+} + DNA \rightarrow Ru(bpy)_3^{2+} + DNA_{ox} \quad (3)$$

where DNA_{ox} is a DNA molecule with a guanine residue that is oxidized by one electron. Precise potentials are difficult to determine in the melts, so complex **2** was dissolved in ether and determined to have a potential of 1.04 V by use of an internal ferrocene standard. Thus, complex **2** should be capable of oxidizing guanine in DNA in reactions analogous to eqs 2 and 3.

A DNA melt was prepared by equilibrium dialysis of a solution of **1** and herring testes DNA at a stoichiometry of two nucleotides of DNA per one dicationic Co complex. After extensive dialysis to remove the perchlorate counterions from **1** and the sodium cations from DNA, the solution was placed on a rotary evaporator to yield a highly viscous melt, Co(MePEG-bpy)$_3$·DNA (**3**). Compound **3** was dried under vacuum, and elemental analysis showed a purity of ≥90% with virtually no detectable sodium ion present, indicating that all of the DNA counterions had been replaced by $Co(MePEG\text{-}bpy)_3^{2+}$. The remainder of the composition of **3** is made up of some perchlorate anions in place of DNA.

The cyclic voltammogram of **3** showed a characteristic oxidation wave for the Co(III/II) couple at $E_{1/2}$ = 0.40 V (Figure 3A) with currents considerably lower than those for the perchlorate melt **1**. Chronoamperometry experiments were performed, and the collected current was plotted as a function

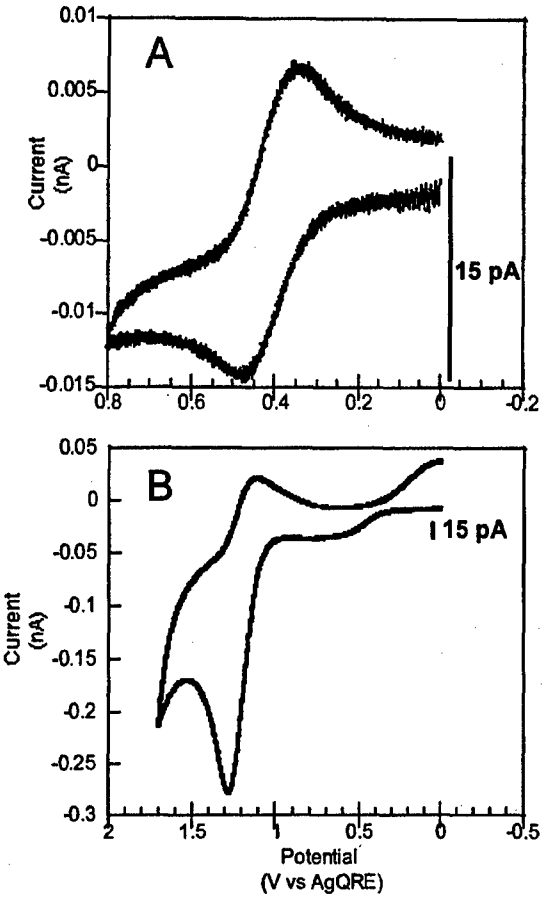

Figure 3. Cyclic voltammograms of (A) **3** and (B) a 1:1 mixture of **2** and **3**. Conditions were the same as in Figure 2.

of $t^{-1/2}$. These plots were linear, and the slope was used along with the Cottrell equation as described previously[12] to give a D_{PHYS} for the complex in the DNA melt of 6×10^{-12} cm^2/s. The peak current in cyclic voltammograms was also a linear function of the square root of the scan rate and gave a D_{PHYS} of 5×10^{-12} cm^2/s. A smaller D_{PHYS} in the DNA melt (compared to the perchlorate melt) is not surprising, since the polymeric counterion provokes a qualitatively higher viscosity and the relatively rigid helices should impede transport of the metal complex to the electrode.

The DNA in the melts is double-stranded. Compound **3** was dissolved in water, and the DNA fragments were separated on an agarose gel. The DNA fragments on the gel were 50–100 bp in length and stained well with ethidium bromide. Since heterogeneous polynucleotides such as herring testes DNA cannot reanneal, this experiment shows that the DNA in the melt was double-stranded. To confirm this point, another melt was prepared using a polyether-decorated ammonium cation, which formed a 1:1 melt with DNA nucleotides, MePEG-NEt_3·DNA (Figure 1, **4**). Compound **4** was characterized by elemental analysis and NMR and was found to give a CD spectrum in water that was identical with that for native herring testes DNA (Figure 4). Compound **3** could not be characterized by CD spectroscopy because the absorptions for the metal complex interfered with the DNA signals. This experiment further demonstrates that the DNA molecules in the melt remain double-stranded. Because **4** contains a countercation that does not exhibit optical absorption in the 250–300 nm range, the melt could be placed between glass plates and scanned in an optical spectrometer. The absorbance spectrum of the neat DNA melt is similar to that of DNA in solution. A pictorial representation

(17) Henle, E. S.; Linn, S. *J. Biol. Chem.* **1997**, *272*, 19095–19098.
(18) Beckman, K. B.; Ames, B. N. *J. Biol. Chem.* **1997**, *272*, 19633–19636.
(19) Saito, I.; Takayama, M.; Sugiyama, H.; Nakatani, K.; Tsuchida, A.; Yamamoto, M. *J. Am. Chem. Soc.* **1995**, *117*, 6406–6405.
(20) Meggers, E.; Michel-Beyerle, M. E.; Giese, B. *J. Am. Chem. Soc.* **1998**, *120*, 12950–12955.
(21) Lewis, F. D.; Wu, T.; Zhang, Y.; Letsinger, R. L.; Greenfield, S. R.; Wasielewski, M. R. *Science* **1997**, *277*, 673–676.
(22) Wan, C.; Fiebig, T.; Kelley, S. O.; Treadway, C. R.; Barton, J. K.; Zewail, A. H. *Proc. Natl. Acad. Sci. U.S.A.* **1999**, *96*, 6014–6019.
(23) Jortner, J.; Bixon, M.; Langenbacher, T.; Michel-Beyerle, M. E. *Proc. Natl. Acad. Sci. U.S.A.* **1998**, *95*, 12759–12765.
(24) Lewis, F. D.; Liu, X.; Liu, J.; Miller, S. E.; Hayes, R. T.; Wasielewski, M. R. *Nature* **2000**, *406*, 51–53.
(25) Johnston, D. H.; Glasgow, K. C.; Thorp, H. H. *J. Am. Chem. Soc.* **1995**, *117*, 8933–8938.
(26) Johnston, D. H.; Thorp, H. H. *J. Phys. Chem.* **1996**, *100*, 13837–13843.
(27) Sistare, M. F.; Holmberg, R. C.; Thorp, H. H. *J. Phys. Chem. B* **1999**, *103*, 10718–10728.
(28) Szalai, V. A.; Thorp, H. H. *J. Phys. Chem. B* **2000**, *104*, 6851–6859.

Oxidation Kinetics of Guanine in DNA Molecules Adsorbed onto Indium Tin Oxide Electrodes

Paul M. Armistead and H. Holden Thorp

Department of Chemistry and the Lineberger Comprehensive Cancer Center, University of North Carolina at Chapel Hill, Chapel Hill, North Carolina 27599-3290

ANALYTICAL® CHEMISTRY

Reprinted from
Volume 73, Number 3, Pages 558–564

Anal. Chem. 2001, *73*, 558–564

Oxidation Kinetics of Guanine in DNA Molecules Adsorbed onto Indium Tin Oxide Electrodes

Paul M. Armistead and H. Holden Thorp*

Department of Chemistry and the Lineberger Comprehensive Cancer Center, University of North Carolina at Chapel Hill, Chapel Hill, North Carolina 27599-3290

Oligonucleotides containing the guanine nucleobase were adsorbed onto ITO electrodes from mixtures of DMF and acetate buffer. Chronocoulometry and chronoamperometry were performed on the modified electrodes in both phosphate buffer and buffer containing low concentrations of the inorganic complex $Ru(bpy)_3^{2+}$ (bpy = 2,2′ bipyridine), which catalyzes guanine oxidation. The charge and current evolution with and without the catalyst were compared to the charge and current evolution for electrodes that were treated with identical oligonucleotides that were substituted at every guanine with the electrochemically inert nucleobase hypoxanthine. Chronocoulometry over 2.5 s shows that roughly 2 electrons per guanine were transferred to the electrode in both the presence and absence of $Ru(bpy)_3^{2+}$, although at a slower rate for the uncatalyzed process. Chronoamperograms measured over 250 ms can be fit to a double exponential decay, with the intensity of the fast component roughly 6–20 times greater than that of the slow component. First- and second-order rate constants for catalytic and direct guanine oxidation were determined from the fast component. The maximum catalytic enhancement for immobilized guanine was found to be $i_{cat}/i_d = 4$ at 25 μM $Ru(bpy)_3^{2+}$. The second-order rate constant for the catalyzed reaction was 1.3×10^7 M^{-1} s^{-1}, with an apparent dissociation constant of 8.8 μM. When compared to parallel studies in solution, a smaller value of the dissociation constant and a larger value of the second-order rate constant are observed, probably due to distortion of the immobilized DNA, an increase in the local negative charge due to the oxygen sites on the ITO surface, and redox cycling of the catalyst, which maintains the surface concentration of the active form.

Oxidative damage of cellular DNA is currently viewed as a leading cause in disease processes as diverse as aging and cancer.[1-3] Because guanine is the most easily oxidized nitrogenous base, the chemical mechanism of its oxidation has been studied in detail.[4,5] While the mechanism of guanine oxidation in solution has been well investigated, there have been very few mechanistic studies of guanine oxidation at the surface of an electrode. This information would be useful for the design of electrochemical nucleic acid biosensors based on the detection of guanine oxidation.[6-9] Specifically, it would be important to know how many electrons can be transferred to the electrode from each guanine base and the rate of that electron transfer. Previous solution electrochemistry studies have shown that uncatalyzed guanine electron transfer is slow at most electrode surfaces;[10] however, guanine oxidation has been observed when the guanine is adsorbed onto carbon paste electrodes.[9] In addition to base oxidation, many other electrochemical schemes for sensing DNA are being pursued.[11-16]

Our laboratory has developed a catalytic guanine oxidation system with the inorganic metal complex $Ru(bpy)_3^{2+}$ as the oxidation catalyst. Catalytic guanine oxidation proceeds through the following reactions[17]

$$Ru(bpy)_3^{2+} \rightarrow Ru(bpy)_3^{3+} + e^- \quad (1)$$

$$Ru(bpy)_3^{3+} + \text{guanine} \rightarrow Ru(bpy)_3^{2+} + \text{guanine}^{\bullet+} \quad (2)$$

This reaction has been studied by digital simulation of solution electrochemistry and by stopped-flow spectroscopy.[17,18] Recently, we have developed a simple method for adsorbing DNA onto ITO electrodes that, when combined with the electrocatalytic scheme

(1) Mecocci, P.; Fano, G.; Fulle, S.; MacGaverty, U.; Shinobu, L.; Polidori, M. C.; Cherubini, A.; Vecchiet, J.; Senin, U.; Flint Beal, M. *Free Radical Biol. Med.* **1999**, *26*, 303–308.
(2) Dreher, D.; Junod, A. F. *Eur. J. Cancer* **1996**, *32A*, 30–38.
(3) Loft, S.; Poulsen, H. E. *J. Mol. Med.* **1996**, *74*, 297–312.
(4) Burrows, C. J.; Muller, J. G. *Chem. Rev.* **1998**, *98*, 1109–1151.
(5) Steenken, S. *Chem. Rev.* **1989**, *89*, 503–520.
(6) Napier, M. E.; Thorp, H. H. *Langmuir* **1997**, *13*, 6342–6344.
(7) Napier, M. E.; Loomis, C. R.; Sistare, M. F.; Kim, J.; Eckhardt, A. E.; Thorp, H. H. *Bioconjugate Chem.* **1997**, *8*, 906–913.
(8) Ontko, A. C.; Armistead, P. M.; Kircus, S. R.; Thorp, H. H. *Inorg. Chem.* **1999**, *38*, 1842–1846.
(9) Wang, J.; Bollo, S.; Paz, J. L. L.; Sahlin, E.; Mukherjee, B. *Anal. Chem.* **1999**, *71*, 1910–1913.
(10) Armistead, P. M.; Thorp, H. H. *Anal. Chem.* **2000**, *72*, 3764–3770.
(11) Millan, K. M.; Saraullo, A.; Mikkelsen, S. R. *Anal. Chem.* **1994**, *66*, 2943–2948.
(12) Wang, J.; Cai, X.; Rivas, G.; Shiraishi, H.; Farias, P. A. M.; Dontha, N. *Anal. Chem.* **1996**, *68*, 2629–2634.
(13) Kelley, S. O.; Boon, E. M.; Barton, J. K.; Jackson, N. M.; Hill, M. G. *Nucleic Acids Res.* **1999**, *27*, 4830–4837.
(14) Creager, S.; Yu, C. J.; Bamdad, C.; O'Connor, S.; MacLean, T.; Lam, E.; Chong, Y.; Olsen, G. T.; Luo, J.; Gozin, M.; Kayyem, J. F. *J. Am. Chem. Soc.* **1999**, *121*, 1059–1064.
(15) Singhal, P.; Kuhr, W. G. *Anal. Chem.* **1997**, *69*, 4828–4832.
(16) Xu, X.-H.; Bard, A. J. *J. Am. Chem. Soc.* **1995**, *117*, 2627–2631.
(17) (a) Johnston, D. H.; Glasgow, K. C.; Thorp, H. H. *J. Am. Chem. Soc.* **1995**, *117*, 8933–8938. (b) Sistare, M.; Holmberg, R.; Thorp, H. H. *J. Phys. Chem.* **1999**, *103*, 10718–10728.
(18) Yang, I. V.; Thorp, H. H. *Inorg. Chem.* **2000**, *39*, 4969–4976.

10.1021/ac001286t CCC: $20.00
Published on Web 01/03/2001

above, enabled us to detect DNA adsorbed onto ITO electrodes at surface densities as low as 44 amol/mm^2.[10] The adsorption procedure involves treatment of the electrodes with DNA dissolved in DMF/acetate, which is a denaturing medium and, therefore, leads to attachment of single-stranded DNA to the electrode. Because the detection system relies on oxidation of guanine, the modified electrodes can be interrogated on only one scan; in fact, we have shown previously that repeated scanning leads to a decrease in the catalytic current on successive scans.[10]

To probe the surface reaction in the electrocatalytic system, experiments were performed in which both direct oxidation of adsorbed guanine and $Ru(bpy)_3^{2+}$-catalyzed oxidation of adsorbed guanine could be monitored in the same experiment. In our previous studies, catalytic current enhancements were detected through cyclic voltammetry at fast scan rates (10 V s^{-1}).[10] In those experiments, guanine oxidation in the absence of catalyst was barely detectable, so the extent of catalysis could not be quantitatively evaluated. Here we report on chronocoulometry and chronoamperometry experiments on ITO electrodes that were treated with large amounts DNA of a specific sequence. These experiments were extended for much longer times (2.5 s), which allowed the slow direct guanine oxidation to be measured accurately. From these data, the number of electrons transferred to the electrode per guanine was quantified, and the rate constants for both the catalyzed and uncatalyzed reactions could be estimated. To obtain the kinetic information from the chronoamperograms, a second term was added to the standard Cottrell equation. This term takes into account the catalytic reactions occurring near the electrode surface and accurately predicts the initial currents from such a reaction. This modification of the Cottrell equation potentially constitutes a general description of other electrochemical systems in which a scarce substrate is adsorbed onto the electrode surface and an electrocatalyst is present in the bulk solution.

EXPERIMENTAL SECTION

Materials and Reagents. Oligonucleotides were synthesized at the Lineberger Comprehensive Cancer Center Nucleic Acid Core Facility at the University of North Carolina. All water used was in-house distilled water that was further purified on a Milli-Q water purification system. *N,N*-Dimethyl formamide, sodium phosphate, sodium acetate, and sodium chloride were from Mallinckrodt (Paris, KY). $[Ru(bpy)_3]Cl_2$ was purchased as the chloride salt from Aldrich and was recrystallized from acetonitrile. ITO electrodes were purchased from Delta Technologies (Stillwater, MN). All electrochemical measurements were performed in a one-compartment cell on a BAS (Lafayette, IN) 100B potentiostat that was connected to a 200 MHz Pentium computer. A Ag/AgCl reference electrode from Cypress Systems was used (Lawrence, KS), and a platinum wire was used as an auxiliary electrode. All radiolabeling data were collected on a phosphorimager screen that was subsequently scanned on a Molecular Dynamics Storm 860 (San Jose, CA). Phosphorimager data analysis was performed using ImagQuaNT software.

Immobilization of DNA onto ITO Electrodes. Oligonucleotides containing the sequences 5′-AAA TAT $(AGT)_{20}$ ATA AAA (20G72), 5′-AAA TAT $(AIT)_{20}$ ATA AAA (20I72), and 5′-TTT TAT $(ACT)_{20}$ ATA TTT (20C72) were purified in 100 mM sodium acetate, pH = 6.8, on 3000 molecular-weight-cutoff filters. The oligonucleotides were annealed by adding one volume of 20 μM oligonucleotide (either 20G72 or 20I72) to an equal volume of 20 μM 20C72. The solutions were heated to 95 °C for 5 min and allowed to slowly cool to room temperature. All experiments were performed on annealed samples, hereafter denoted as either 20G72 or 20I72.

ITO electrodes were cleaned by sonicating in Alconox (4 g/L) for 15 min; 2-propanol for 15 min; and Milli-Q water twice, for 15 min each.[19] The annealed DNA was added to 9 volumes of DMF, and 50 μL of the mixture were pipetted onto each cleaned ITO electrode. The electrodes were placed in a constant humidity chamber for 4 h. The electrodes were then immersed in different solutions that were agitated on a rotary mixer. The electrodes were first placed in water for 3 min; followed by 500 mM sodium chloride and 50 mM sodium phosphate, pH = 7.0, for 3 min; with three final water washes, each for 3 min. The electrodes were then allowed to air-dry. As we discussed in detail previously,[10] the adsorbed DNA is single-stranded, so treating the electrode with annealed DNA simply leads to the adsorption of both single strands in the duplex.

Quantification of DNA Adsorbed onto ITO Electrodes. Double-stranded 20G72 was 5′-labeled using T4 polynucleotide kinase (Life Technologies) and α-^{32}P ATP (Amersham). Briefly, 1 μL of 1 μM annealed oligonucleotide was added to 1 μL of α-^{32}P ATP, 1 μL of 5× forward reaction buffer, 1 μL of water, and 1 μL of kinase. The reaction was allowed to proceed at 37 °C for 15 min. The reaction was diluted to 70 μL by adding 65 μL of water. Unincorporated ATP was removed by passing the entire mix through a NucTrap purification column (Stratagene). The purified oligonucleotides were in a final volume of roughly 100 μL. From this volume, 1 μL was added to 100 μL of 10 μM annealed 20G72 in 100 mM sodium acetate, pH = 6.8. The doped sample was added to 9 volumes of DMF. The mixture was added to cleaned ITO electrodes and placed in a constant humidity chamber for 4 h. The electrodes were washed identically to nonradiolabeled ITO electrodes and allowed to air-dry. Quantification standards were produced by pipetting a 1-μL drop of the doped annealed solution (before addition of DMF) onto a piece of filter paper. The filter paper was dried and wrapped with the radiolabeled ITO electrodes in plastic wrap. The electrodes and standards were placed on a phosphorimager screen overnight. The screen was scanned on a Storm 860 phosphorimager, and analysis of the electrodes was performed using ImageQuaNT software.

Chronocoulometry of DNA Adsorbed onto ITO Electrodes. Solutions of annealed 10 μM 20G72 and 20I72 were prepared in 100 mM sodium acetate, pH = 6.8. The oligonucleotides were adsorbed, washed, and dried on cleaned ITO electrodes as described above. Chronocoulometry was performed with a double potential step from 900 to 1300 to 900 mV vs Ag/AgCl reference. A platinum wire was used as the auxiliary electrode. The step time was set at 2.5 s. Chronocoulometry was performed on ITO electrodes treated with 20G72 or 20I72 in 50 mM sodium phosphate buffer, pH = 7.0, in the presence or absence of 25 μM $Ru(bpy)_3^{2+}$. The $Q-t$ curve taken on electrodes treated with 20I72 was subtracted from the $Q-t$ curves taken on 20G72 electrodes.

(19) Willit, J. L.; Bowden, E. F. *J. Phys. Chem.* **1990**, *94*, 8241–8246.

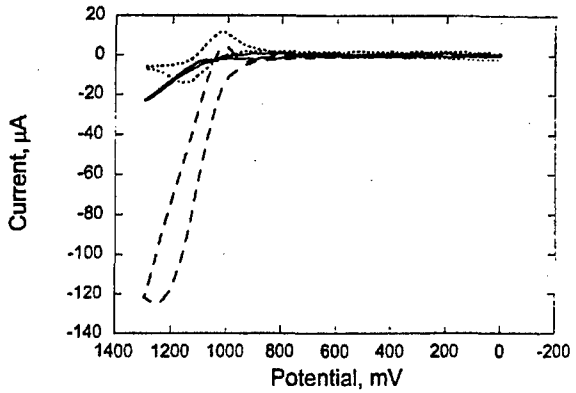

Figure 1. Cyclic voltammograms of calf thymus DNA-modified ITO electrodes at 10 V/s in the presence (dashed) and absence (solid) of 100 μM $Ru(bpy)_3^{2+}$. A cyclic voltammogram of 100 μM Ru(bpy) at an unmodified electrode is also shown (dotted).

Chronoamperometry of DNA Adsorbed onto ITO Electrodes. Chronoamperometry data were obtained by taking the derivative of chronocoulometry data. Solutions of annealed 10 μM 20G72 and 20I72 were prepared in 100 mM sodium acetate, pH = 6.8. The oligonucleotides were adsorbed, washed, and dried on cleaned ITO electrodes, as described above. Chronocoulometry was performed with a double potential step from 900 to 1300 to 900 mV vs Ag/AgCl reference. A platinum wire was used as the auxiliary electrode. The step time was set at 250 ms, and $Q-t$ curves were collected at varying concentrations of $Ru(bpy)_3^{2+}$ (0, 5, 10, 25, and 100 μM). For each $Ru(bpy)_3^{2+}$ concentration, 16 electrodes were modified with 20G72 and interrogated by chronocoulometry; the 16 $Q-t$ curves were averaged to generate a single $Q-t$ curve for that $Ru(bpy)_3^{2+}$ concentration. Similarly, 16 electrodes were modified with 20I72 for each $Ru(bpy)_3^{2+}$ concentration, interrogated by chronocoulometry, and averaged. The averaged $Q-t$ curve for each concentration for 20I72 was subtracted from the corresponding averaged $Q-t$ curve for 20G72. The derivative with respect to time was taken of the subtracted $Q-t$ curves, which yielded a chronoamperogram. These chronoamperomograms were fitted to double-exponentials shown in Figure 3.

RESULTS

Cyclic Voltammetry of Adsorbed DNA on ITO Electrodes. Previous electrochemical experiments on single-stranded DNA adsorbed onto ITO electrodes used cyclic voltammetry to measure catalytic oxidation of the adsorbed guanine bases. In these studies, electrocatalysis was measured by monitoring the increase in the $Ru(bpy)_3^{2+}$ oxidation wave in the cyclic voltammograms.[10] Although these experiments gave quantitative data on the nature of the electrocatalytic reaction being observed, the cyclic voltammograms did not yield any useful information on direct guanine oxidation in the absence of $Ru(bpy)_3^{2+}$.

Figure 1 shows representative cyclic voltammograms at 10 V/s of 100 μM $Ru(bpy)_3^{2+}$ at an unmodified ITO electrode, a DNA-modified electrode in the absence of $Ru(bpy)_3^{2+}$, and a DNA-modified electrode in a solution containing 100 μM $Ru(bpy)_3^{2+}$. The background charging current obtained from a bare ITO electrode in buffer was subtracted from all of the voltammograms. Direct DNA oxidation is only observable as a poorly defined

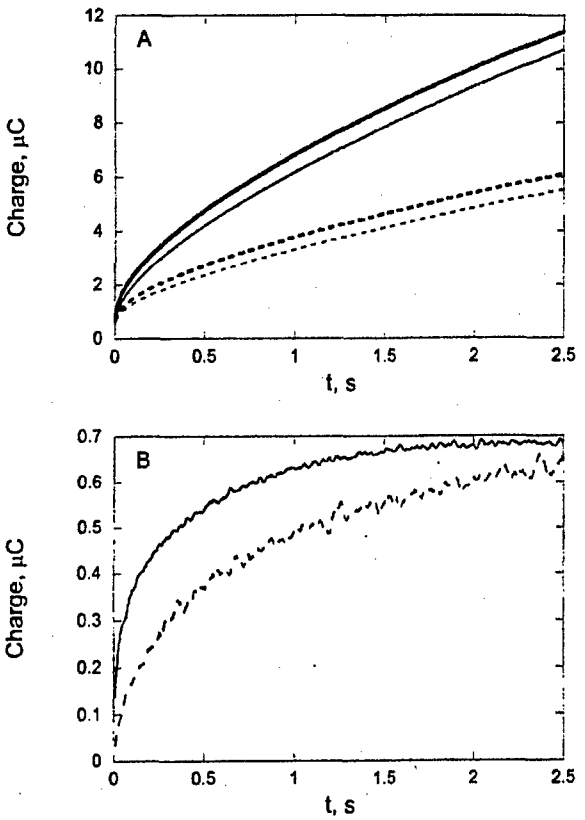

Figure 2. (A) $Q-t$ curves of electrodes modified with 20I72 or 20G72 (bold) with 25 μM $Ru(bpy)_3^{2+}$ (solid) or in buffer alone (dashed). (B) $Q-t$ curves of ITO electrodes treated with 20G72, minus the signals from the corresponding electrodes modified with 20I72 in 25 μM $Ru(bpy)_3^{2+}$ (solid) or in buffer (dashed).

oxidative wave with no peak, but there is a large catalytic enhancement in the oxidative wave for $Ru(bpy)_3^{2+}$. Detailed analysis of this phenomenon has been reported elsewhere.[17] As we have discussed, the cyclic voltammetry experiments provide the largest differences in absolute currents for the catalyzed and uncatalyzed reactions but do not allow for direct analysis of the extent of catalysis. Chronocoulometry and chronoamperometry were, therefore, used here under conditions of long times and high DNA loading to allow measurement of the slow, direct guanine oxidation and to quantify the catalytic rate enhancement due to $Ru(bpy)_3^{3+/2+}$. As we have discussed,[17] the rate of guanine oxidation can be a strong function of the secondary structure of the DNA; however, this effect is observed only at high salt concentration. At the low salt concentrations that was used here, the guanine oxidation rate is independent of the secondary structure;[18] thus, all of the guanines in the adsorbed DNA molecules contribute equally to the catalytic current observed in Figure 1.

Prior to electrochemical analysis of the reactions, we needed to know the precise quantity of DNA adsorbed to the electrodes, which was determined by analysis of electrodes that were modified with radiolabeled oligonucleotides using a phosphorimager. It was found that 180 fmol of DNA were adsorbed onto the 12.6 mm^2 electrodes. This value was further corrected to represent the number of moles of guanine present. Because each duplex used to treat the electrode contained 20 guanines, the total amount of guanine sampled during an electrochemical measurement was 3.7

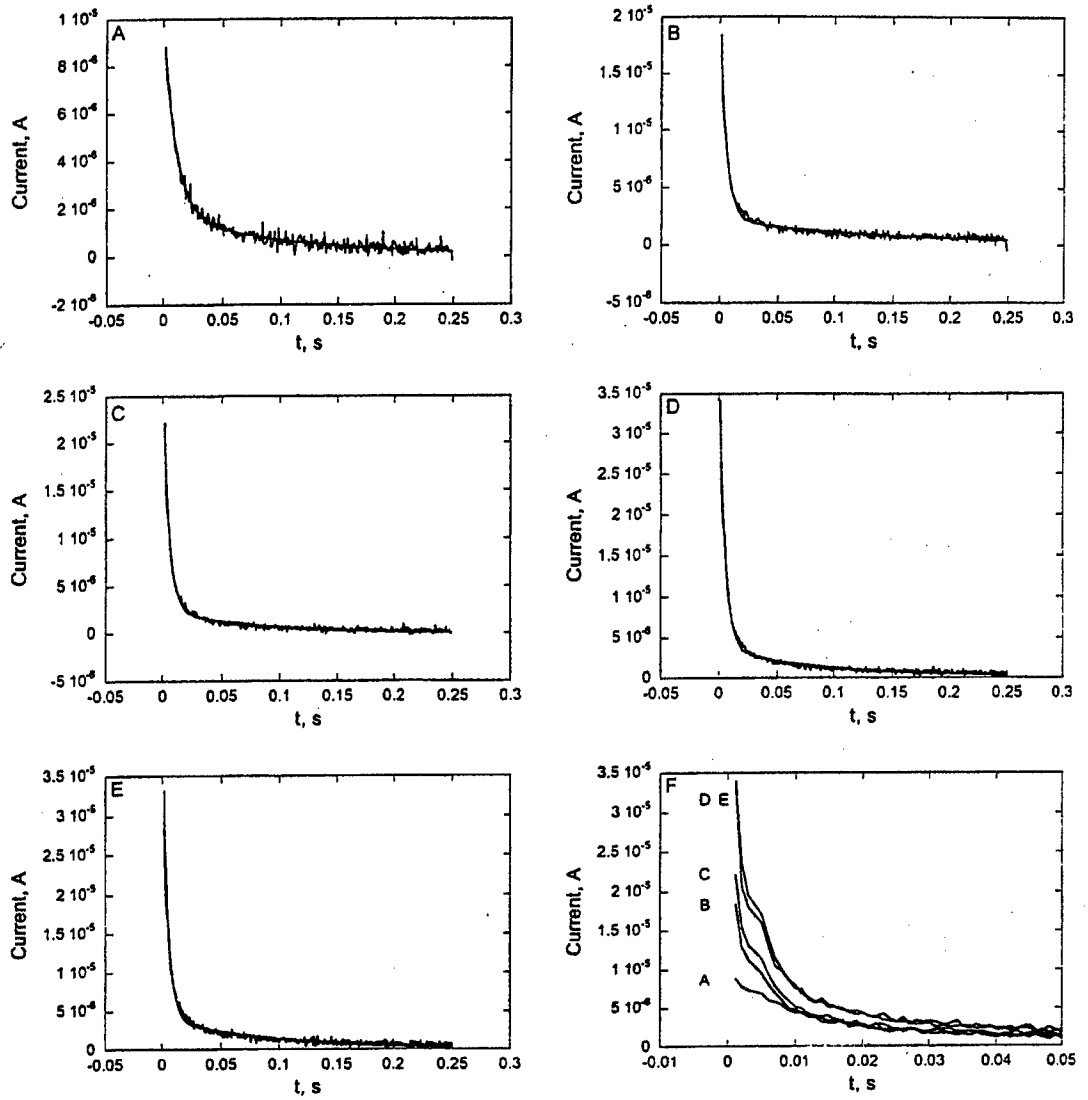

Figure 3. Chronoamperomograms of 20G72 taken at 0, 5, 10, 25, and 100 μM $Ru(bpy)_3^{2+}$, minus data for 20I72 at the same $Ru(bpy)_3^{2+}$ concentrations (panels A–E, respectively). Each chronoamperomogram was generated from 16 20G72 and 16 20I72 electrodes; see Experimental Section. Chronoamperomograms were generated by taking the derivative of the corresponding Q–t curve. Each trace was fit to a double exponential curve. Panel F shows all five traces overlaid; note the difference in time axis for panel F.

± 1.1 pmol (representing an average over six measurements). Note that the oligonucleotides used in this study were annealed to their complements prior to adsorption onto the electrodes; however, later experiments showed that the adsorbed molecules were single-stranded.[10] Thus, the electrode modifications carried out here simply produced equal amounts of each single strand immobilized to the electrode.

Chronocoulometry of Adsorbed DNA. Although ITO electrodes exhibit very small water oxidation currents, simple background subtraction was still needed to detect low levels of catalysis. The background subtraction was performed using electrodes that had 20I72 adsorbed onto the ITO in the same manner as 20G72. The hypoxanthine base is electrochemically inert at guanine oxidation potentials,[7] so subtraction of signals due to 20I72 accurately reflects the effects of electrode poisoning without artificially reducing the amount of charge transferred from guanine. When electrodes modified with 20G72 and 20I72 were interrogated by cyclic voltammetry, large current enhancements were observed with 20G72 (as in Figure 1), but the signals for electrodes modified with 20I72 were identical to those for $Ru(bpy)_3^{2+}$ alone. As a further control, electrodes were modified with analogues of 20I72 where all of the hypoxanthines were changed to thymine. These electrodes gave currents identical to those from electrodes modified with 20I72. Thus, using 20I72-modified electrodes as a background also allowed any minor charge contributions from the other bases to be effectively subtracted.

Figure 2A shows unsubtracted chronocoulometry traces over 2.5 s for both 20G72- and 20I72-modified electrodes with and without $Ru(bpy)_3^{2+}$. If the 20I72 trace from Figure 2A is subtracted from the 20G72 trace made at the same concentration of $Ru(bpy)_3^{2+}$, a charge vs time plot can be drawn that reflects the charge transfer due solely to guanine oxidation. These plots are shown in Figure 2B for both the uncatalyzed (0 μM $Ru(bpy)_3^{2+}$) and catalyzed (25 μM $Ru(bpy)_3^{2+}$) reactions. At sufficiently long times, the same amount of charge is transferred from guanine to the electrode with and without $Ru(bpy)_3^{2+}$. The number of electrons transferred per guanine, n, can be determined using the Faraday relation

$$Q = nFm \quad (3)$$

where Q is the charge, F is the Faraday constant (96,485 C mol^{-1}), and m is the number of moles of guanine. By combining data from the radiolabeled experiments with chronocoulometry, it was found that 1.9 ± 0.6 electrons per guanine were transferred to the electrode. A similar value of 2.2 ± 0.4 electrons per guanine was determined from integration of cyclic voltammograms in our previous study.[10] A two-electron oxidation is readily accounted for by a number of proposed oxidation mechanisms.[20-25]

Chronoamperometry of Adsorbed DNA on ITO. To gain a more quantitative understanding of the extent to which $Ru(bpy)_3^{2+}$ catalyzes guanine electron transfer, analysis of guanine oxidation currents was performed at various $Ru(bpy)_3^{2+}$ concentrations. Chronocoulometry was performed with 250-ms step-times on electrodes that were treated with either 20G72 or 20I72. These measurements were performed with $Ru(bpy)_3^{2+}$ concentrations of 0, 5, 10, 25, and 100 μM. The $Q-t$ curves of the 20I72-treated electrodes were subtracted from those for the 20G72-treated electrodes, and the derivatives with respect to time of the subtracted $Q-t$ curves were taken.

The current vs time traces obtained from the subtraction procedure are shown for varying $Ru(bpy)_3^{2+}$ concentrations in Figure 3. The guanine oxidation current drops off rapidly (within 30 ms) for all of the electrodes; however, the most rapid drop and the greatest initial oxidation current occurs at higher $Ru(bpy)_3^{2+}$ concentrations. The initial currents at each $Ru(bpy)_3^{2+}$ concentration are shown in Figure 4A and show that catalyzed guanine electron transfer is roughly 4 times faster than the uncatalyzed reaction under these conditions. The initial current from guanine oxidation at 25 μM $Ru(bpy)_3^{2+}$ is 34 μA, but at 0 μM, the initial current is 7.7 μA. The initial currents from Figure 4A begin to plateau at higher $Ru(bpy)_3^{2+}$ concentrations, which suggests the saturation of a binding preequilibrium. The initial currents from Figure 4A were normalized so that current from direct guanine oxidation [at 0 μM $Ru(bpy)_3^{2+}$] was zero. These data points were then fit to a standard binding isotherm

$$i = \frac{i_{max}[Ru(bpy)_3^{2+}]}{[Ru(bpy)_3^{2+}] + K_D} \quad (4)$$

where i_{max} is the maximum current obtained and K_D is the apparent dissociation constant for $Ru(bpy)_3^{3+}$ and the immobilized DNA. As described below, we can assume that the concentration of $Ru(bpy)_3^{3+}$ at the surface is the same as the concentration of $Ru(bpy)_3^{2+}$ in the bulk, so the concentration of $Ru(bpy)_3^{2+}$ is used in eq 4. From this curve, a value of K_D = 8.8 ± 3.7 μM was determined.

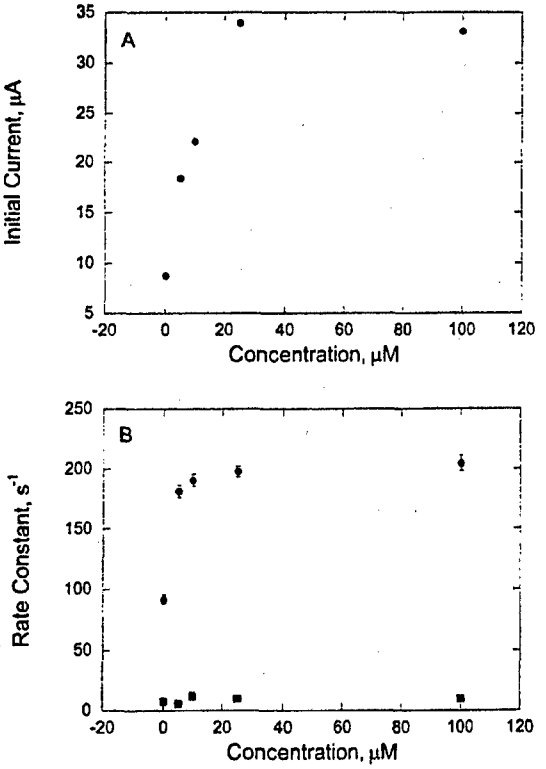

Figure 4. (A) Plot of the initial currents at each concentration of $Ru(bpy)_3^{2+}$, determined from the current vs time traces shown in Figure 3. (B) Plot showing both the fast (●) and slow (■) exponential terms from each double exponential fit of the traces in Figure 3. The error bars were determined from the fit of each trace (16 trials per concentration).

The current vs time traces in Figure 3 did not follow a simple $t^{1/2}$ dependence that would be expected for diffusion controlled-process.[26] Instead, the curves could be fit to double-exponential functions [i.e., $A_1 \exp(-k_1 t) + A_2 \exp(-k_2 t)$]. The rate constants for both the fast and slow components are shown in Figure 4B. In all of the fits, the fast component was 10–20 times more intense than the slow component (i.e., $A_1/A_2 > 10$). In addition, the slow component does not vary with the $Ru(bpy)_3^{2+}$ concentration, but the fast component increases with increasing $Ru(bpy)_3^{2+}$ concentrations and reaches a maximum value of 205 s^{-1} at 100 μM $Ru(bpy)_3^{2+}$. Figure 5 shows the total decay curve, with both the fast and slow components illustrated, for 25 μM $Ru(bpy)_3^{2+}$. The fast component dominates the current trace for the first 15 ms of the reaction. Because of its low intensity and lack of variation with $Ru(bpy)_3^{2+}$ concentration, the slow component was not analyzed further.

DISCUSSION

Catalytic Current Analysis. Kinetic analysis of electrocatalysis has typically been limited to the study of systems in which the substrate is in solution and the catalyst is either in solution or immobilized on the electrode surface. These types of systems have shown great utility in the detection of both small molecule and biomolecule analytes.[27,28] In an electrochemical detection system

(20) Hickerson, R. P.; Prat, F.; Muller, J. G.; Foote, C. S.; Burrows, C. J. *J. Am. Chem. Soc.* **1999**, *121*, 9423–9428.
(21) Arkin, M. R.; Stemp, E. D. A.; Pulver, S. C.; Barton, J. K. *Chem. Biol.* **1997**, *4*, 389–400.
(22) Cullis, P. M.; Malone, M. E.; Mreson-Davis, L. A. *J. Am. Chem. Soc.* **1996**, *118*, 2775–2781.
(23) Muller, J. G.; Duarte, V.; Hickerson, R. P.; Burrows, C. J. *Nucleic Acids Res.* **1998**, *26*, 2247–2249.
(24) Duarte, V.; Muller, J. G.; Burrows, C. J. *Nucleic Acids Res.* **1999**, *27*, 496–502.
(25) Kino, K.; Saito, I.; Sugiyama, H. *J. Am. Chem. Soc.* **1998**, *120*, 7373–7374.
(26) Bard, A. J.; Faulkner, L. R. *Electrochemical Methods*, 2nd ed.; John Wiley and Sons: New York, 1980.
(27) Pikulski, M.; Gorski, W. *Anal. Chem.* **2000**, *72*, 2696–2702.
(28) Wilkins, E.; Atanasov, P. *Med. Eng. Phys.* **1996**, *18*, 273–288.

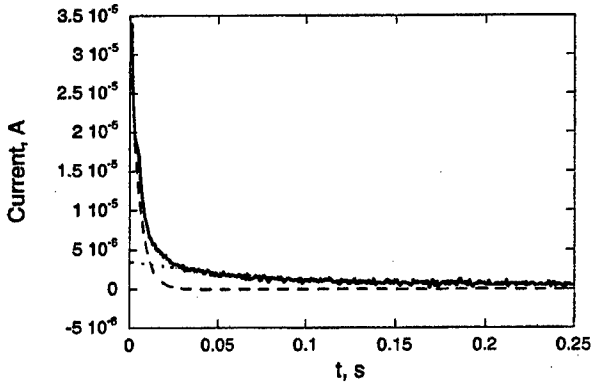

Figure 5. Current vs time plot taken at 25 μM $Ru(bpy)_3^{2+}$ (solid) showing the slow (dotted) and fast (dashed) components from the double-exponential fit.

in which the analyte is the scarce component to be detected (e.g., a large biomolecule), attachment of the analyte to the electrode surface increases its surface concentration and hence the sensitivity.[29] The catalytic DNA oxidation reaction described here involves the adsorption of a scarce analyte and the use of a solution-bound electrocatalyst, $Ru(bpy)_3^{2+}$. Our goal here was to observe both the catalyzed and uncatalyzed oxidations using the same technique, which was possible only with high DNA loadings and on long time scales with chronocoulometry. Under these conditions, the rate enhancements provided by the redox couple were modest; however, the results in Figure 1 show that much larger catalytic effects are apparent with cyclic voltammetry. Detailed analysis of the results in Figure 1 is not possible, due to the poor resolution of the uncatalyzed reaction.

Oxidation of $Ru(bpy)_3^{2+}$ in solution at a bare electrode (or one with adsorbed inosine) yields a normal chronamperogram. When the potential is such that the concentration of reduced ruthenium at the electrode is zero (i.e., $[Ru(bpy)_3^{2+}]_{x=0} = 0$), the diffusion-controlled current response for such a system is described by the Cottrell equation[26]

$$i_{\text{Cottrell}} = FA\left(\frac{\sqrt{D}C_{\text{red,bulk}}}{\sqrt{\pi t}}\right) \tag{5}$$

where i is the current, n is the number of electrons transferred in the process, A is the electrode area, D is the diffusion coefficient of the electroactive species, and $C_{\text{red,bulk}}$ is the concentration of the electroactive species in solution. Under these conditions, we can also write that

$$C_{\text{ox},x=0} = C_{\text{red,bulk}}\sqrt{\frac{D_{\text{ox}}}{D_{\text{red}}}} \simeq C_{\text{red,bulk}} \quad (\text{if } D_{\text{ox}} = D_{\text{red}}) \tag{6}$$

where $C_{\text{ox},x=0} = [Ru(bpy)_3^{3+}]_{x=0}$ and D_{ox} and D_{red} are the diffusion coefficients of $Ru(bpy)_3^{2+}$ and $Ru(bpy)_3^{3+}$, respectively. Thus, $[Ru(bpy)_3^{3+}]_{x=0}$ is maintained at a constant concentration at the electrode surface. The adsorbed species, which is electrochemically inert, can react with the $Ru(bpy)_3^{3+}$ according to

$$\text{DNA}_s + [Ru(bpy)_3^{3+}]_{x=0} \xrightarrow{k} \text{DNA}_{s,\text{ox}} + [Ru(bpy)_3^{2+}]_{x=0} \tag{7}$$

where k is the second-order rate constant ($M^{-1}\,s^{-1}$), DNA_s is the adsorbed DNA, and $\text{DNA}_{s,\text{ox}}$ is the adsorbed DNA in which the guanine has been oxidized by one electron. The electrochemical reaction proceeds by diffusion control (see eq 1) and retains the interfacial concentrations of the solution species, that is, $[Ru(bpy)_3^{3+}]_{x=0} = C_{\text{red,bulk}}$ and $[Ru(bpy)_3^{2+}]_{x=0} = 0$ (eqs 6 and 7). Thus, there will be an additional current, i_{surface}, affected by reaction 7, for which

$$i_{\text{surface}} = -FA\frac{d\Gamma_{\text{red}}}{dt} = FAk\Gamma_{\text{red}}[Ru(bpy)_3^{3+}]_{x=0} = FAk\Gamma_{\text{red}}C_{\text{red,bulk}} = FAk'\Gamma_{\text{red}} \tag{8}$$

where k' ($= kC_{\text{red,bulk}}$) is the effective pseudo-first-order rate constant, and Γ_{red} (mol/cm^2) is the surface concentration of the oxidizable units. Equation 8 gives

$$i_{\text{surface}} = FAk'\Gamma_T e^{-k't} \tag{9}$$

where Γ_T is the amount of guanine initially present on the electrode surface, that is, the total amount of guanine on the electrode surface. Then, the total current for the redox process is[30]

$$i_{\text{total}} = i_{\text{Cottrell}} + i_{\text{surface}} = \text{FA}\left[\frac{\sqrt{D}C_{\text{red, bulk}}}{\sqrt{\pi t}} + k'\Gamma_T e^{-k't}\right] \tag{10}$$

where $\Gamma_T = \Gamma_{\text{red}} + \Gamma_{\text{ox}}$. According to eq 10, the kinetic current is maximized compared to the Cottrell current when $t = 1/2\,k'$. To analyze the kinetic current directly, we use eq 9, where Γ_T is approximately equal to the surface concentration of guanine in mol/cm^2.

Comparison of Rate Constants. Equation 9 was used to determine the rate constants for the fast component in Figure 4B. At high ruthenium concentrations (100 μM), the measured rate constant describes the electron transfer via a guanine·$Ru(bpy)_3^{3+}$ complex. At lower ruthenium concentrations, the observed rate constant contains contributions from both direct guanine oxidation and oxidation via the guanine·$Ru(bpy)_3^{3+}$ complex. As the ruthenium concentration decreases, the contribution from direct guanine oxidation increases, resulting in an overall decrease in the observed first-order rate constant. The observed first-order rate constant for adsorbed guanine at 0 μM $Ru(bpy)_3^{2+}$ (92 s^{-1}) describes the uncatalyzed first-order electron-transfer reaction of guanine to the electrode. Thus, the maximum rate constant of 205 s^{-1} is likely a sum of the uncatalyzed and catalyzed rates, giving a rate for the catalyzed electron transfer of 110 s^{-1}. With a $k' = 205\ s^{-1}$, the optimal time for measuring the kinetic current from eq 6 is 2.5 ms, which is near the time resolution of the present experiment, but provides support for analyzing the reaction at the earliest possible times, which we have done here.

(29) Palecek, E. *Electroanalysis* **1996**, *8*, 7–14.

(30) Feldberg, S. W., personal communication.

The understanding developed through analysis of the first-order rate constant and the binding isotherm provides a strong basis for the large current enhancements that are seen in cyclic voltammetry (Figure 1 and ref 10). The first-order rate constant of 110 s^{-1} is somewhat larger than the corresponding first-order rate constants determined for electron transfer within the Ru(bpy)$_3^{3+}$·DNA complex in solution.[17b] In the solution cases, the first-order rate constants were about 30 s^{-1} for similar sequences and conditions. Thus, the DNA–Ru^{3+} electron transfer at the surface is similar to that in solution. The somewhat faster electron-transfer rate observed at the surface is likely due to a distortion of the immobilized DNA that increases the solvent accessibility of the oxidized guanine.

The surface immobilization has a much larger effect on the affinity of the catalyst for DNA than on the electron-transfer rate. In solution, Ru(bpy)$_3^{3+}$ binds to DNA with a dissociation constant of about 1 mM,[31] and the apparent affinity at the electrode surface is 8.8 μM, as determined from eq 4. This 100-fold increase in affinity is likely due to partial negative charges on the ITO surface,[32] which increase the electrostatic attraction of the cationic catalyst to the DNA-modified ITO surface. In addition, there is likely an increase in the *apparent* affinity arising from the redox cycling of the catalyst, which imposes a large driving force for accumulation of Ru(bpy)$_3^{3+}$ at the electrode surface. This driving force arises because the electrode is poised at potentials capable of oxidizing Ru(bpy)$_3^{2+}$, while reduction by the adsorbed DNA is simultaneously suppressing the surface concentration of Ru(bpy)$_3^{3+}$.

CONCLUSIONS

Oxidation of an adsorbed analyte by a solution-based electrocatalyst provides a potential solution to the direct detection of a native biomolecule.[33] In such a system, adsorption of the analyte increases its effective concentration, but addition of the solution-based catalyst increases the rate of electron transfer, which is often slow for biomolecules.[27] We have described here the kinetic analysis for such a system in which DNA is adsorbed onto ITO electrodes, and Ru(bpy)$_3^{3+/2+}$ is used to increase the rate of electron transfer from guanines in DNA to the electrode surface. The particular system discussed is one in which the DNA molecules are single-stranded and oriented parallel to the ITO surface. In this configuration, the electrogenerated Ru(bpy)$_3^{3+}$ is reduced back to Ru(bpy)$_3^{2+}$ at the electrode surface, prohibiting the diffusion of Ru(bpy)$_3^{3+}$ away from the electrode surface at short times. The kinetics of this scenario are described by a modification to the Cottrell equation that accounts for both the diffusive current, giving a $t^{1/2}$ dependence, and a catalytic current, which gives an e^{-kt} dependence. The contribution to the catalytic current is, therefore, maximized at early times.

Although the present system does not allow for flux of Ru(bpy)$_3^{3+}$ away from the electrode surface, such a system could be designed using an intervening layer that would position the DNA at some larger distance from the electrode, such that reduction of Ru(bpy)$_3^{3+}$ immediately at the electrode surface would not occur. In such a system, additional terms would need to be added to eq 10 to describe the catalytic reaction in solution.[34] Ordinarily, detection of catalytic current for solution reactions is limited to electrodes large enough to exhibit planar diffusion;[35–37] however, systems described by eq 6 would not be subject to this limitation. Thus, systems such as that described here might allow for further miniaturization of the detection electrode and, hence, to greater sensitivity.

ACKNOWLEDGMENT

We thank Drs. R. M. Wightman, S. W. Feldberg, and C. A. Golden for helpful discussions. This research was supported by the Department of Defense and Xanthon, Inc.

Received for review October 31, 2000. Accepted November 13, 2000.

AC001286T

(31) Johnston, D. H.; Thorp, H. H. *J. Phys. Chem.* **1996**, *100*, 13837–13843.
(32) *Oxides and Oxide Films*; Ahmed, S. M., Ed.; Marcel Dekker: New York, 1972; Vol. 1, pp 320–402.
(33) Thorp, H. H. *Trends Biotechnol.* **1998**, *16*, 117–121.
(34) Nicholson, R. S.; Shain, I. *Anal. Chem.* **1964**, *36*, 706–735.
(35) Heinze, J. *Ber. Bunsen-Ges. Phys. Chem.* **1981**, *85*, 1096–1103.
(36) Dayton, M. A.; Ewing, A. G.; Wightman, R. M. *Anal. Chem.* **1980**, *52*, 2392–2396.
(37) Szalai, V. A.; Thorp, H. H. *J. Phys. Chem. B* **2000**, *104*, 6851–6859.

Kinetics of Metal-Mediated One-Electron Oxidation of Guanine in Polymeric DNA and in Oligonucleotides Containing Trinucleotide Repeat Sequences

Ivana V. Yang and H. Holden Thorp

Department of Chemistry, The University of North Carolina, Chapel Hill, North Carolina 27599-3290

Inorganic Chemistry®

Reprinted from
Volume 39, Number 21, Pages 4969–4976

Kinetics of Metal-Mediated One-Electron Oxidation of Guanine in Polymeric DNA and in Oligonucleotides Containing Trinucleotide Repeat Sequences

Ivana V. Yang and H. Holden Thorp*

Department of Chemistry, The University of North Carolina, Chapel Hill, North Carolina 27599-3290

Received June 6, 2000

The oxidation of guanines in DNA by Ru(III) is investigated by catalytic electrochemistry and stopped-flow spectrophotometry. The reactions of calf thymus DNA (20% guanine) and herring testes DNA (25% guanine) with $Ru(bpy)_3^{3+}$ (bpy = 2,2′-bipyridine) show biexponential decays in stopped-flow spectrophotometric experiments with the fast and slow components in 2:1 ratios and average rate constants in 880 mM NaCl of $\langle k \rangle = 18\,700\ M^{-1}\ s^{-1}$ for calf thymus DNA and $\langle k \rangle = 24\,600\ M^{-1}\ s^{-1}$ for herring testes DNA. The higher rate constant for the more guanine-rich DNA is possibly due to a higher density of electron-rich guanine multiplets. The observation of a biexponential decay is incorporated into digital simulations of the catalytic voltammograms observed for $Ru(bpy)_3^{2+}$ in the presence of DNA. For both DNAs, the rates observed by voltammetry are somewhat slower than those observed by stopped-flow spectrophotometry and the dependence of the rate constants on scan rate using the biexponential model is less pronounced than when only one decay is treated, supporting the notion that the scan rate dependence arises from the multiphasic decay. At low salt concentrations, where binding of the metal complex to DNA increases the effective catalytic rate constant, rates can be measured by stopped-flow spectrophotometry only with a less oxidizing complex, $Fe(bpy)_3^{3+/2+}$, which yields trends in the rate constants similar to those observed for the case of $Ru(bpy)_3^{3+/2+}$ at high ionic strength. Oligonucleotides based on the trinucleotide repeat sequences $(AGT)_n$ and $(GAA)_n$ produce significant catalytic currents, which are readily interpreted in terms of the guanine concentration and the secondary structure discerned from gel electrophoresis experiments. These experiments may provide a basis for sensing secondary structures and repeat numbers in biologically relevant DNAs.

Introduction

Electrochemistry offers an attractive approach to genetic analysis for a number of reasons that have been previously discussed.[1−16] A challenge in developing electrochemical methods for nucleic acid analysis is the identification of the appropriate redox-active moiety to analyze. For direct analysis, oxidation of the nucleic acid bases is the most facile; however, the potentials required for these reactions are high and generally near those where most electrodes oxidize water.[11,13] Other electrochemical approaches center on detection of exogenous redox labels that either interact specifically with double-stranded DNA[3−5,7−9,12,14−16] or are covalently attached to the target nucleic acid.[1,2,6,10]

We have described an electrochemical approach to nucleic acid analysis where DNA sequence and structure are probed by $Ru(bpy)_3^{2+}$-mediated oxidation of guanine nucleobases ($E_{1/2}$[Ru(III/II)] = 1.06 V and $E_{1/2}$[G(1+/0)] ~1.1 V vs Ag/AgCl).[17−19] This method is based on the detection of current enhancement in the cyclic voltammogram of $Ru(bpy)_3^{2+}$ measured at indium tin oxide (ITO) electrodes in the presence of DNA (bpy = 2,2′-bipyridine). The large number of guanine bases present in polymeric DNA combined with the use of miniaturized electrodes may allow detection of small amounts of genomic DNA fragments. In fact, we recently reported detection of immobilized DNA on ITO electrodes at a density of only 44 amol/mm².[20] This method is attractive because the ITO electrodes do not oxidize water or guanine significantly at the potential where the $Ru(bpy)_3^{3+/2+}$ couple occurs and the rate constant for $Ru(bpy)_3^{3+}$-guanine electron transfer is ex-

(1) Caruana, D. J.; Heller, A. *J. Am. Chem. Soc.* **1999**, *121*, 769−774.
(2) Hartwich, G.; Caruana, D. J.; deLumley-Woodyear, T.; Wu, Y.; Campbell, C. N.; Heller, A. *J. Am. Chem. Soc.* **1999**, *121*, 10803−10812.
(3) Hashimoto, K.; Ito, K.; Ishimori, Y. *Anal. Chem.* **1994**, *66*, 3830−3833.
(4) Kelley, S. O.; Barton, J. K.; Jackson, N. M.; Hill, M. G. *Bioconjugate Chem.* **1997**, *8*, 31−37.
(5) Kelley, S. O.; Boon, E. M.; Barton, J. K.; Jackson, N. M.; Hill, M. G. *Nucleic Acids Res.* **1999**, *27*, 4830−4837.
(6) Korri-Youssoufi, H.; Garnier, F.; Srivastava, P.; Godillot, P.; Yassar, A. *J. Am. Chem. Soc.* **1997**, *119*, 7388−7389.
(7) Marrazza, G.; Chianella, I.; Mascini, M. *Biosens. Bioelectron.* **1999**, *14*, 43−51.
(8) Millan, K. M.; Mikkelsen, S. R. *Anal. Chem.* **1993**, *65*, 2317−2323.
(9) Millan, K. M.; Saraullo, A.; Mikkelsen, S. R. *Anal. Chem.* **1994**, *66*, 2943−2948.
(10) O'Connor, S. D.; Olsen, G. T.; Creager, S. E. *J. Electroanal. Chem. Interfacial Electrochem.* **1999**, *466*, 197−202.
(11) Palecek, E.; Fojta, M. *Anal. Chem.* **1994**, *66*, 1566−1571.
(12) Takenaka, S.; Yamashita, K.; Takagi, M.; Uto, Y.; Kondo, H. *Anal. Chem.* **2000**, *72*, 1334−1341.
(13) Wang, J.; Rivas, G.; Fernandes, J. R.; Paz, J. L. L.; Jiang, M.; Waymire, R. *Anal. Chim. Acta* **1998**, *375*, 197−203.
(14) Wang, J.; Fernandes, J. R.; Kubota, L. T. *Anal. Chem.* **1998**, *70*, 3699−3702.
(15) Xu, X.-H.; Yang, H. C.; Mallouk, T. E.; Bard, A. J. *J. Am. Chem. Soc.* **1994**, *116*, 8386-8387.
(16) Xu, X.-H.; Bard, A. J. *J. Am. Chem. Soc.* **1995**, *117*, 2627−2631.
(17) Johnston, D. H.; Thorp, H. H. *J. Phys. Chem.* **1996**, *100*, 13873−13843.
(18) Johnston, D. H.; Glasgow, K. C.; Thorp, H. H. *J. Am. Chem. Soc.* **1995**, *117*, 8933−8938.
(19) Steenken, S.; Jovanovic, S. V. *J. Am. Chem. Soc.* **1997**, *119*, 617−618.
(20) Armistead, P. M.; Thorp, H. H. *Anal. Chem.* **2000**, *72*, 3764−3770.

10.1021/ic000607g CCC: $19.00
Published on Web 09/29/2000

tremely large, approaching 10^6 M^{-1} s^{-1}.[21] Accordingly, large current enhancements are obtained for micromolar concentrations of $Ru(bpy)_3^{2+}$ even when the DNA concentration is less than that of the catalyst.[21]

We have utilized the cyclic voltammetry simulation program DigiSim[22] to analyze the catalytic mechanism and extract rate constants for guanine oxidation in different DNA environments.[17,18,21] A relatively simple mechanism can be used for the case at high ionic strength where binding of the metal complex to DNA can be neglected:

$$Ru(bpy)_3^{3+} + e^- \rightleftharpoons Ru(bpy)_3^{2+} \quad (1)$$

$$Ru(bpy)_3^{3+} \rightleftharpoons Ru(bpy)_3^{2+} \quad (2)$$

$$Ru(bpy)_3^{3+} + DNA \rightarrow Ru(bpy)_3^{2+} + DNA' \quad (3)$$

$$Ru(bpy)_3^{3+} + DNA' \rightarrow Ru(bpy)_3^{2+} + DNA'' \quad (4)$$

Here DNA′ is a DNA molecule where one electron has been removed from guanine and DNA″ is a DNA molecule where two electrons have been removed from guanine. The mechanism accounts for slow spontaneous conversion of the oxidized metal complex back to the reduced form (eq 2), which is known to occur at neutral pH.[23] The mechanism also provides for DNA overoxidation (eq 4), since many guanine oxidation products are more easily oxidized than guanine itself.[24] At high salt concentration, the rate constant for oxidation of guanine in calf thymus DNA (eq 3) is $\sim 1 \times 10^4$ M^{-1} s^{-1} according to cyclic voltammetry; this value has been confirmed independently by pulsed voltammetry, chronoamperometry, and stopped-flow spectrophotometry.[18]

At low ionic strength, electrostatic binding of the mediator to the nucleic acid increases the catalytic current enhancement and accelerates the rate of guanine oxidation by an order of magnitude. This binding equilibrium complicates the mechanism, however, because square schemes accounting for bound and free ruthenium must be added for each electron transfer.[17] In addition, chronoamperometry studies have shown that, at low salt concentrations, the reaction exhibits biphasic kinetics with rates that differ by roughly an order of magnitude.[21] The biphasic nature of the reaction is also apparent in the scan rate dependence of the rate constants obtained from cyclic voltammetry. We have shown that the Λ and Δ enantiomers of $Ru(bpy)_3^{2+}$ oxidize guanine with similar rates, eliminating the possibility that the biphasic kinetics are a result of the stereoisomerism of the metal complex.[21]

We now extend our studies to $Ru(bpy)_3^{2+}$-mediated oxidation of polymeric and oligomeric DNAs containing different numbers of guanines. The primary question we address is whether the scan rate dependence from cyclic voltammetry is apparent as biphasic kinetics in homogeneous reactions that do not involve a solid electrode. This question was investigated by performing parallel studies of the oxidations of polymeric and oligonucleotide DNAs by stopped-flow spectrophotometry and cyclic voltammetry. A consistent model has been developed for analyzing both kinds of kinetic data where the stopped-flow results can be used to guide the electrochemical analysis. We also address three additional questions. First, what is the effect of changing the density of guanine in each strand of DNA? Second, how do noncanonical DNA structures affect the electrochemical response and apparent rate constant? Finally, since samples such as calf thymus DNA contain many sequences and fragment lengths, what is the role of polydispersity in the DNA sample? These questions have been addressed by studying the reactions of genomic DNAs from calf thymus and herring testes, which have different percentages of guanine (20% and 25%, respectively).[25] In addition, we have studied monodisperse oligonucleotides consisting of triplet repeats that contain a single guanine; such sequences are relevant to the disease-causing trinucleotide expansions that occur in genomic DNAs.[26–28]

Experimental Section

Materials. Calf thymus and herring testes DNA samples were purchased from Sigma and sheared by repeated sonication and passage through a 22-gauge needle.[29] Synthetic oligonucleotides were purchased from the Nucleic Acid Core Facility at the Lineberger Comprehensive Cancer Center of The University of North Carolina at Chapel Hill and purified on Microcon YM-3 centrifugal filters (Millipore). Water was purified with a Milli-Q purification system (Millipore). Salts for buffer preparation were purchased from Mallinckrodt, and ligands and metal salts were purchased from Aldrich. Published procedures were used to prepare the metal complexes $[Ru(bpy)_3]Cl_3$, $[Fe(bpy)_3]Cl_3$,[30] and $[Os(bpy)_2(dppz)]Cl_2$,[31] (bpy = 2,2′-bipyridine, dppz = dipyridophenazine). Gel electrophoresis reagents (acrylamide, agarose, TBE buffer) were purchased from Bio-Rad. All solution concentrations were determined spectrophotometrically using a Hewlett-Packard HP 8452 diode array spectrophotometer and known extinction coefficients.[18,31,32] Extinction coefficients for oligonucleotides were calculated using the nearest-neighbor equation,[33] giving the concentration of nucleic acid in strand concentration. Solutions of double-stranded oligonucleotide were prepared by mixing 1:1.2 guanine-containing and complementary oligonucleotides in the desired buffers, heating at 90 °C for 5 min, and cooling the mixtures to room temperature over a period of 3 h.

Stopped-Flow Spectrophotometry. Kinetic experiments were carried out using an On Line Instrument Systems RSM-1000 stopped-flow spectrophotometer. The reactions were monitored spectrophotometrically from 350 to 580 nm for 2.0 s at 1000 scans/s for $Ru(bpy)_3^{3+}$ and for 5 min at 21 scans/s for $Fe(bpy)_3^{3+}$. Solutions were maintained at 25 ± 1 °C. $M(bpy)_3^{3+}$ (M = Ru, Fe) and DNA were dissolved in ~10 mM H_2SO_4 (pH 2) and pH 8 phosphate buffer, respectively, and these solutions were then mixed to give a solution that was 50 mM in sodium phosphate, pH 7, with or without 800 mM NaCl after mixing. Concentrations of $Ru(bpy)_3^{2+}$ and $Fe(bpy)_3^{3+}$ in each run were obtained from A_{min} and $A_{max}-A_{min}$ at 452 nm (ϵ = 14 600 M^{-1} cm^{-1}) and at 524 nm (ϵ = 8400 M^{-1} cm^{-1}), respectively. Second-order oxidation rate constants were determined by global analysis[34] of all the data using the SPECFIT software (Spectrum Software Associates, Chapel Hill, NC).

Voltammetry and Digital Simulation. Voltammograms were collected using an EG&G Princeton Applied Research 273A poten-

(21) Sistare, M. F.; Holmberg, R.; Thorp, H. H. *J. Phys. Chem. B* **1999**, *103*, 10718–10728.
(22) Rudolph, M.; Reddy, D. P.; Feldberg, S. W. *Anal. Chem.* **1994**, *66*, 595A–600A.
(23) Creutz, C.; Sutin, N. *Proc. Natl. Acad. Sci. U.S.A.* **1975**, *72*, 2858–2862.
(24) Burrows, C. J.; Muller, J. G. *Chem. Rev.* **1998**, *98*, 1109–1151.
(25) Sigma Technical Support, 1997.
(26) Paulson, H. L.; Fischbeck, K. H. *Annu. Rev. Neurosci.* **1996**, *19*, 79–107.
(27) Sutherland, G. R.; Richards, R. I. *Proc. Natl. Acad. Sci. U.S.A.* **1995**, *92*, 3636–3641.
(28) Wells, R. D. *J. Biol. Chem.* **1996**, *271*, 2875–2878.
(29) Chaires, J. B.; Dattagupta, N.; Crothers, D. M. *Biochemistry* **1982**, *21*, 3933–3940.
(30) DeSimone, R. E.; Drago, R. S. *J. Am. Chem. Soc.* **1970**, *92*, 2343–2352.
(31) Welch, T. W.; Corbett, A. H.; Thorp, H. H. *J. Phys. chem.* **1995**, *99*, 11757–11763.
(32) Sambrook, J.; Fritsch, E. F.; Maniatis, T. *Molecular cloning: a laboratory manual*; Cold Spring Harbor: Plainview, NY, 1989.
(33) *CRC Handbook of Biochemistry and Molecular Biology*,3rd ed.; Fasman, G. D., Ed.; CRC Press: Cleveland, OH, 1976; Section B, Vol. 1.
(34) Meader, M.; Zuberbuhler, A. D. *Anal. Chem.* **1990**, *62*, 2220–2224.

tiostat/galvanostat with a single-compartment cell[35] equipped with a tin-doped indium oxide (ITO) working electrode having a geometric area of 0.32 cm^2 (Delta Technologies), a Pt-wire auxiliary electrode, and a Ag/AgCl reference electrode (Cypress Sytems). ITO electrodes were cleaned as described previously,[36] and a freshly cleaned electrode was used for each experiment. Normal-pulse voltammograms were collected and simulated using the COOL software package according to a published procedure.[31] For cyclic voltammetry experiments, the electrode was conditioned by scanning in buffer between 0.0 and 1.3−1.4 V for seven cycles, followed by a background scan of buffer alone that was subtracted from subsequent scans. Cyclic voltammograms of 50 μM $Ru(bpy)_3^{2+}$ in the absence and the presence of DNA were collected for each electrode. Second-order rate constants for DNA oxidation by $Ru(bpy)_3^{2+}$ were determined by fitting of cyclic voltammetric data using the DigiSim 2.1 software package (Bioanalytical Systems). The complete fitting procedure and parameters used have been described elsewhere.[17,21] Diffusion coefficients of calf thymus and herring testes DNAs were obtained by normal-pulse voltammetry (see below), and those of synthetic oligonucleotides were calculated using the equation of Tirado and Garcia de la Torre.[37−39]

Gel Electrophoresis. Sizes of sheared DNA fragments were determined on a 0.9% agarose gel according to standard procedures.[32] $d(GAA)_n$ and $d(AGT)_n$ (n = 6 or 9) oligonucleotides were 5′-radiolabeled using T4 polynucleotide kinase (New England Biolabs) and 5′-[γ-^{32}P]dATP (Amersham).[32] Unreacted 5′-[γ-^{32}P]dATP was removed from the labeled oligonucleotide using a NucTrap column from Stratagene. Radiolabeled oligonucleotide (25−50 000 cpm) was added to a solution of cold oligonucleotide alone (25 μM) or cold oligonucleotide with 30 μM complementary $d(TTC)_9$ or $d(ACT)_9$ oligonucleotide in 50 mM sodium phosphate buffer with 800 mM NaCl. Oligonucleotides were annealed, loaded on a 20% nondenaturing polyacrylamide gel, and electrophoresed at 4 °C and 200 V for 8 h. The gel was exposed on a phosphorimager screen overnight and scanned using a Storm 840 system (Molecular Dynamics).

Results and Discussion

Polymeric DNA: High Salt. (a) Stopped-Flow Spectrophotometry. Our experimental strategy was to study the kinetics of the homogeneous DNA oxidation by stopped-flow spectrophotometry and then to use the results of these experiments in modifying the electrochemical model. Initial investigations centered on reactions at high sodium ion concentration where binding of $Ru(bpy)_3^{3+/2+}$ to DNA can be neglected.[18] As expected from the scan rate dependence of the cyclic voltammetry,[21] single-wavelength kinetic traces exhibited biphasic kinetics and fit best to double-exponential functions (i.e., $A_1 \exp(-k_1 t) + A_2 \exp(-k_2 t)$). The ratios of the intensities of the fast and slow components (i.e., A_1:A_2) for these curves were ~2:1. These ratios were used in subsequent global fitting of the data at multiple wavelengths (350−600 nm), which was performed in SPECFIT according to a kinetic model consisting of two parallel oxidations by noninterconvertible Ru^{3+} populations:

$$Ru1^{3+} + DNA \xrightarrow{k_1} Ru^{2+} + DNA' \qquad (5)$$

$$Ru2^{3+} + DNA \xrightarrow{k_2} Ru^{2+} + DNA' \qquad (6)$$

where $Ru1^{3+}$ and $Ru2^{3+}$ indicate species of Ru(III) and the ratio $[Ru1^{3+}]/[Ru2^{3+}]$ was constrained to a value of 2. A representative kinetic trace at 452 nm with the global analysis fit is shown in Figure 1A. The calculated absorption spectra shown in Figure 1B agree well with the known spectra of $Ru(bpy)_3^{2+}$ and $Ru(bpy)_3^{3+}$.[40] From inspection of the early-time points in Figure 1A, there appears to be another minor contribution from an even faster process not accounted for by the two species in eqs 5 and 6. We have chosen not to analyze this minor process rather than to add another set of parameters, although triexponential processes in DNA have been described.[41,42]

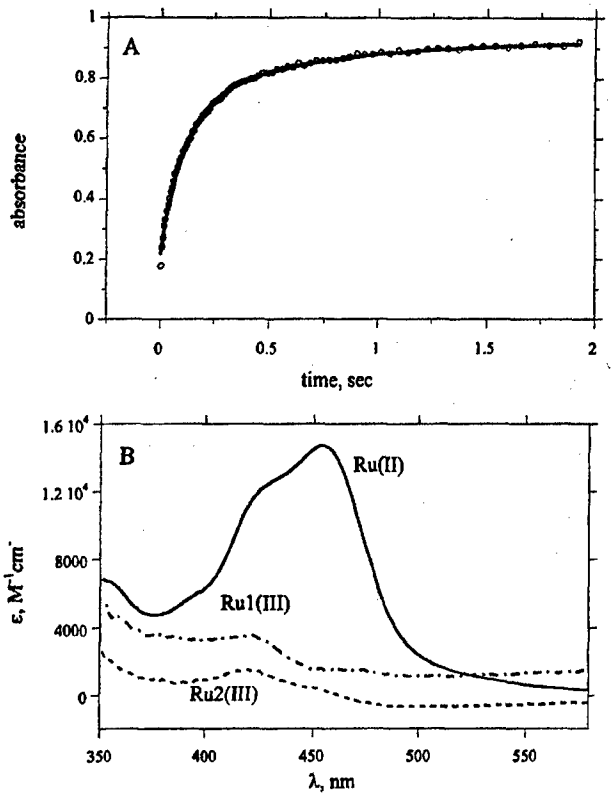

Figure 1. (A) Absorbance at 452 nm versus time for the oxidation of herring testes DNA by $Ru(bpy)_3^{3+}$ at high ionic strength. The solid line shows the calculated time dependence from global analysis. (B) Calculated spectra of Ru^{2+}, $Ru1^{3+}$, and $Ru2^{3+}$ determined in the global analysis.

Second-order rate constants in terms of guanine concentration determined by global analysis of the stopped-flow data (as in Figure 1) are summarized in Table 1. A number of important points are apparent. First, the rate constant for the faster component of the reaction of $Ru(bpy)_3^{3+}$ with calf thymus DNA is in excellent agreement with the value we previously reported for this reaction obtained from stopped-flow spectrophotometry with fitting to a single population (24×10^3 M^{-1} s^{-1}).[18] Second, the rate constant for the slower component of the reaction of $Ru(bpy)_3^{3+}$ with calf thymus DNA agrees well with the rate constant obtained by chronoamperometry (3.5×10^3 M^{-1} s^{-1}).[21] Third, the more abundant $Ru1^{3+}$ population oxidizes guanines in double-stranded DNA almost an order of magnitude faster than $Ru2^{3+}$. This ratio of rates is similar to that obtained for the two observed components in oxidation of calf thymus DNA from recent chronoamperometry experiments at low ionic strength.[21]

(35) Willit, J. L.; Bowden, E. F. *J. Phys. Chem.* **1990**, *94*, 8241−8246.
(36) Welch, T. W.; Thorp, H. H. *J. Phys. Chem.* **1996**, *100*, 13829−13836.
(37) Tirado, M. M.; Garcia de la Torre, J. *J. Chem. Phys.* **1980**, *73*, 1986−1993.
(38) Tirado, M. M.; Garcia de la Torre, J. *J. Chem. Phys.* **1979**, *71*, 2581−2587.
(39) Garcia de la Torre, J.; Lopez Martinez, M. C.; Tirado, M. M. *Biopolymers* **1984**, *23*, 611−615.
(40) Kalyanasundaram, K. *Coord. Chem. Rev.* **1982**, *46*, 159.
(41) Netzel, T. L.; Zhao, M.; Nafisi, K.; Headrick, J.; Sigman, M. S.; Eaton, B. E. *J. Am. Chem. Soc.* **1995**, *117*, 9119−9128.
(42) Netzel, T. L.; Nafisi, K.; Zhoa, M. *J. Phys. Chem.* **1995**, *99*, 17936−17947.

Table 1. Second-Order Rate Constants from Stopped-Flow Spectrophotmetry for Guanine Oxidation by $Ru(bpy)_3^{3+}$

DNA[a]	M	% guanine	[NaCl], mM	k_1,[b] $M^{-1}\,s^{-1}$	k_2,[b] $M^{-1}\,s^{-1}$	$\langle k \rangle$, $M^{-1}\,s^{-1}$
calf thymus	Ru	20	800	26 400 ± 700	3300 ± 600	18 700[c]
	Fe		0	480 ± 40	45 ± 9	260[d]
herring testes	Ru	25	800	34 100 ± 800	5500 ± 300	24 600[c]
	Fe		0	720 ± 60	86 ± 4	400[d]
$(GAA)_9(TTC)_9$	Ru	16	800	31 000 ± 600	3900 ± 200	17 500[d]
	Fe		0	240 ± 60	26 ± 4	130[d]

[a] [G] = [nucleotide phosphate DNA]/5 for calf thymus DNA and nucleotide phosphate DNA/4 for herring testes DNA. [G] = 9 [strand DNA] for the $(GAA)_9(TTC)_9$ oligonucleotide. [b] Each reported value is a mean (±1 standard deviation) of four to six rate constants at different DNA and metal concentrations. [c] $\langle k \rangle = (2k_1 + k_2)/3$. [d] $\langle k \rangle = (k_1 + k_2)/2$.

A final point from Table 1 is that both k_1 and k_2 are higher for herring testes DNA than for calf thymus DNA. The rate constants are given in terms of moles of guanine, so the higher fraction of guanine in herring testes DNA is already accounted for in the model. A possible explanation for this increase is a higher number of GG steps in herring testes DNA. The 5′ guanine in GG sequences is more easily oxidized than guanines that are 5′ to other bases due to more favorable stacking interactions with the adjacent guanine.[43-45] As shown previously with defined sequences, larger numbers of GG steps in the sequence increase the apparent rate constant when normalized to the total number of guanines.[45] For comparison, the weighted average rate constants, $\langle k \rangle = (2k_1 + k_2)/3$, are also given in Table 1.

In addition to the two-population model in eqs 5 and 6, two alternative kinetic models were tested. The first involved overoxidation of guanine instead of a parallel oxidation process, since we have shown that overoxidation steps improve the fitting of cyclic voltammetry results and are easily envisioned on the basis of the chemistry of guanine oxidation.[17,21,24] We also examined the possibility of nonproductive Ru^{3+} reduction (i.e., eq 3) accounting for the second exponential in the kinetic trace, since $Ru(bpy)_3^{3+}$ is known to convert independently to the 2+ form at neutral pH.[23] The data were not fit well by either mechanism; these two steps are probably too slow to contribute to the decay on the stopped-flow time scale.

(b) Cyclic Voltammetry. Having established that the homogeneous reaction proceeds with biphasic kinetics and a 2:1 ratio of subpopulations, we next sought to use this information in the electrochemical simulations. However, we first required values for the diffusion coefficients of the biopolymers. These were determined by electrochemistry of a nonoxidizing probe molecule with high DNA-binding affinity, as previously described.[31] Calf thymus DNA and herring testes DNA were sheared to generate shorter and more homogeneous DNA samples. Sizes of these sheared DNA fragments were estimated independently by gel electrophoresis to be between 1000 and 3000 base pairs (bp) for calf thymus (compared to >12 000 bp for unsheared) and between 500 and 1000 bp for herring testes (compared to 700−3000 bp for unsheared). Apparent diffusion coefficients of the fragments were determined using normal-pulse voltammetry with the $Os(bpy)_2(dppz)^{2+}$ intercalator (dppz = dipyridophenazine).[31] This technique provides diffusion coefficients for DNA molecules with an accuracy comparable to that of light-scattering experiments and theoretical calculations.[31,37-39,46,47] Analysis of normal-pulse voltammograms of $Os(bpy)_2(dppz)^{2+}$ in the presence of sheared calf thymus and herring testes DNAs gave diffusion coefficients of 1.8×10^{-7} and 2.1×10^{-7} cm^2/s, respectively.

With the DNA diffusion coefficients known, the mechanism established by stopped-flow spectrophotometry could then be used as the basis for simulating the electrochemical data. Cyclic voltammograms of $Ru(bpy)_3^{2+}$ in the presence of 1.0, 1.5, and 2.0 mM calf thymus or herring testes DNA at a range of scan rates (10−250 mV/s) were collected. High concentrations and relatively slow scan rates were necessary to observe different amounts of catalytic current enhancement for calf thymus and herring testes DNAs at the same nucleotide concentration. The mechanism employed in the fitting of cyclic voltammograms was similar to the mechanism we have previously reported (eqs 1−4),[17] except that two noninterconvertible ruthenium populations were used for the initial electron transfer, as observed in the stopped-flow studies. The ratio $[Ru1^{3+}]/[Ru2^{3+}] = 2$ was taken from the fitting of the stopped-flow data. Two further oxidations by the more reactive $Ru1^{3+}$ population were required to fit the data, which are in contrast to the stopped-flow spectrophotometry data, where no overoxidation reactions are apparent. The complete mechanism entered into DigiSim simulation program is shown in eqs 7−14, where DNA‴ is DNA that has been oxidized by three electrons.

$$Ru1^{2+} \rightleftharpoons Ru1^{3+} + e^- \quad (7)$$

$$Ru2^{2+} \rightleftharpoons Ru2^{3+} + e^- \quad (8)$$

$$Ru1^{3+} \rightleftharpoons Ru1^{2+} \quad (9)$$

$$Ru2^{3+} \rightleftharpoons Ru2^{2+} \quad (10)$$

$$Ru1^{3+} + DNA \xrightarrow{k_1} Ru1^{2+} + DNA' \quad (11)$$

$$Ru1^{3+} + DNA' \xrightarrow{k_1'} Ru1^{2+} + DNA'' \quad (12)$$

$$Ru1^{3+} + DNA'' \xrightarrow{k_1''} Ru1^{2+} + DNA''' \quad (13)$$

$$Ru2^{3+} + DNA \xrightarrow{k_2} Ru2^{2+} + DNA' \quad (14)$$

A representative set of cyclic voltammograms overlaid with DigiSim fits is shown in Figure 2A. The rate constants obtained from the simulations did not show a systematic dependence on the DNA concentration and are given in Table 2 as averages from three concentrations at 10 and 250 mV/s for both calf thymus and herring testes DNAs. The values of k_1 agree well with the rate constant we have previously determined for oxidation of guanine in calf thymus DNA at high ionic strength by cyclic voltammetry ($\sim 1 \times 10^4$ $M^{-1}s^{-1}$),[18] where the data were fit to only one population. The ratio of rates for the initial electron transfer in the faster and the slower components varied with the scan rate between 10 and 60, with the lower limit being

(43) Saito, I.; Nakamura, T.; Nakatani, K.; Yoshioka, Y.; Yamaguchi, K.; Sugiyama, H. *J. Am. Chem. Soc.* **1998**, *120*, 12686−12687.
(44) Sugiyama, H.; Saito, I. *J. Am. Chem. Soc.* **1996**, *118*, 7063−7068.
(45) Sistare, M. F.; Codden, S. J.; Heimlich, G.; Thorp, H. H. *J. Am. Chem. Soc.* **2000**, *122*, 4742−4749.
(46) Eimer, W.; Pecora, R. *J. Chem. Phys.* **1991**, *94*, 2324−2329.
(47) Goinga, H. T.; Pecora, R. *Macromolecules* **1991**, *24*, 6128−6138.

Table 2. Second-Order Rate Constants from Electrochemistry for Guanine Oxidation by $Ru(bpy)_3^{3+}$ in Polymeric DNA at High Salt Concentrations

DNA[a]	ν, mV/s	10^3k_1,[b] M^{-1} s^{-1}	$10^3k_1'$,[b] M^{-1} s^{-1}	$10^3k_1''$,[b] M^{-1} s^{-1}	10^3k_2,[b] M^{-1} s^{-1}	$\langle k\rangle$,[c] M^{-1} s^{-1}
calf	10	6.2 ± 1.1	5.9 ± 3.0	6.0 ± 3.5	0.59 ± 0.38	4 300
thymus	250	17 ± 3.1	11 ± 1.6	0	0.75 ± 0.30	11 600
herring	10	6.8 ± 1.4	5.1 ± 0.90	5.3 ± 1.4	0.39 ± 0.26	4 700
testes	250	21.4 ± 5.1	12 ± 2.5	0	0.89 ± 0.30	14 600

[a] [G] = [nucleotide phosphate DNA]/5 for calf thymus and [nucleotide phosphate DNA]/4 for herring testes DNA. [b] Each reported value is a mean (±1 standard deviation) of three rate constants (1.0, 1.5, and 2.0 mM nucleotide phosphate DNA). [c] $\langle k\rangle = (2k_1 + k_2)/3$.

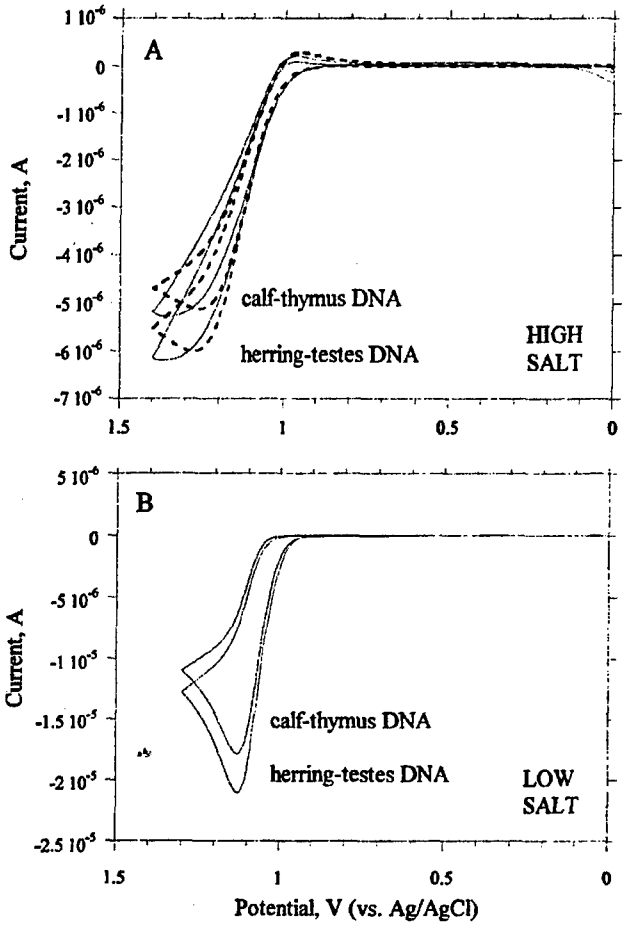

Figure 2. Cyclic voltammograms (solid) and digital simulations (dashed; calculated using eqs 7–14) for 50 μM $Ru(bpy)_3^{2+}$ with 2.0 mM calf thymus or herring testes DNA in (A) 50 mM sodium phosphate, pH 7, with 800 mM NaCl and (B) 50 mM sodium phosphate, pH 7, at 50 mV/s.

in good agreement with the ratio of the two components determined by chronoamperometry.[21]

Rate constants for both the faster and the slower component are lower than those obtained from stopped-flow spectrophotometry. We suspect that this relationship is a result of the longer time scale in the cyclic voltammetric experiment and the subsequent need for the addition of overoxidation steps, which provide an additional pathway for Ru(III) reduction not needed in the stopped-flow model. Accordingly, fitting of cyclic voltammograms collected at higher scan rates, i.e., shorter reaction times, required fewer overoxidation steps and gave k_1 values that approach the values obtained in the stopped-flow experiment (Table 2). However, the relative amount of catalytic current enhancement decreases with increasing scan rate because of the lower number of catalytic cycles at shorter reaction times, which leads to a larger error. At present, we are unsure as to whether the overoxidation steps are required because the longer time scale allows for additional reactions or because the simulation model is in some way limited. Parallel investigation of oxidation products and reaction kinetics should allow us to clarify this point in the future.

As discussed above, our primary goal was to determine whether the inclusion of multiple rate constants in the fitting of the electrochemical data reduces the dependence of the simulated rate constants on the scan rate observed when only one population is used. In Table 2, the rate constants obtained from the simulation of cyclic voltammograms with two populations of Ru(III) do show a modest scan rate dependence: the values of k_1 and k_1' increase with an increase in scan rate and the value of k_1'' becomes negligible at 250 mV/s. The values of k_2 do not change in a systematic fashion over the studied range of scan rates. Although the rate constants in Table 2 still show an experimentally significant scan rate dependence, the variation is much less pronounced than when only one population is used in the fit. In Table 2, the value of k_1 changes by a factor of 2 from 10 to 250 mV/s, which is much smaller than the scan rate dependence of the rate constant when only one ruthenium population is entered in the mechanism. In the latter case, the apparent rate changes by an order of magnitude on going from 25 to 250 mV/s.[21] Thus, use of two ruthenium populations reduces the scan rate dependence previously observed by digital simulation, supporting the proposal that biphasic kinetics in the guanine–Ru(III) electron transfer are responsible for the scan rate dependence.

Polymeric DNA: Low Salt. (a) Stopped-Flow Spectrophotometry. Studies on calf thymus and herring testes DNA were performed at low ionic strength to examine the effect of ruthenium binding to the DNA on the kinetics of guanine oxidation in the two polymers containing different amounts of guanine. Binding of $Ru(bpy)_3^{3+}$ to DNA in the absence of additional NaCl renders the rate of guanine oxidation approximately an order of magnitude faster than at high ionic strength,[17] making it difficult to study by stopped-flow spectrophotometry. To follow the faster reaction at low ionic strength, we decided to employ $Fe(bpy)_3^{3+}$, which is a close structural analogue of $Ru(bpy)_3^{3+}$ but has a lower redox potential ($E_{1/2}$ [Fe(III/II)] = 0.85 V), slowing the rate of guanine oxidation considerably.[18] The reaction was monitored at 524 nm in the same manner as the reaction of DNA with ruthenium at high ionic strength. SPECFIT analysis was also performed analogously to that for the ruthenium case, using the same mechanism (eq 5 and 6). The ratio of two iron populations was established by fitting of a double exponential to single-wavelength data and gave a ratio of $[Fe1^{3+}]/[Fe2^{3+}] = 1$, which differs from the 2:1 ratio of two ruthenium populations at high ionic strength. The difference in the ratios of the faster and the slower components is probably not significant. Second-order rate constants in terms of guanine concentrations for calf thymus and herring testes DNAs at various DNA concentrations are summarized in Table 1. The ratio of rate constants for the faster and slower component is similar to the ratio of the two components at high ionic strength, but the difference in rates of guanine oxidation in calf

thymus and herring testes DNAs is much more pronounced when binding of the metal complex is occurring, giving nearly a factor of 2 difference between herring testes and calf thymus DNAs. This difference could be due to an even more greatly enhanced reactivity of GG steps at low ionic strength compared to high ionic strength.

(b) Cyclic Voltammetry. Electrochemical studies on polymeric DNA substrates were also performed under conditions where metal complex binding to the polyanion must be considered. Cyclic voltammograms of $Ru(bpy)_3^{2+}$ at low ionic strength in the presence of 1.0, 1.5, and 2.0 mM calf thymus or herring testes DNA at 25 and 50 mV/s were collected; representative data are shown in Figure 2B. While the amount of current is much higher than that in the high ionic strength case, the binding of ruthenium to DNA does not enhance the relative difference in the amount of current enhancement in the presence of different amounts of guanine. This result demonstrates that small differences in the guanine content (20% vs 25%) can be detected in our system regardless of the ionic strength. We were not able to extract rate information from the cyclic voltammograms because the mechanism that accounts for both the ruthenium binding and the presence of the faster and the slower components has too many parameters, which were therefore not well determined.

Oligonucleotides. (a) Stopped-Flow Spectrophotometry—High Salt. Stopped-flow spectrophotometric studies with $Ru(bpy)_3^{3+}$ at high ionic strength were extended to smaller DNA molecules, namely, synthetic oligonucleotides containing trinucleotide repeat sequences. We chose to investigate the trinucleotide repeat effect in oligonucleotides based on $(GAA)_n$, which is expanded in the genomes of Friederich's ataxia patients.[26-28] This motif was chosen over other physiologically relevant sequences because of the lack of guanines in the complementary strand, which makes possible direct comparison the data for single- and double-stranded oligonucleotide in subsequent voltammetry experiments. The rate constants for oxidation of guanine in the double-stranded $(GAA)_9(TTC)_9$ oligonucleotide were extracted from stopped-flow data in the same manner as that used for the case of polymeric DNA molecules and are shown in Table 1. The most important observation is the biphasic nature of the electron-transfer reaction, with the ratio of two Ru^{3+} populations of 1:1. The biphasic kinetics of the reaction with oligonucleotides as the substrate suggests that polydispersity and sequence heterogeneity of DNA molecules are not the origin of the biphasic kinetics since synthetic oligonucleotides are all of the same length and their hybrids are too short to have unusual secondary structures. Rate constants for guanine oxidation are nearly identical in double-stranded oligonucleotides and in polymeric DNA samples (Table 1), which is reasonable since calf thymus and herring testes DNAs are almost completely double-stranded. The ratio of the faster and the slower component also remains constant regardless of the DNA sample. Thus, potential polydispersity in polymeric DNA samples does not appear to affect the rate of electron transfer.

(b) Cyclic Voltammetry—High Salt. Guanine oxidation in oligonucleotides containing triplet repeats was also investigated by cyclic voltammetry. Two trinucleotide repeat sequences were examined: $(GAA)_n$ and $(AGT)_n$, where $n = 6$ or 9. The $(AGT)_n$ repeat was included to study the effect of the base 3′ to the guanine, since the GA step in the $(GAA)_n$ repeat may be more reactive than the GT step in the $(AGT)_n$ repeat due to differential stacking of two purines compared to a purine and a pyrimidine.[43]

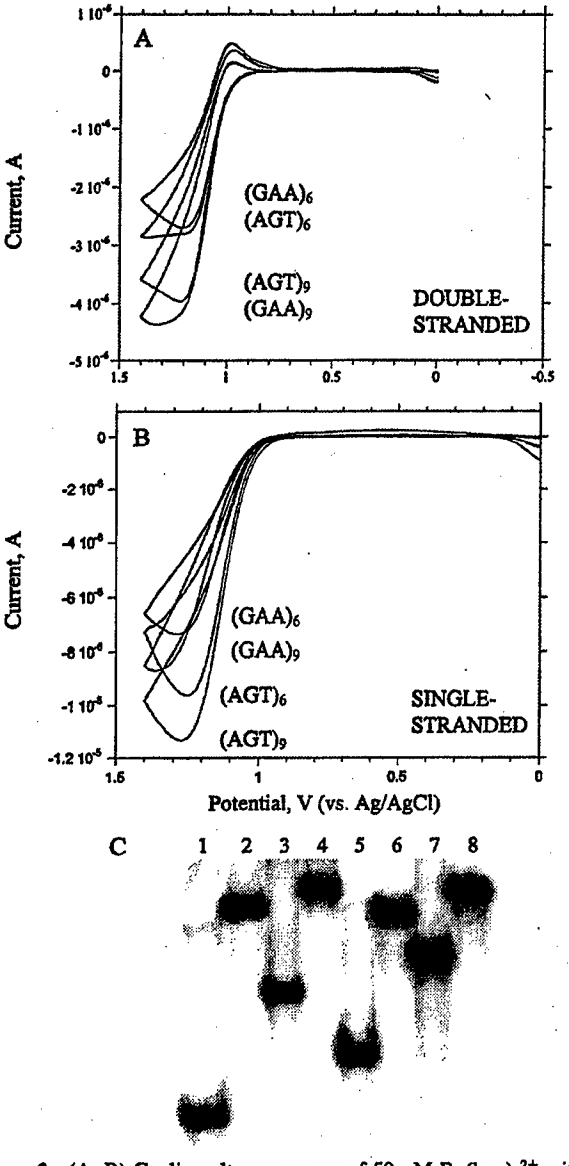

Figure 3. (A, B) Cyclic voltammograms of 50 μM $Ru(bpy)_3^{2+}$ with 25 μM double-stranded (ds) (A) and single-stranded (ss) (B) oligonucleotides in 50 mM sodium phosphate, pH 7, with 800 mM NaCl at 25 mV/s. (C) Nondenaturing polyacrylamide gel of $(GAA)_n$ and $(AGT)_n$ oligonucleotides visualized by phosphorimagery. Lanes: 1, ss $(GAA)_6$; 2, ds $(GAA)_6$; 3, ss $(GAA)_9$; 4, ds $(GAA)_9$; 5, ss $(AGT)_6$; 6, ds $(AGT)_6$; 7, ss $(AGT)_9$; 8, ds $(AGT)_9$.

Representative sets of cyclic voltammograms are shown in Figure 3A,B. Oligonucleotides containing six and nine triplet repeats are easily distinguished when single- or double-stranded. More catalytic current is observed for single-stranded oligonucleotides because of the higher solvent accessibility of single-stranded guanines compared to guanines inside the double helix.[18] Double-stranded $(GAA)_n$ and $(AGT)_n$ oligonucleotides show the same amount of current enhancement within experimental error, whereas single-stranded $(AGT)_n$ oligonucleotides produce more current than $(GAA)_n$ oligonucleotides. We suspected that this difference may be due to the presence of noncanonical secondary structures in $(GAA)_n$ oligonucleotides imposed by the ability of guanine and adenine to form Hoogsteen base pairs.[48] Nondenaturing gel electrophoresis under conditions identical to those in our electrochemical experiments

(48) *Nucleic Acids in Chemistry and Biology*; 2nd ed.; Blackburn, G. M., Gait, M. J., Eds.; Oxford University Press: New York, 1996.

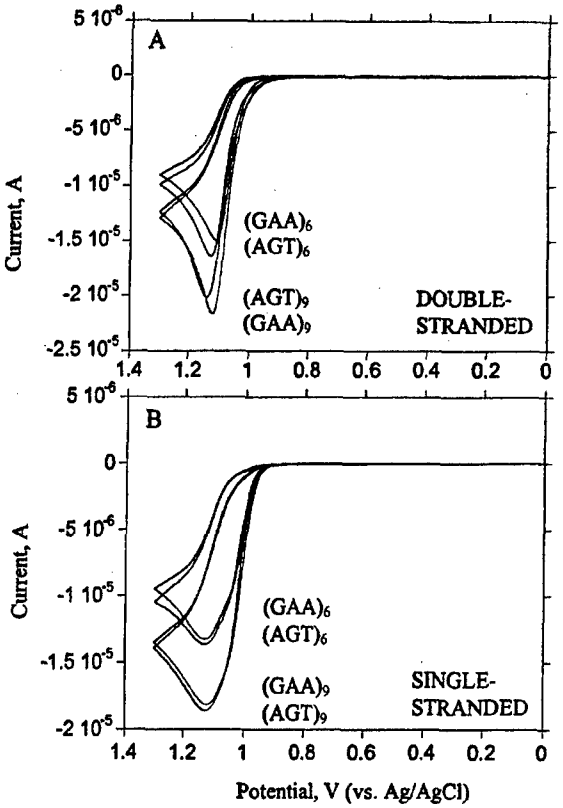

Figure 4. Cyclic voltammograms of 50 μM $Ru(bpy)_3^{2+}$ with 25 μM double-stranded (A) and single-stranded (B) oligonucleotides in 50 mM sodium phosphate, pH 7, at 25 mV/s.

(25 μM oligonucleotide in 50 mM sodium phosphate with 800 mM added sodium chloride; Figure 3C) supports this hypothesis, since the single-stranded forms of this oligonucleotide (lanes 1 and 3) migrate much faster than the single-stranded forms of the $(AGT)_n$ sequence (lanes 5 and 7). All of the annealed samples migrate as expected for the duplex forms. The results in Figure 3 provide a satisfying demonstration of how the electrochemistry can indicate changes in structure that can then be confirmed by traditional biochemical techniques.

(c) Cyclic Voltammetry—Low Salt. Cyclic voltammograms of $Ru(bpy)_3^{2+}$ in the presence of 25 μM single- and double-stranded $(GAA)_6$, $(GAA)_9$, $(AGT)_6$, and $(AGT)_9$ oligonucleotides at low ionic strength are shown in Figure 4. While the absolute amount of observed current is higher than that observed at high ionic strength (Figure 3), the relative difference between six and nine repeats remains the same both in double- (Figure 4A) and in single-stranded (Figure 4B) oligonucleotides. This situation is analogous to the comparison of calf thymus and herring testes DNAs at low and high ionic strengths and indicates that binding of the metal complex to DNA increases the overall signal but neither improves nor decreases the sensitivity for distinguishing different amounts of guanine. In contrast to the high ionic strength case, single-stranded $(GAA)_n$ and $(AGT)_n$ oligonucleotides show the same amount of current enhancement possibly because the noncanonical secondary structures in $(GAA)_n$ repeats (Figure 3C) form only at high sodium ion concentration.

A striking feature in Figure 4 compared to the voltammograms collected at high ionic strength is the similar currents observed for double- (Figure 4A) and single-stranded (Figure 4B) DNAs. In Figure 3 and in many other experiments performed at high salt concentration, we have observed much higher reactivity of single-stranded and mismatched guanines due to higher solvent accessibility.[18,49] Tighter binding of the metal cation to the double helix enhances the reactivity of double-stranded oligonucleotides; however, the guanines of single-stranded oligonucleotides are more solvent accessible and therefore more reactive. These effects are apparently contradictory; thus, the difference in absolute current for double- and single-stranded DNAs is small at low salt concentration. The voltammograms do differ in shape, where voltammograms of single-stranded DNA are much wider and voltammograms of double-stranded DNA have much sharper peaks.

(d) Distinguishing Repeat Numbers. In the final set of experiments, we examined the reactivity of oligonucleotides containing $(GAA)_n$ ($n = 5-9$) trinucleotide repeats. Here our goal was to determine whether the catalytic current was sufficient to distinguish addition of a single repeat to the sequence. To combine the advantages of better sensitivity at lower ionic strength and a simpler mechanism at high ionic strength, an intermediate ionic strength regime (50 mM sodium phosphate with 400 mM sodium chloride) was chosen. Cyclic voltammograms of 25 μM single- and double-stranded oligonucleotides at 25 mV/s are shown in Figure 5A,B, and plots of peak current vs number of repeats, n, are shown in Figure 5C. The peak current increases linearly with the number of repeats in both single- and double-stranded $(GAA)_n$ oligonucleotides. More current enhancement is observed in the case of single-stranded oligonucleotides, suggesting that the unbound ruthenium dominates at this ionic strength. However, the amount of current enhancement for $(GAA)_6$ and $(GAA)_9$ oligonucleotides is higher and the difference between single- and double-stranded DNAs is less pronounced when compared to those at high ionic strength (Figure 2), which implies that binding of ruthenium to DNA is detectable.

Conclusions

Biphasic Kinetics. The electron-transfer reaction of $M(bpy)_3^{3+}$ (M = Ru, Fe) with guanine nucleobases exhibits biphasic kinetics both in DNA polymers of heterogeneous sequences and in trinucleotide-repeat oligonucleotides at both high and low ionic strengths. This suggests that conformation, polydispersity, and sequence heterogeneity are not the origin of the two populations. Simple binding of the metal complex is likely not the source of the two populations either, since the two populations are present even when binding of the metal complex is negligible, i.e., at high Na^+ concentrations. We believe that the biphasic kinetics result simply from inclusion of guanine in a macromolecule (even in small oligonucleotides), which is supported by many observations of biphasic reaction kinetics for similar reactions.[50-53] As has been discussed elsewhere,[50-53] the two species likely result from different binding geometries that undergo a reaction (in this case electron transfer) that is fast compared to the diffusive interconversion of the two species.

Scan Rate Dependence. The scan rate dependence of the rate constants obtained from cyclic voltammetry is greatly diminished when the voltammograms are fit to the two-population model (Table 2) instead of the mechanism with only

(49) Ropp, P. A.; Thorp, H. H. *Chem. Biol.* **1999**, *6*, 599–605.
(50) Arkin, M. R.; Stemp, E. D. A.; Holmlin, R. E.; Barton, J. K.; Hormann, A.; Olson, E. J. C.; Barbara, P. F. *Science* **1996**, *273*, 475–480.
(51) Arkin, M. R.; Stemp, E. D. A.; Turro, C.; Turro, N. J.; Barton, J. K. *J. Am. Chem. Soc.* **1996**, *118*, 2267–2274.
(52) Barton, J. K.; Kumar, C. V.; Turro, N. J. *J. Am. Chem. Soc.* **1986**, *108*, 6391–6393.
(53) Kumar, C. V.; Barton, J. K.; Turro, N. J. *J. Am. Chem. Soc.* **1985**, *107*, 5518–5523.

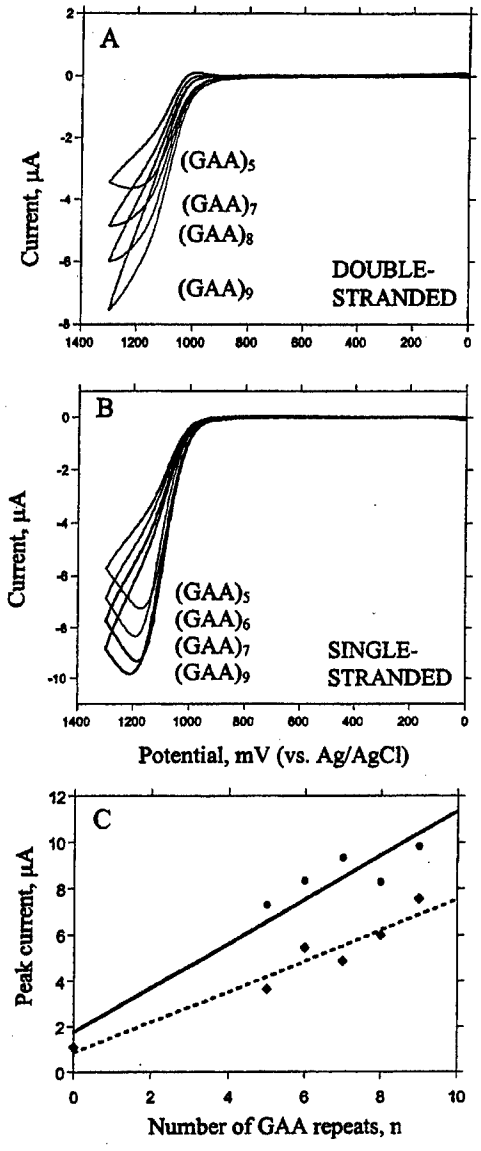

Figure 5. (A, B) Cyclic voltammograms of 50 μM $Ru(bpy)_3^{2+}$ with 25 μM double-stranded (A) and single-stranded (B) oligonucleotides in 50 mM sodium phosphate, pH 7, with 400 mM NaCl at 25 mV/s. (C) Plots of peak currents taken from voltammograms for double-stranded (◆) and single-stranded (●) oligonuclotides vs the number of GAA repeats, *n*. Solid and dashed lines are best linear fits of the data; $R = 0.96$.

one population used previously.[17,45] The apparent rate constants obtained from fits to the one-population model are therefore an average of the rate constants for two phases of the reaction with the relative contributions of the two phases varying with the scan rate. Thus, inclusion of the two populations in the model reduces the effect on the apparent rate constant of sampling a fraction of the reaction course at any given scan rate.

Effect of Guanine Density. Heterogeneous-sequence DNA polymers that differ in their guanine contents by only ~5% are easily distinguished by the current observed in cyclic voltammetry in both high and low ionic strength regimes. This effect is due in part to the increased guanine concentration, which increases the observed current. However, the change in absolute guanine concentration is accounted for in the modeled rate constants, which are given in terms of moles of guanine. Therefore, the polymers with higher guanine content are intrinsically more reactive than those with less. This effect may arise from a higher number of electron-rich GG doublets, which are 12 times more reactive than an isolated guanine.[45] Alternatively, the higher numbers of guanines may provide greater intrinsic reactivity due to an increase in the frequency of collisions that lead to electron-transfer. We have discussed these issues in detail elsewhere and examined these effects in oligonucleotides of known sequences.[21,45] Because the sequences present in calf thymus and herring testes DNAs are heterogeneous, this issue cannot be resolved with certainty.

Guanine-containing trinucleotide repeat sequences of different lengths are readily differentiated at high, low, and intermediate ionic strengths. The observed current enhancement increases linearly with the number of repeats at intermediate ionic strength. This is of special significance because it should allow for future detection of trinucleotide repeat expansion in clinical samples from patients with neurodegenerative disorders such as fragile X syndrome, Friedrich's ataxia, and myotonic dystrophy.[26-28]

Secondary-Structure Dependence. Single-stranded oligonucleotides are much more reactive than their double-stranded counterparts under high ionic strength conditions as a result of higher solvent accessibility of guanine nucleobases. This is not the case in the low-salt regime, where the more pronounced solvent accessibility of single-stranded guanines is counteracted by an enhanced affinity of the positively charged metal complex for the more negatively charged double-stranded DNA, leading to comparable reactivities of single- and double-stranded sequences. Noncanonical secondary structures of $(GAA)_n$ are apparent in the electrochemistry and are verified independently by native gel electrophoresis. These observations demonstrate that detection of guanine secondary structures is best performed at high ionic strength, while simple quantitation of guanine concentrations is best performed at low ionic strength, where different secondary structures exhibit similar rate constants.

Acknowledgment. The U.S. Army Medical Research and Materiel Command under contract DAMD17-98-1-8224 supported this work along with Xanthon, Inc. We thank Stephanie Weatherly, Brian Farrer, Carole Golden, and Veronika Szalai for helpful discussions.

IC000607G

Modification of Indium Tin Oxide Electrodes with Nucleic Acids: Detection of Attomole Quantities of Immobilized DNA by Electrocatalysis

Paul M. Armistead and H. Holden Thorp

Department of Chemistry and Lineberger Comprehensive Cancer Center, University of North Carolina, Chapel Hill, North Carolina 27599-3290

ANALYTICAL® CHEMISTRY

Reprinted from
Volume 72, Number 16, Pages 3764–3770

Anal. Chem. **2000**, *72*, 3764–3770

Modification of Indium Tin Oxide Electrodes with Nucleic Acids: Detection of Attomole Quantities of Immobilized DNA by Electrocatalysis

Paul M. Armistead and H. Holden Thorp*

Department of Chemistry and Lineberger Comprehensive Cancer Center, University of North Carolina, Chapel Hill, North Carolina 27599-3290

Indium tin oxide electrodes were modified with DNA, and the guanines in the immobilized nucleic acid were used as a substrate for electrocatalytic oxidation by $Ru(bpy)_3^{3+}$ (bpy = 2,2′-bipyridine). Nucleic acids were deposited onto 12.6-mm^2 electrodes from 9:1 DMF/water mixtures buffered with sodium acetate. The DNA appeared to denature in the presence of DMF, leading to adsorption of single-stranded DNA. The nucleic acid was not removed by vigorous washing or heating the electrodes in water, although incubation in phosphate buffer overnight liberated the adsorbed biomolecule. Acquisition of cyclic voltammograms or chronoamperomograms of $Ru(bpy)_3^{2+}$ at the modified electrodes produced catalytic signals indicative of oxidation of the immobilized guanine by Ru(III). The electrocatalytic current was a linear function of the extent of modification with a slope of 0.5 μA/pmol of adsorbed guanine; integration of the current–time traces gave 2.2 ± 0.4 electrons/guanine molecule. Use of long DNA strands therefore gave steep responses in terms of the quantity of adsorbed DNA strand. For example, electrodes modified with a 1497-bp PCR product from the HER-2 gene produced detectable catalytic currents when as little as 550 amol of strand was adsorbed, giving a sensitivity of 44 amol/mm^2.

Spatial resolution of nucleic acids immobilized on solid surfaces has enabled the parallel detection of nucleic acids in array formats that have been applied to monitoring the presence of infectious organisms, quantitating mRNA expression levels, and sequencing genomic DNA.[1-3] Factors that have made these advancements possible include fluorescence microscopy, methods to label DNA and RNA with fluorophores, and the ability to attach nucleic acids on small, spatially resolved features. Electrochemical techniques are ideally suited to miniaturization and have the potential to simplify nucleic acid analysis by circumventing the need for fluorescent labeling steps and fluorescent microscopy.[4,5] Numerous methods for attaching DNA to electrode materials have been described.[6-12]

Direct electrochemistry of nucleic acids has been achieved through a number of approaches. The electrochemical detection of nucleic acids was first demonstrated by Palecek using reduction of the guanine, cytosine, and adenine bases at mercury electrodes.[13] This original work has been modified and improved to such an extent that the reduction can be used to detect DNA with a sensitivity of roughly 100 pg.[14,15] Wang et al. have focused on the detection of direct oxidation of the guanine and adenine bases adsorbed on carbon electrodes.[8,16-18] The major difficulty with this approach is that water is also oxidized at the potentials needed to oxidize guanine and adenine; however, by combining square wave voltammetry and standard background subtraction, a detection limit estimated to be 15.4 fmol of tRNA has been achieved on a 2.5-mm-diameter carbon paste electrode.[18] Kuhr et al. have also achieved a sensitive detection system based upon catalytic oxidation of the deoxyribose (or ribose) sugar in nucleic acid at a copper microelectrode.[19-21] To detect low concentrations of nucleotides, a 20-μm-diameter copper wire is used as the working electrode, and sinusoidal voltammetry is performed. To date, this system has been used to detect nucleotide concentrations of 70–200 nM and DNA concentrations of 3.2 pM.[20,21]

(1) Spargo, C. A.; Haaland, P. D.; Jurgensen, S. R.; Shank, D. D.; Walker, G. T. *Mol. Cell. Probes* **1993**, *7*, 395–404.
(2) Schena, M.; Shalon, D.; Davis, R. W.; Brown, P. O. *Science* **1995**, *270*, 467–470.
(3) Chee, M.; Yang, R.; Hubbell, E.; Berno, A.; Huang, X. C.; Stern, D.; Winkler, J.; Lockhart, D. J.; Morris, M. S.; Fodor, S. P. A. *Science* **1996**, *274*, 610–614.
(4) Thorp, H. H. *Trends Biotechnol.* **1998**, *16*, 117–121.
(5) Mikkelsen, S. R. *Electroanalysis* **1996**, *8*, 15–19.
(6) Millan, K. M.; Spurmanis, A. J.; Mikkelsen, S. R. *Electroanalysis* **1992**, *4*, 929–932.
(7) Palecek, E. *Electroanalysis* **1996**, *8*, 7–14.
(8) Wang, J.; Cai, X.; Rivas, G.; Shiraishi, H.; Farias, P. A. M.; Dontha, N. *Anal. Chem.* **1996**, *68*, 2629–2634.
(9) Kouri-Yousoufi, H.; Garnier, F.; Srivasta, P.; Yassar, A. *J. Am. Chem. soc.* **1997**, *119*, 7388–7389.
(10) Herne, T. M.; Tarlov, M. J. *J. Am. Chem. Soc.* **1997**, *119*, 8916–8920.
(11) de Lumley-Woodyear, T.; Caruana, D. J.; Campbell, C. N.; Heller, A. *Anal. Chem.* **1999**, *71*, 394–398.
(12) de Lumley-Woodyear, T.; Campbell, C. N.; Freeman, E.; Freeman, A.; Georgiou, G.; Heller, A. *Anal. Chem.* **1999**, *71*, 535–538.
(13) Palecek, E. *Nature* **1960**, *188*, 656–657.
(14) Palecek, E.; Fojta, M. *Anal. Chem.* **1994**, *66*, 1566–1571.
(15) Palecek, E.; Tomschik, M.; Stankova, V.; Havran, L. *Electroanalysis* **1997**, *9*, 990–997.
(16) Wang, J.; Cai, X.; Jonsson, C.; Balakrishnan, M. *Electroanalysis* **1996**, *8*, 20–24.
(17) Wang, J.; Fernandes, J. R.; Kubota, L. T. *Anal. Chem.* **1998**, *70*, 3699–3702.
(18) Wang, J.; Bollo, S.; Paz, J. L. L.; Sahlin, E.; Mukherjee, B. *Anal. Chem.* **1999**, *71*, 1919–1931.
(19) Singhal, P.; Kawagoe, K. T.; Christian, C. N.; Kuhr, W. G. *Anal. Chem.* **1997**, *69*, 1662–1668.
(20) Singhal, P.; Kuhr, W. G. *Anal. Chem.* **1997**, *69*, 3552–3557.
(21) Singhal, P.; Kuhr, W. G. *Anal. Chem.* **1997**, *69*, 4828–4832.

10.1021/ac000051e CCC: $19.00
Published on Web 07/11/2000

The poor electron-transfer kinetics from nucleic acids to most electrode materials has led many research groups to investigate the utility of having the detection of nucleic acids coupled to the detection of some second reporter molecule. Mikkelsen and coworkers detected DNA on carbon electrodes by immobilizing the DNA onto the electrode and then measuring the enhanced faradaic current of $Co(bpy)_3^{2+/3+}$ in the presence of the surface-attached DNA; the detection limit of this system was estimated to be 250 pg of a 400-bp PCR product.[22,23] Another indirect detection system recently reported by Heller et al. involves the modification of DNA to allow coupling to a "wired" polymer on the electrode surface.[12] A genetically modified horseradish peroxidase is added to the DNA-treated polymer, and in the presence of hydrogen peroxide substrate, Heller et al. detected a modified PCR product in 10 min and a single base mismatch in an oligonucleotide on a 7-μm microelectrode.[12,24] Another recent indirect system involves monitoring the redox chemistry of methylene blue on alkanethiol monolayers of DNA on gold electrodes.[25,26]

An approach taken by our laboratory to address the issue of creating a sensitive nucleic acid detection system involves using $Ru(bpy)_3^{2+/3+}$ as a guanine oxidation catalyst (bpy = 2,2′-bipyridine).[4,27] Using $Ru(bpy)_3^{2+}$ as the oxidation catalyst for guanine offers an advantage over detecting guanine oxidation directly because it exhibits rapid electron-transfer kinetics with most electrode materials including the tin-doped indium oxide (ITO) electrodes used in this study.[28] $Ru(bpy)_3^{3+}$ has a reduction potential of 1.06 V vs Ag/AgCl, which is close to that of guanosine radical cation (E° = 1.07 V vs Ag/AgCl);[29] second-order rate constants for electron transfer from guanine in DNA to $Ru(bpy)_3^{3+}$ are as high as $10^6\ M^{-1}\ s^{-1}$.[30-33] The $Ru(bpy)_3^{3+}$–guanine electron transfer is observed as a current enhancement in the oxidation wave of $Ru(bpy)_3^{2+}$ in a cyclic voltammogram through an EC′ mechanism.[34-36]

$$Ru(bpy)_3^{2+} \rightarrow Ru(bpy)_3^{3+} + e^- \quad (1)$$

$$Ru(bpy)_3^{3+} + \text{guanine} \rightarrow Ru(bpy)_3^{2+} + (\text{guanine})^+ \quad (2)$$

The ITO electrodes exhibit little water oxidation current at the potentials needed to achieve the electrocatalysis.[28]

To make this reaction scheme practical for use as a nucleic acid biosensor, surface immobilization of the nucleic acid must be achieved.[4] We have pursued a number of immobilization schemes involving self-assembled monolayers,[35] electropolymerized films,[37] and porous membranes attached to the ITO surface.[36] Here we describe a very simple system for immobilizing DNA on ITO without the use of a coupling agent or an additional layer on the electrode. In this approach, strands of DNA 435–1497 bp long were prepared by polymerase chain reaction (PCR) and directly attached to an ITO surface by irreversible adsorption of the DNA from a *N,N*-dimethylformamide (DMF)/acetate solution. Repeated washing or heating of the electrodes did not liberate the immobilized DNA. Guanines in the immobilized DNA did not show significant direct oxidation current, but did act as a substrate for the electrocatalysis scheme shown in eqs 1 and 2 with $Ru(bpy)_3^{2+}$ in solution. Quantification of the adsorbed DNA by radiolabeling and phosphorimagery showed that less than 1 fmol of long strands of DNA gave measurable catalytic currents on relatively large electrodes (12.6 mm^2), giving a detection limit of only 44 amol/mm^2. The fragments detected were RT-PCR amplicons of the HER-2 mRNA from BT-474 cancer cells. Amplification of the HER-2 gene correlates with decreased survival in women with node-positive breast cancer.[38]

EXPERIMENTAL SECTION

Preparation of Nucleic Acids. BT-474 cells were kindly provided by the laboratory of Dr. Bill Cance at the UNC Lineberger Comprehensive Cancer Center. RNA was extracted and purified by means of an RNeasy RNA purification kit from Qiagen. Polymerase chain reaction was performed using a Hybaid PCR Sprint with a 0.2-mL tube configuration heating block. PCR products were purified on Life Technologies Concert PCR purification columns (Life Technologies). Quantification of radiolabeled PCR products was performed on a Molecular Dynamics Storm 860 phosphorimager with subsequent analysis performed using ImageQuaNT software. All water used was in-house distilled water that was further purified through a Milli-Q ultrafiltration system. Water used for RNA manipulations was further treated with diethyl pyrocarbonate (DEPC; Sigma).

Reverse transcription was performed by mixing 2 μL of total RNA (0.8 μg/μL), 2 μL of Random hexamers (Promega), 4 μL of dNTPs (10 mM, Amersham), and 6 μL of RNase-free water. The reverse transcription mix was heated to 70 °C for 3 min to denature the RNA and then immediately placed on ice. To the mix was added 1 μL of RNasin (Promega), 1 μL of M-MLV reverse transcriptase (Life Technologies, 200 units/μL), and 4 μL of 5× reverse transcription buffer (Life Technologies). The reactants were mixed and incubated at 42 °C for 1 h. PCR was performed on the reverse transcription products to amplify segments of the HER-2 gene. A 50-μL PCR mix was assembled from 5 μL of the reverse transcription reaction, 2.5 μL of the forward primer (5 μM), 2.5 μL of the reverse primer (5 μM), 2.5 μL of $MgCl_2$ (50 mM), 2.5 μL of dNTPs (10 mM), 5 μL of 10× PCR buffer, 30 μL of water, and 1 unit of Taq polymerase (Life Technologies, 5 units/μL). The 435-bp product (forward primer, GGC TGT GCC

(22) Millan, K. M.; Mikkelsen, S. R. *Anal. Chem.* **1993**, *65*, 2317–2323.
(23) Millan, K. M.; Saraulio, A.; Mikkelsen, S. R. *Anal. Chem.* **1994**, *66*, 2943–2948.
(24) Carauna, D. J.; Heller, A. *J. Am. Chem. Soc.* **1999**, *121*, 769–774.
(25) Kelley, S. O.; Boon, E. M.; Barton, J. K.; Jackson, N. M.; Hill, M. G. *Nucleic Acids Res.* **1999**, *27*, 4830–4837.
(26) Kelley, S. O.; Barton, J. K.; Jackson, N. M.; Hill, M. G. *Bioconjugate Chem.* **1997**, *8*, 31–37.
(27) Johnston, D. H.; Welch, T. W.; Thorp, H. H. *Metal Ions Biol. Syst.* **1996**, *33*, 297–324.
(28) Johnston, D. H.; Glasgow, K. C.; Thorp, H. H. *J. Am. Chem. Soc.* **1995**, *117*, 8933–8938.
(29) Steenken, S.; Jovanovic, S. V. *J. Am. Chem. Soc.* **1997**, *119*, 617–618.
(30) Sistare, M. F.; Holmberg, R. C.; Thorp, H. H. *J. Phys. Chem. B* **1999**, *103*, 10718–10728.
(31) Johnston, D. H.; Thorp, H. H. *J. Phys. Chem.* **1996**, *100*, 13837–13843.
(32) Szalai, V. A.; Thorp, H. H. *J. Am. Chem. Soc.* **2000**, *122*, 4524–4525.
(33) Ropp, P. A.; Thorp, H. H. *Chem. Biol.* **1999**, *6*, 599–605.
(34) Napier, M. E.; Loomis, C. R.; Sistare, M. F.; Kim, J.; Eckhardt, A. E.; Thorp, H. H. *Bioconjugate Chem.* **1997**, *8*, 906–913.
(35) Napier, M. E.; Thorp, H. H. *Langmuir* **1997**, *13*, 6342–6344.
(36) Napier, M. E.; Thorp, H. H. *J. Fluoresc.* **1999**, *9*, 181–186.
(37) Ontko, A. C.; Armistead, P. M.; Kircus, S. R.; Thorp, H. H. *Inorg. Chem.* **1999**, *38*, 1842–1846.
(38) Slamon, D. J.; Clark, G. M.; Wong, S. G.; Levin, W. J.; Ullrich, A.; McGuire, W. L. *Science* **1987**, *235*, 177–182.

CGC TGC AAG GGG CCA; reverse primer, GCA GCC AGC AAA CTC CTG GAT ATT), 1,020 bp product (forward primer, GGC TGT GCC CGC TGC AAG GGG CCA; reverse primer, CGG CAA ACAGTG CCT GGC ATT) and 1497-bp PCR product (forward primer, GGC TGT GCC CGC TGC AAG GGG CCA; reverse primer, CCT CAG CTCCGT CTCTTT CAG) were prepared using 1 cycle at 95 °C for 5 min, 30 cycles at 94 °C for 20 s, 62 °C for 30 s (64 °C for the 1020-bp fragment and 55 °C for the 435-bp fragment), 72 °C for 2 min (1.5 min for the 1020-bp fragment and 40 s for the 435-bp fragment), and 1 cycle at 72 °C for 10 min (5 min for the 435-bp fragment). Each PCR product was tested for purity by gel electrophoresis on a 2% agarose gel. Both the 435- and 1497-bp sequences yielded one product of the appropriate size as determined on the gel. The 1020-bp sequence consistently yielded a low molecular weight band that was less than 1% as intense as the major band of the appropriate size observed on the gel. RT-PCR products were purified on Concert purification columns (Life Technologies) before subsequent manipulations. These products were used as templates for further amplifications as more product was needed. The purified PCR products were ethanol precipitated and resuspended in 100 mM sodium acetate at pH 6.8. This procedure typically yielded ~70 μL of 1 mM PCR product (concentration determined in moles of nucleotide) from 20 reaction tubes. Only purified PCR products were used in all of these experiments because the pyrophosphate and unreacted dNTPs in the unpurified PCR mixture adsorb to the electrode. The adsorption of these small molecules prevents adsorption of the DNA product and results in no catalytic current enhancement when electrochemical measurements are performed.

Electrode Modification. ITO electrodes (12.6 mm^2) were purchased from Delta Technologies. ITO electrodes were sonicated in an Alconox (Alconox, New York, NY) solution (8 g of Alconox/L of water) for 15 min, rinsed, and then sonicated in 2-propanol for 15 min followed by two 15-min sonications in water.[39] The electrodes were then allowed to air-dry. Purified PCR products were prepared for immobilization onto the ITO surface by mixing 5 μL of the PCR product in 100 mM sodium acetate, pH 6.8, with 45 μL of DMF. The 50-μL mixture was pipetted onto each electrode, and the electrodes were placed in a constant-humidity chamber for 1 h. The electrodes were then rinsed by immersion in solutions that were agitated on a rotary mixer. The electrodes were subjected to two water washes for 3 min each, one wash in 1 M sodium chloride for 5 min, one wash in 100 mM sodium phosphate (pH 7.0) for 5 min, and three final washes in water each for 3 min. The electrodes were then allowed to dry. The amount of DNA attached to the surface was controlled by changing the concentration of the PCR product that was applied to the ITO.

Electrochemical Measurements. All electrochemical experiments were performed in a one-compartment electrochemical cell using a BAS 100B potentiostat. The modified ITO was used as the working electrode, a Ag/AgCl (Cypress Systems) minielectrode was used as the reference, and a platinum wire was used as the auxiliary electrode. For each batch of 10 electrodes cleaned, one electrode was used to perform a background scan. This electrode was not treated with DNA; however, cyclic voltammetry was performed on it at the above parameters without $Ru(bpy)_3^{2+}$ in 50 mM sodium phosphate, pH 7.0. This buffer cyclic voltammogram was subtracted from those later measured on the DNA-modified electrodes. As measurements at lower DNA concentrations were performed, the effect of background-subtraction error increased. Background-subtracted cyclic voltammograms whose charging current contribution was greater than the actual faradaic signal of $Ru(bpy)_3^{2+}$ oxidation were not used in subsequent analyses.

DNA Quantification by Phosphorimagery. Radiolabeled PCR products were synthesized according to a method similar to that of Mertz and Rashtchian.[40] Briefly, a 20-μL PCR mixture was prepared containing 1 μL of template DNA (100 pg/μL), 1 μL of forward primer (5 μM), 1 μL of reverse primer (1 μL of $MgCl_2$ (10 mM), 1 μL of dNTP's (100 μM), 2 μL of 10× PCR buffer, 3 μL of α-^{32}P-dCTP (1.8 μM), 10 μL of water, and 1 unit of Taq polymerase. Preparation of the appropriate fragment was verified by electrophoresis of parallel, nonradioactive PCR products on a 5% native polyacrylamide gel stained with SYBR-green (Molecular Probes). All of the parallel reactions yielded one visible product that was the appropriate length. The radiolabeled PCR products were purified on Concert PCR purification cartridges, ethanol precipitated, and dried on a speed vacuum. To each dried radiolabeled PCR product was added 40 μL of 1 mM unlabeled PCR product of the same length in 100 mM sodium acetate, pH 6.8. The newly doped PCR products were used within 1 day of synthesis to minimize the effects of radiolysis. Electrodes modified with radiolabeled DNA were air-dried, wrapped in plastic wrap, and placed on a phosphorimager screen. Aliquots of 1 μL of certain concentrations from the labeled PCR products were used as quantification standards. These aliquots were applied to filter paper, dried, wrapped in plastic wrap, and placed on the phosphorimager screen. The phosphorimager screen was exposed for ~12 h and scanned on a Molecular Dynamics Storm 860 phosphorimager.

RESULTS

Electrocatalysis at DNA-Modified Electrodes. To maximize the sensitivity of the electrocatalytic system, conditions were established to minimize current due to $Ru(bpy)_3^{2+}$ alone and to maximize the contribution of the catalytic signal. The ratio of the catalytic current (i_{cat}) to current at the unmodified electrode (i_d) was determined as a function of scan rate and $Ru(bpy)_3^{2+}$ concentration. The maximum value of i_{cat}/i_d was observed when voltammograms were collected at a scan rate of 10 V/s, and the $Ru(bpy)_3^{2+}$ concentration was kept at only 10 μM. At lower scan rates or higher concentrations of $Ru(bpy)_3^{2+}$, the catalytic current was more difficult to distinguish over the current due to the metal complex alone. Shown in Figure 1A are cyclic voltammograms of $Ru(bpy)_3^{2+}$ at a DNA-modified electrode (solid line) and of an unmodified electrode over the same potential range in 50 mM phosphate buffer with no $Ru(bpy)_3^{2+}$ (dashed line). The DNA-modified electrode gave faradaic currents that were large in the forward direction current and small in the reverse direction, as is typical of electrocatalysis. This faradaic wave was superimposed on a relatively high charging current that results from the large electrode area (12.6 mm^2) and the high scan rate.

Figure 1B shows background-subtracted voltammograms of $Ru(bpy)_3^{2+}$ at DNA-modified (solid line) and unmodified (dashed

(39) Willit, J. L.; Bowden, E. F. *J. Phys. Chem.* **1990**, *94*, 8241–8246.

(40) Mertz, L. M.; Rashtchian, A. *Focus* **1994**, *16*, 45–48.

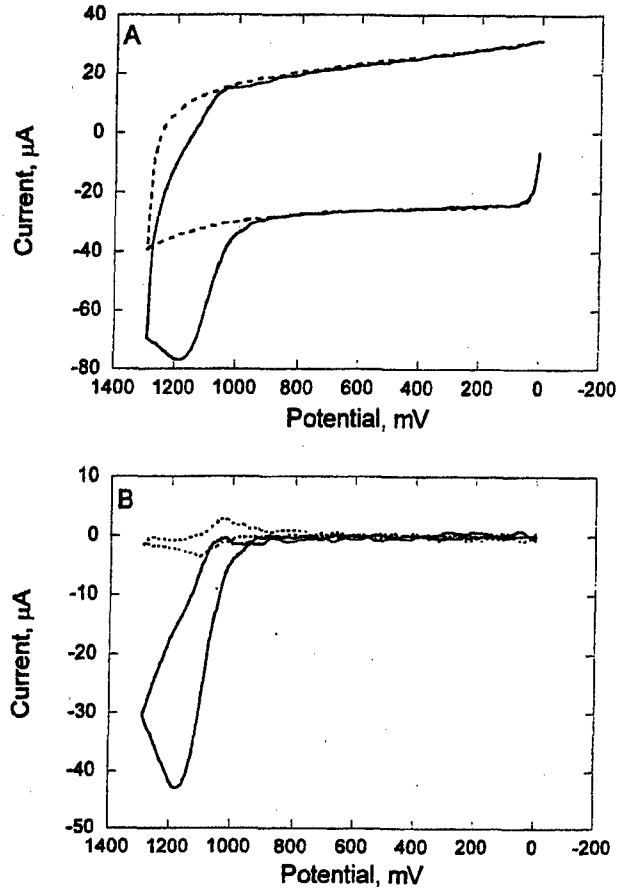

Figure 1. (A) Cyclic voltammograms taken at 10 V/s for bare ITO in 50 mM sodium phosphate, pH 7 (dashed line) and for a DNA-modified electrode in 10 μM $Ru(bpy)_3^{2+}$ (solid line). (B) Cyclic voltammograms obtained after subtraction for 10 μM $Ru(bpy)_3^{2+}$ at an unmodified electrode (dashed line) and at the DNA-modified electrode from (A) (solid line). Subtractions used as a background scan of bare ITO in 50 mM sodium phosphate, as shown as the dashed line in (A).

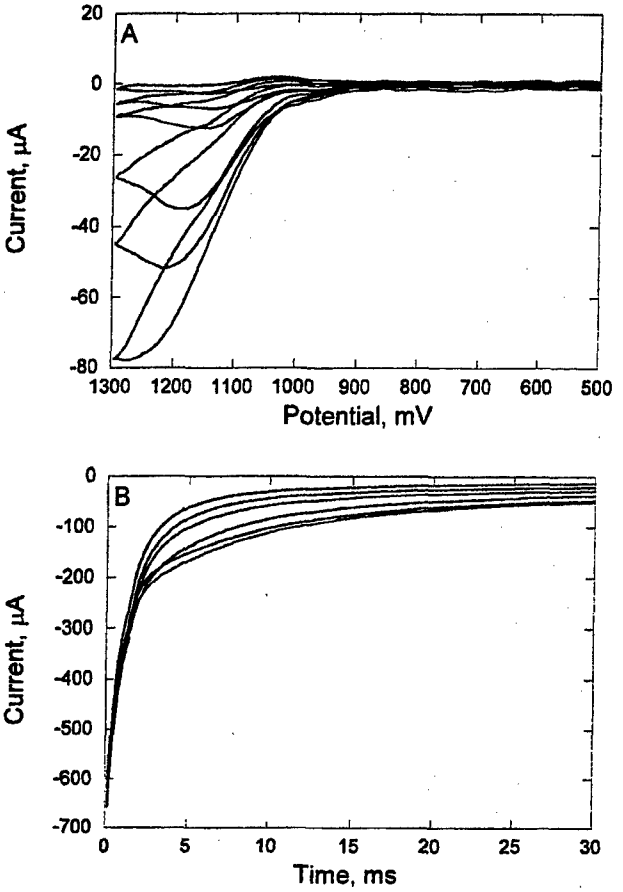

Figure 2. (A) Cyclic voltammograms of 10 μM $Ru(bpy)_3^{2+}$ at ITO electrodes modified with 1497-bp PCR product at nucleotide concentrations of 50, 20, 10, 2.5, 1.0, and 0.5 μM. Increasingly larger currents were observed as the DNA concentration increased. (B) Representative chronoamperograms of 10 μM $Ru(bpy)_3^{2+}$ at ITO electrodes modified with the 435-bp PCR product at the same nucleotide concentrations as in (A).

line) electrodes. The catalytic enhancement due to the immobilized DNA is apparent in comparing the two voltammograms. The voltammogram at the unmodified electrode shows the typical quasi-reversible response for $Ru(bpy)_3^{2+}$ at these scan rates and gives an oxidative peak current of 3.6 ± 0.6 μA over more than 20 trials. Voltammograms of the DNA-modified electrodes in the *absence* of $Ru(bpy)_3^{2+}$ produced a barely detectable current above that observed for the unmodified electrodes; i.e., very little oxidation of guanine in the immobilized DNA was detected without $Ru(bpy)_3^{2+}$. Further, repeated scanning of the electrodes modified with 100 μM DNA in the presence of $Ru(bpy)_3^{2+}$ produced much smaller currents on the second scan, and by the tenth scan, the signal had decreased to 4... μA, within experimental error of the value for $Ru(bpy)_3^{2+}$ at an unmodified electrode. This result suggests that the electrocatalysis irreversibly damages the guanine bases in the DNA.

The DNA-modified electrode in Figure 1 was prepared by treating an ITO electrode with a 20 μM (nucleotide) solution of DNA in 9:1 DMF/acetate buffer at constant humidity for 1 h followed by numerous washing steps that did not remove the immobilized DNA. No DNA was lost even after heating the electrodes to 95 °C for 2 min; however, the DNA could be removed by incubation in phosphate buffer at room temperature overnight. This competition by phosphate did cause removal of up to 50% of the immobilized DNA during the sodium phosphate rinsing step; however, provided the washing time was carefully followed, reproducible results were obtained. Figure 2A shows representative cyclic voltammetry data obtained from electrodes modified with increasingly concentrated solutions of DNA. As the quantity of DNA exposed to the electrode was increased, the catalytic current increased both in cyclic voltammetry (Figure 2A) and in chronoamperometry (Figure 2B). Note that the voltammograms in Figure 2A were performed with electrodes modified with the larger PCR product while the chronoamperometry data were collected on electrodes modified with the shorter fragment and thus were modified with less total guanine (vide infra). Nevertheless, increases in current attributable to DNA oxidation were generally more readily apparent in the raw data obtained by cyclic voltammetry than by chronoamperometry.

An important question was whether the immobilized DNA was in the single-stranded or duplex form. In the experiments thus far, double-stranded PCR products were added to the DMF solution that was then placed on the ITO electrode for immobilization. We suspected that the DMF solution denatured the duplexes, leading to immobilization of single-stranded DNA. Cyclic voltam-

Table 1. Immobilization of PCR Products on ITO Electrodes

strand length (bp)	nucleotide concn[a] (μM)	strand concn[b] (nM)	nucleotide immobilized[c] (pmol)	strand immobilized[d] (fmol)	% immobilized[e]	peak current[f] (μA)
435	20	23.0	7.7	8.9	14	22.0 ± 4.0
	2	2.30	0.89	1.0	16	3.8 ± 0.5
1020	20	9.80	15	7.4	27	27.0 ± 5.0
	2	0.980	1.4	0.69	25	5.2 ± 0.5
1497	20	6.7	19	6.1	33	38.0 ± 3.0
	2	0.67	1.7	0.55	29	7.1 ± 1.4

[a] Concentration is nucleotide phosphates in the 9:1 DMF/acetate solution applied to the electrode. [b] Strand concentration determined dividing the nucleotide concentration by twice the strand length. [c] Nucleotide immobilized determined by phosphorimagery of ITO electrodes compared to standards of known molar amounts. [d] Strand immobilized determined by dividing the moles of immobilized nucleotide by twice the strand length. [e] Percent immobilized determined by dividing the moles of nucleotide immobilized by the moles of nucleotide applied to the electrode. [f] Oxidative peak current determined for four cyclic voltammograms of $Ru(bpy)_3^{2+}$ at electrodes modified with the given strand concentration; peak current for $Ru(bpy)_3^{2+}$ at an unmodified electrode was 3.6 ± 0.6 μA.

mograms of electrodes with calf thymus DNA that was thermally denatured before the addition of DMF were indistinguishable from cyclic voltammograms obtained from electrodes that were treated with double-stranded DNA. Since calf thymus DNA does not reanneal upon cooling after thermal denaturation, this result strongly suggests that the immobilized DNA is single-stranded.

Characterization of DNA Adsorption. To confirm that DNA was irreversibly adsorbing to the ITO electrodes and that the quantity of adsorbed DNA was increasing as the concentration of the modifying solution was increased, DNA fragments were radiolabeled and quantified using a phosphorimager. The fragments were "body labeled" by performing PCR with α-^{32}P-dCTP, which inserts many radioactive phosphorus nuclei per DNA fragment. The body-labeling scheme was used so that the majority of DNA attached to the electrode could be unlabeled and doped with small quantities of the radiolabeled DNA that had a high specific activity. After the radioactive DNA fragments were attached, the electrodes were placed on a phosphorimager screen and analyzed against standards of known quantity. To determine whether the length of the DNA strands impacted the extent of modification of the electrode, PCR fragments of 435, 1020, and 1497 bp were prepared and used to modify the ITO electrodes. The relevant quantities that need to be considered in the analysis are the nucleotide concentration in the solution, the strand concentration in solution, the quantity of nucleotides immobilized, and the quantity of strands immobilized. Since the immobilized DNA is single-stranded, the number of strands immobilized on the electrode is equal to the quantity of nucleotides on the electrode divided by twice the length of the (double-stranded) PCR product.

The quantities of immobilized strands and nucleotides are compared in Figure 3 and Table 1. For all three PCR products, the number of strands immobilized increases rapidly with the concentration of nucleotides in the application solution until ~40 μM nucleotide, where the fraction of adsorbed DNA begins to decrease (Figure 3A). As a control, the procedure was repeated with borosilicate glass, and the quantity of adsorbed DNA was at least 50 times lower than that adsorbed to ITO. The number of strands immobilized is higher for a given nucleotide concentration for the shorter strands, as also shown in Figure 3A. This effect arises in part because, at a particular nucleotide concentration, a solution of shorter fragments contains a higher number of strands. In fact, when the number of strands immobilized onto the

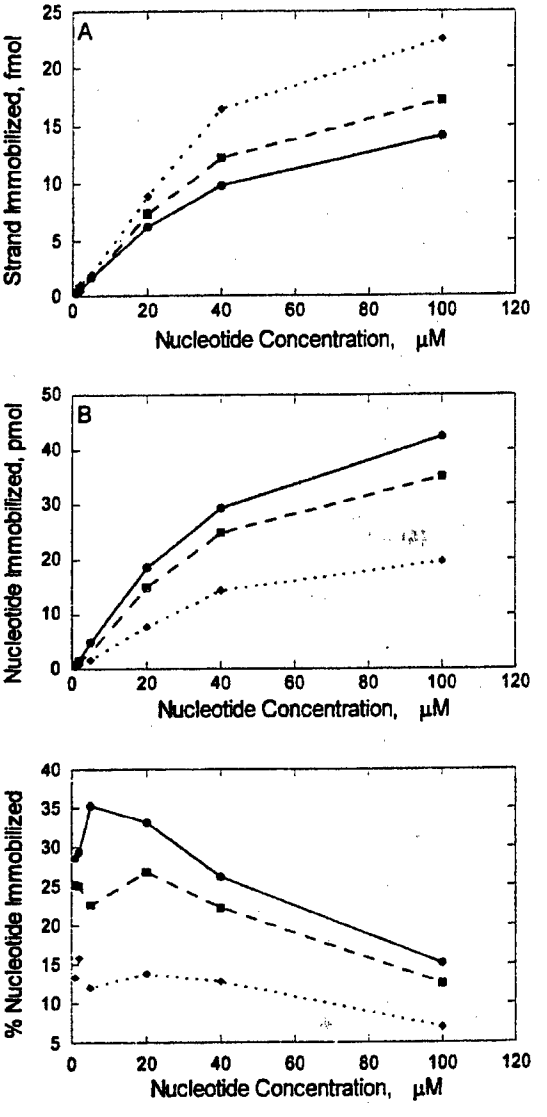

Figure 3. (A) Moles of radiolabeled PCR products immobilized onto ITO electrodes for the PCR products of 1497 (●), 1020 (■), or 435 bp (◆) as a function of the concentration of nucleotide originally applied to the electrode. (B) Moles nucleotides immobilized taken directly from the data in (A). (C) Fraction of nucleotides adsorbed from the deposition solution as a function of the original concentration of the applied solution for the three PCR products.

electrode is converted to the number of nucleotides immobilized (Figure 3B), it is apparent that more total nucleotides are immobilized for the longer fragments. This relationship is also seen in Table 1 by comparing, for example, the results for application of 20 μM nucleotide of the 435-bp fragment, which leads to 7.7 pmol of immobilized nucleotide, while application of 20 μM of the 1497-bp fragment leads to immobilization of 19 pmol of nucleotide. Thus, more than twice the number of nucleotides are immobilized for the longer fragment from solutions containing the same number of nucleotides for each fragment.

The results in Figure 3A and B show that the mechanism of DNA adsorption is one in which generally longer strands lead to a higher efficiency of surface modification at any given nucleotide concentration. Thus, we expect that, for a given concentration of nucleotides, a greater fraction of the total DNA in the solution will be adsorbed with longer strands. We therefore analyzed the number of nucleotides that were adsorbed to the electrode compared to the total number of nucleotides in the solution used to treat the electrode. As expected, a greater fraction of the nucleotides was adsorbed for the longer strands (Figure 3C, Table 1). As much as 33% of the total nucleotides applied to the electrode could be immobilized for the longest strand. In addition, it was apparent for the long strand that the efficiency of modification increases at low nucleotide concentrations and then decreases at higher nucleotide concentrations, as shown in Figure 3C.

The results to this point demonstrate that when more DNA is applied to the electrode, greater catalytic enhancement is obtained for the cyclic voltammetry and chronoamperometry of $Ru(bpy)_3^{2+}$. The independent quantification of the immobilized DNA by phosphorimagery shows that more nucleotides are in fact adsorbed to the electrode at the higher concentrations, and we know from numerous previous studies that the guanines in DNA are the ultimate source of the electrons.[34-37,41]

Sensitivity of Electrocatalytic Detection. We next sought to establish a quantitative relationship between the number of strands adsorbed and the peak current obtained in cyclic voltammograms acquired as in Figure 1. The three fragments chosen all contain ~30% guanine: the 435-bp fragment contains 264 guanines (30.3%), the 1020-bp fragment contains 626 guanines (30.7%), and the 1497-bp fragment contains 918 guanines (30.7%).[42] We therefore expect a direct relationship between the quantity of immobilized nucleotides and the catalytic enhancement, which should be the same for all three sequences. We prepared electrodes modified with all three strands, collected cyclic voltammograms of $Ru(bpy)_3^{2+}$ at each modified electrode, and independently quantified the number of immobilized strands by phosphorimagery. Figure 4A shows there is an excellent linear correlation between the peak current and the number of nucleotides immobilized. The slope of the linear fit is 1.7 μA/pmol nucleotide immobilized, which corresponds to 0.5 μA/pmol guanine. Integrating the peak currents reveals that 2.2 ± 0.4 electrons are transferred per guanine. There are a number of oxidation pathways for guanine that can result in a two-electron oxidation.[43-47] Representative peak currents are also shown in Table 1 with standard errors.

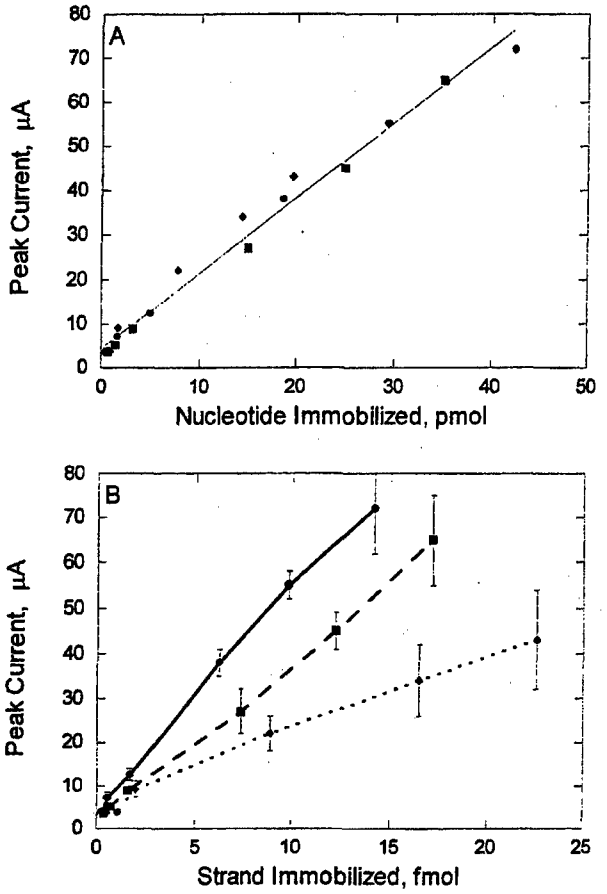

Figure 4. (A) Oxidative peak currents from cyclic voltammograms of 10 μM $Ru(bpy)_3^{2+}$ at the modified electrodes as a function of the quantity of immobilized nucleotides (1497- (●), 1020- (■), and 435-bp PCR product (◆)) determined by phosphorimagery of the radiolabeled PCR products. Voltammograms were acquired as in Figures 1 and 2A. (B) Peak current as a function of moles of strand immobilized for the 1497- (●), 1020- (■), and 435-bp PCR product (◆).

A final prediction that can be made from the results thus far is that the sensitivity of the electrocatalysis to the number of immobilized strands should be steeper for longer fragments that contain more guanines. The data from Figure 4A are replotted in Figure 4B for each fragment as a function of the number of immobilized strands. As expected, the longer fragments show steeper responses. To assess the lower detection limit, the standard error was determined for $Ru(bpy)_3^{2+}$ at unmodified electrodes over numerous trials. Catalytic currents that were more than 3 times greater than this error were detected for the long strand when as little as 550 amol was adsorbed. Thus, the electrocatalysis provides detectable currents at a density of immobilized DNA of 44 amol/mm^2. Even longer DNA fragments

(41) Johnston, D. H.; Cheng, C.-C.; Campbell, K. J.; Thorp, H. H. *Inorg. Chem.* **1994**, *33*, 6388–6390.

(42) Yamamoto, T.; Ikawa, S.; Akiyama, T.; Semba, K.; Nomura, N.; Miyajima, N.; Saito, T.; Toyoshima, K. *Nature* **1986**, *319*, 230–234.

(43) Duarte, V.; Muller, J. G.; Burrows, C. J. *Nucleic Acids Res.* **1999**, *27*, 496–502.

(44) Doddridge, Z. A.; Cullis, P. M.; Jones, G. D. D.; Malone, M. E. *J. Am. Chem. Soc.* **1998**, *120*, 10998–10999.

(45) Cullis, P. M.; Malone, M. E.; Merson-Davies, L. A. *J. Am. Chem. Soc.* **1996**, *118*, 2775–2781.

(46) Vialas, C.; Pratviel, G.; Claparols, C.; Meunier, B. *J. Am. Chem. Soc.* **1998**, *120*, 11548–11553.

(47) Vialas, C.; Claparols, C.; Pratviel, G.; Meunier, B. *J. Am. Chem. Soc.* **2000**, *122*, 2157–2167.

would contain more guanines and give higher signals per strand; however, most reverse transcriptase enzymes cannot reverse transcribe through RNA that has regions containing a high degree of secondary structure, thereby prohibiting production of significantly longer fragments.[48]

DISCUSSION

DNA–Electrode Interaction. When DNA is dissolved in aqueous solution, relatively little adsorption to ITO electrodes is observed. In fact, the direct oxidation of DNA at ITO is difficult to detect in contrast to other electrode materials such as carbon paste and mercury, which give strong DNA adsorption and faradaic current due to base redox chemistry.[15,18] However, when DNA is dissolved in a medium that contains mostly DMF, strong adsorption occurs to produce modified electrodes where the DNA cannot be removed by agitated washing or heating to 95 °C. Given that DNA immobilized in this fashion is slowly released in the presence of phosphate buffer and that longer strands adsorb more efficiently than shorter strands (on a per nucleotide basis), we suspect that a metal–phosphate interaction is partly responsible for the surface modification. Such a model would also explain why borosilicate did not adsorb DNA under the same conditions. Phosphates and phosphonates exhibit high-affinity interactions with metal oxides,[49–51] and it seems reasonable to propose that DNA can form strong associations with ITO through multiple interactions with the phosphate backbone. The fact that DNA remains attached to the surface at high temperatures but can be competed away from the surface by small molecules is a characteristic of polyelectrolyte adsorption.[52]

The extent of surface coverage in these experiments can be assessed from the quantities of adsorbed DNA. With the large fragment, the maximum amount of DNA adsorbed was 14 fmol of duplex. Since the DNA appears to be single-stranded, this translates to 28 fmol of single strands or 1.3×10^9 strands/mm^2. Estimating the footprint of a 1497-base strand as 10 Å × 3.4 Å × 1497 suggests that this quantity of strands covers 8.7 mm^2 or 69% of a full monolayer.[53] The lower limit of detection observed at 550 amol corresponds to 2.7% of a full monolayer.

Electrocatalysis. In general, electrocatalysis is performed under conditions where the catalyst is immobilized on the electrode and the substrate is in solution.[54–56] However, in the system described here, the scenario is essentially reversed and the substrate (guanine in DNA) is immobilized on the electrode and the catalyst ($Ru(bpy)_3^{2+}$) is dissolved in the solution. The observations that repeated scanning gives lower currents suggests that the catalytic reaction consumes a large amount of the immobilized DNA in the early times of the reaction. Further, the chronoamperometry data in Figure 2B show that the majority of the catalysis is over within the first 30 ms, which is also consistent with the observation that the catalytic current was easiest to detect by cyclic voltammetry when the scan rate was 10 V/s. These features are in agreement with numerous observations made when both $Ru(bpy)_3^{2+}$ and DNA are in solution, which show that the rate constant for oxidation of guanine by Ru(III) is as high as 10^6 M^{-1} s^{-1}.[28,30,31]

With the low quantities of DNA adsorbed onto the electrode, it is likely that a large fraction of the guanines has been oxidized in a single sweep, which at 10 V/s provides ~60 ms during which there is a significant concentration of Ru(III) at the electrode surface. In fact, roughly 2 electrons/guanine were transferred to the electrode during the cyclic voltammetry experiments. After the adsorbed DNA is consumed, the catalytic cycle does not occur, so large current enhancements are not observed at lower scan rates.

The appeal of a direct electrochemical technique for detecting nucleic acids is that long strands that contain many of the redox-active unit exhibit high responses for individual strands.[4] This concept has been exploited in numerous schemes involving redox chemistry of the DNA bases and recently by Kuhr et al. for oxidation of ribose sugars at copper electrodes.[21] As stated above, the drawback to these direct techniques is that the redox chemistry is either slow or occurs at potentials where the electrode also electrolyzes water. The advantage of the $Ru(bpy)_3^{2+}$-mediated system here is that, like many indirect detection schemes, the electrons are delivered to the electrode by a molecule that exhibits a fast heterogeneous electron transfer. However, the counted electrons originate in the biopolymer, providing some of the advantages of the direct approaches. As in the indirect detection scheme, the ITO electrode exhibits little water oxidation current at the operative potential. At the same time, strands with more guanines give more signal, a point that is well exemplified by Figure 4 and is an advantage typical of direct electrochemistry. This latter point enables subfemtomole detection limits using long DNA strands that contain many oxidizable guanines. Further gains in sensitivity can be effected by miniaturization of the electrode, which could enable the development of a detection scheme for direct analysis of small quantities of nucleic acid derived from biological mixtures.

(48) Thiel, V.; Rashtchian, A.; Herold, J.; Schuster, D. M.; Guan, N.; Siddell, S. G. *Anal. Biochem.* **1997**, *252*, 62–70.

(49) Nooney, M. G.; Campbell, A.; Murrel, T. S.; Lin, X.-F.; Hossner, L. R.; Chusuei, C. C.; Goodman, D. W. *Langmuir* **1998**, *14*, 2750–2755.

(50) Gao, W.; Dickinson, L.; Grozinger, C.; Morin, F. G.; Reven, L. *Langmuir* **1996**, *12*, 6429–6435.

(51) Cao, G.; Hong, H.-G.; Mallouk, T. E. *Acc. Chem. Res.* **1992**, *25*, 420–427.

(52) Hesselink, F. T. In *Adsorption from Solution at the Solid/Liquid Interface*; Parfitt, G. D., Rochester, C. H., Eds.; Academic Press: New York, 1983; pp 377–412.

(53) Stryer, L. *Biochemistry*; 3rd ed.; W. H. Freeman and Co.: New York, 1988.

(54) Glass, A. E. G.; Davis, G.; Francis, G. D.; Hill, H. A. O.; Aston, W. J.; Higgins, I. J.; Plotkin, E. V.; Scott, L. D. L.; Turner, A. P. F. *Anal. Chem.* **1984**, *56*, 667–671.

(55) Kenausis, G.; Chen, Q.; Heller, A. *Anal. Chem.* **1997**, *69*, 1054–1060.

(56) Wilkins, E.; Atanasov, P. *Med. Eng. Phys.* **1996**, *18*, 273–288.

ACKNOWLEDGMENT

We thank the Department of Defense and Xanthon, Inc. for support of this research. Helpful discussions with Drs. Carole Golden, Mary Napier, Patty Ropp, Natasha Popovich, and Allen Eckhardt are gratefully acknowledged.

Received for review January 12, 2000. Accepted June 5, 2000.

AC000051E

[This page is intentionally left blank.]